THIS REPORT WAS INADVERTENTLY DISSEMINATED IN THE PUBLIC DOMAIN/ONLINE SINCE 12/2018 WITHOUT A DISCLAIMER. DISCLAIMER HAS BEEN ADDED – "THIS INFORMATION IS DISTRIBUTED SOLELY FOR THE PURPOSE OF PEER REVIEW UNDER APPLICABLE INFORMATION QUALITY GUIDELINES. IT HAS NOT BEEN FORMALLY DISSEMINATED BY BSEE. IT DOES NOT REPRESENT AND SHOULD NOT BE CONSTRUED TO REPRESENT ANY AGENCY DETERMINATION OR POLICY."

TECHNICAL REPORT ON LEAKAGE SIMULATIONS AND RISK ASSESSMENTS

AUTHORS:

Saeed Salehi (PhD), Principal Investigator

Ramadan Ahmed (PhD), Co-Principal Investigator

Catalin Teodoriu (PhD), Co-Principal Investigator

Harshkumar Patel, Graduate Research Assistant

Chinedum Peter Ezeakacha, Graduate Research Assistant

Prepared under BSEE Project NO: E17PC00005

by

THE UNIVERSITY OF OKLAHOMA

July 2018

THIS REPORT WAS INADVERTENTLY DISSEMINATED IN THE PUBLIC DOMAIN/ONLINE SINCE 12/2018 WITHOUT A DISCLAIMER. DISCLAIMER HAS BEEN ADDED – "THIS INFORMATION IS DISTRIBUTED SOLELY FOR THE PURPOSE OF PEER REVIEW UNDER APPLICABLE INFORMATION QUALITY GUIDELINES. IT HAS NOT BEEN FORMALLY DISSEMINATED BY BSEE. IT DOES NOT REPRESENT AND SHOULD NOT BE CONSTRUED TO REPRESENT ANY AGENCY DETERMINATION OR POLICY."

EXECUTIVE SUMMARY

Liner hanger seal assemblies and cement systems are important barrier elements in offshore, shallow depth well design. Currently, the industry lacks adequate standards and guidelines for assessing seal assembly in a conventional liner hanger or a sub-mudline hanger. The guidelines and standards for liner cementing are already in place, but need improvements. The goal of this study is to assess "fitness-for-service" of seal assemblies and cement sheath using the approach of leakage modelling, simulations, and risk assessment. This fills-in some of the existing knowledge gaps and helps regulators and operators improve design, selection, and qualification of these barrier elements (In this report, the term "barrier(s)" defines the use of cement sheath and liner hanger sealing assembly to prevent uncontrolled influx and migration of formation fluid to a shallow formation or surface facilities).

To achieve the objectives, a comprehensive finite element analysis was conducted using three-dimensional computer models consisting of liner, casing, seal assembly, and cement elements. The sealability of an elastomer component in a hanger assembly was evaluated in terms of the contact stress generated at the seal-pipe interface. Performance of cement sheath was assessed by analyzing radial, hoop, and maximum shear stress for mechanical failure. An extensive literature review was conducted to identify various parameters that can affect the performance of barrier elements. Parametric analyses were performed to understand the behavior of elastomer seal and cement sheath under various conditions, considering different design parameters, such as dimensions and material properties. Various potential failure scenarios were selected and examined to identify the effects on seal performance and cement integrity. Operating curves, correlations, and rules of thumbs were generated for quick and easier prediction of performance of both barriers independently. Our results suggest that annular fit, compression ratio, energization quality, elastic modulus, and Poisson's ratio are the most critical factors affecting sealability of elastomer element in seal assembly.

THIS REPORT WAS INADVERTENTLY DISSEMINATED IN THE PUBLIC DOMAIN/ONLINE SINCE 12/2018 WITHOUT A DISCLAIMER. DISCLAIMER HAS BEEN ADDED – "THIS INFORMATION IS DISTRIBUTED SOLELY FOR THE PURPOSE OF PEER REVIEW UNDER APPLICABLE INFORMATION QUALITY GUIDELINES. IT HAS NOT BEEN FORMALLY DISSEMINATED BY BSEE. IT DOES NOT REPRESENT AND SHOULD NOT BE CONSTRUED TO REPRESENT ANY AGENCY DETERMINATION OR POLICY."

TABLE OF CONTENTS

THIS REPORT WAS INADVERTENTLY DISSEMINATED IN THE PUBLIC DOMAIN/ONLINE SINCE 12/2018 WITHOUT A DISCLAIMER. DISCLAIMER HAS BEEN ADDED – "THIS INFORMATION IS DISTRIBUTED SOLELY FOR THE PURPOSE OF PEER REVIEW UNDER APPLICABLE INFORMATION QUALITY GUIDELINES. IT HAS NOT BEEN FORMALLY DISSEMINATED BY BSEE. IT DOES NOT REPRESENT AND SHOULD NOT BE CONSTRUED TO REPRESENT ANY AGENCY DETERMINATION OR POLICY."

THIS REPORT WAS INADVERTENTLY DISSEMINATED IN THE PUBLIC DOMAIN/ONLINE SINCE 12/2018 WITHOUT A DISCLAIMER. DISCLAIMER HAS BEEN ADDED – "THIS INFORMATION IS DISTRIBUTED SOLELY FOR THE PURPOSE OF PEER REVIEW UNDER APPLICABLE INFORMATION QUALITY GUIDELINES. IT HAS NOT BEEN FORMALLY DISSEMINATED BY BSEE. IT DOES NOT REPRESENT AND SHOULD NOT BE CONSTRUED TO REPRESENT ANY AGENCY DETERMINATION OR POLICY."

THIS REPORT WAS INADVERTENTLY DISSEMINATED IN THE PUBLIC DOMAIN/ONLINE SINCE 12/2018 WITHOUT A DISCLAIMER. DISCLAIMER HAS BEEN ADDED – "THIS INFORMATION IS DISTRIBUTED SOLELY FOR THE PURPOSE OF PEER REVIEW UNDER APPLICABLE INFORMATION QUALITY GUIDELINES. IT HAS NOT BEEN FORMALLY DISSEMINATED BY BSEE. IT DOES NOT REPRESENT AND SHOULD NOT BE CONSTRUED TO REPRESENT ANY AGENCY DETERMINATION OR POLICY."

LIST OF FIGURES

THIS REPORT WAS INADVERTENTLY DISSEMINATED IN THE PUBLIC DOMAIN/ONLINE SINCE 12/2018 WITHOUT A DISCLAIMER. DISCLAIMER HAS BEEN ADDED – "THIS INFORMATION IS DISTRIBUTED SOLELY FOR THE PURPOSE OF PEER REVIEW UNDER APPLICABLE INFORMATION QUALITY GUIDELINES. IT HAS NOT BEEN FORMALLY DISSEMINATED BY BSEE. IT DOES NOT REPRESENT AND SHOULD NOT BE CONSTRUED TO REPRESENT ANY AGENCY DETERMINATION OR POLICY."

THIS REPORT WAS INADVERTENTLY DISSEMINATED IN THE PUBLIC DOMAIN/ONLINE SINCE 12/2018 WITHOUT A DISCLAIMER. DISCLAIMER HAS BEEN ADDED – "THIS INFORMATION IS DISTRIBUTED SOLELY FOR THE PURPOSE OF PEER REVIEW UNDER APPLICABLE INFORMATION QUALITY GUIDELINES. IT HAS NOT BEEN FORMALLY DISSEMINATED BY BSEE. IT DOES NOT REPRESENT AND SHOULD NOT BE CONSTRUED TO REPRESENT ANY AGENCY DETERMINATION OR POLICY."

THIS REPORT WAS INADVERTENTLY DISSEMINATED IN THE PUBLIC DOMAIN/ONLINE SINCE 12/2018 WITHOUT A DISCLAIMER. DISCLAIMER HAS BEEN ADDED – "THIS INFORMATION IS DISTRIBUTED SOLELY FOR THE PURPOSE OF PEER REVIEW UNDER APPLICABLE INFORMATION QUALITY GUIDELINES. IT HAS NOT BEEN FORMALLY DISSEMINATED BY BSEE. IT DOES NOT REPRESENT AND SHOULD NOT BE CONSTRUED TO REPRESENT ANY AGENCY DETERMINATION OR POLICY."

LIST OF TABLES

THIS REPORT WAS INADVERTENTLY DISSEMINATED IN THE PUBLIC DOMAIN/ONLINE SINCE 12/2018 WITHOUT A DISCLAIMER. DISCLAIMER HAS BEEN ADDED – "THIS INFORMATION IS DISTRIBUTED SOLELY FOR THE PURPOSE OF PEER REVIEW UNDER APPLICABLE INFORMATION QUALITY GUIDELINES. IT HAS NOT BEEN FORMALLY DISSEMINATED BY BSEE. IT DOES NOT REPRESENT AND SHOULD NOT BE CONSTRUED TO REPRESENT ANY AGENCY DETERMINATION OR POLICY."

1. INTRODUCTION

The importance of maintaining a well in an optimum and safe condition throughout its life is unequivocally accepted by the industry. To address safety, environmental, and operational concerns during all activities, wells are always designed to have two independently tested barriers (NORSOK D-010). The context in which the term "barrier" is used in this report has been defined as the use of cement sheath and liner hanger sealing assembly to prevent uncontrolled influx and migration of formation fluid to a shallow formation or surface facilities. Seal assemblies and cement systems are important barrier elements and provide the backup defense against formation fluid influx and migration.

In a shallow offshore well, one of the biggest concerns regarding well control is shallow gas kick and migration. This is because maintaining sufficient hydrostatic pressure at shallow depth is challenging. A study of blowout events that occurred during drilling operations on the Outer Continental Shelf (OCS) of Gulf of Mexico from 1992 through 2006 revealed that 48% of the incidents occurred in water depth less than 200 ft and 36% of the incidents occurred between the water depths of 201-500 ft (Izod et al. 2007). They also observed that shallow gas kick was associated with 49% of the blowouts.

In offshore wells, as drilling depth increases, it is a common practice for operators to run a liner string instead of running a full casing string back to the wellhead. The liner is typically hung from the previous casing and/or cemented in place. The cement within the liner-casing overlap acts as a barrier to isolate different fluid-bearing zones from one another and from the surface.

Conventionally, liner hanger systems used to rely only upon the cement to provide sealing between liner/casing overlap and maintain well integrity. The challenges associated with obtaining a good quality primary cementing and financial incentive in not running the cement throughout the overlap up to the liner hanger necessitated a backup sealing mechanism or a barrier (Smith and Williford 2006). This led to innovative designs such as liner-top packer or liner hanger with integrated seal assembly. The seal assembly is typically set mechanically by applying weight down or by combined action of weight and rotation. As the weight is applied, the slips travel down and engages the pipe. A load is placed on the elastomer element which expands radially by compression and seals the annulus between the liner and casing (see Figure 1.1).

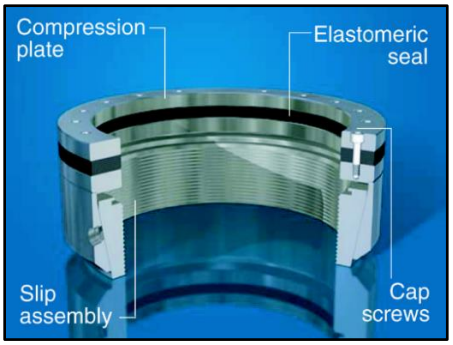

Figure 1.1:Illustration of a mechanical-set slip-and-seal assembly in sub-mudline liner hanger assembly (Speer 2006)

THIS REPORT WAS INADVERTENTLY DISSEMINATED IN THE PUBLIC DOMAIN/ONLINE SINCE 12/2018 WITHOUT A DISCLAIMER. DISCLAIMER HAS BEEN ADDED – "THIS INFORMATION IS DISTRIBUTED SOLELY FOR THE PURPOSE OF PEER REVIEW UNDER APPLICABLE INFORMATION QUALITY GUIDELINES. IT HAS NOT BEEN FORMALLY DISSEMINATED BY BSEE. IT DOES NOT REPRESENT AND SHOULD NOT BE CONSTRUED TO REPRESENT ANY AGENCY DETERMINATION OR POLICY."

1.1. Overview

It has been observed that the failure of seal assembly and/or cement are often responsible for well control incidents. A QC-FIT evaluation report on a recent shallow gas incident (BSEE 2014) revealed potential causes to include failure in casing, seal assembly, and/or cement sheath in liner-casing annulus. An informal survey of several Gulf of Mexico operators indicated that about 30% to 50% of the pressure seals in overlaps failed (Lohoefer et al. 2000). Another report indicates that as many as 18% of offshore wells worldwide are estimated to have some form of weakness or uncertainty in seal assemblies (Van Dort 2009). A study conducted by Izon et al. (2007) indicated that cementing was responsible for 18 out of the 39 major blowouts that occurred between 1992-2006.

Some of the major factors leading to failure of seal assembly are: inability to apply the required weight for energization, wear/tear of seal element, material failure due to temperature and chemical/gas exposure etc. (Wang et al. 2017; Williford and Smith 2007; Smith and Williford 2006). The industry has been exploring alternatives such as expandable liner hangers (Mullins 2016; Mccormick et al. 2012; Walvekar and Jackson 2007; Smith and Williford 2006; Lohoefer et al. 2000) and metal-to-metal seals (Dagle et al. 2016; Stautzenberger et al. 2016). However, these newer technologies are still under development, expensive, have limited material and grade section, and require special technical crews for installing and running the complex tools (Mohamed and Al-Zuraigi 2013). Thus, the conventional liner-hanger assembly is still the most common and widely used solution throughout the industry.

Cement sheath can fail to provide sealability or zonal isolation because of several design, operational, or mechanical factors such as: high inherent permeability, insufficient hydrostatic head or static gel strength, lack of gas migration additive, fluid loss during cementing, presence of micro-annulus due to lack of bonding or volume shrinkage, structural failure in the form of debonding, radial cracking, shear failure, etc. (Lavrov and Torsæter 2016; Khandka 2007). To mitigate these issues, the industry's research efforts have been focused on improving cement slurry design, pumping operation, and strengthening the mechanical properties of set cement for long term integrity.

1.2. Statement of the Problem

Currently, the industry lacks adequate standards and guidelines for assessing seal assembly in a conventional liner hanger or sub-mudline hanger (BSEE 2014). The industry relies on standards developed for packer equipment (ISO 14310:2008E or API Specification 11D1 and 17D). It is unclear at the moment whether the new standard for liner hanger equipment 'API 19LH' - currently being drafted by API, will encompass sufficient guidelines for testing or designing seal assembly. Despite the fact that conventional liner-hanger assemblies have had frequent sealability failure issues, no study is available in the public domain that is focused on assessing the sealability of the elastomer element in hanger seal assemblies under various conditions.

The current industry standards, recommended practices, and technical reports for cement (discussed in section **2.2.3**), are primarily focused on cement slurries, their material properties,

THIS REPORT WAS INADVERTENTLY DISSEMINATED IN THE PUBLIC DOMAIN/ONLINE SINCE 12/2018 WITHOUT A DISCLAIMER. DISCLAIMER HAS BEEN ADDED – "THIS INFORMATION IS DISTRIBUTED SOLELY FOR THE PURPOSE OF PEER REVIEW UNDER APPLICABLE INFORMATION QUALITY GUIDELINES. IT HAS NOT BEEN FORMALLY DISSEMINATED BY BSEE. IT DOES NOT REPRESENT AND SHOULD NOT BE CONSTRUED TO REPRESENT ANY AGENCY DETERMINATION OR POLICY."

laboratory testing, consideration during field operation, etc. All of the documents have helped advance the safety of wells, yet there can still be improvement and expansions in several issues, such as: designing cement for shallow depth wells with potential for gas migration, adequacy of pressure test, and guidelines for evaluating cement system "fitness for service". Further, they lack sufficient discussion on the selection of appropriate mechanical properties for different conditions, performance curves, responses for set cement under various loading conditions, risk assessment of various failure scenarios, etc.

The goal of this study is to assess "fitness-for-service" of seal assemblies and cement sheath under various conditions. This will fill-in some of the existing knowledge gaps and help regulators and operators alike in improving design, selection, and qualification of these barrier elements. It aims to answer following research questions:

Elastomer seal:

- What is the relationship between sealability of elastomer and load applied during setting? What type of elastomer material would yield the highest sealability for a given seal energization load?
- What is the effect of temperature and gas exposure on the elastomer sealability?
- What are the optimum seal dimensions for achieving high and robust sealability for long term service?
- To achieve good sealability, a setting force up to 100,000 lbf is often required. In certain conditions such as shallow liner installation or deviated wells, it may not be possible to apply the required force. Under such low seal energization conditions, what would be the expected loss in sealability?
- How critical is it to exert uniform weight on the seal element for energization?
- What is the effect of improper seal energization on sealability? In other words, during weight application, how does a faulty equipment such as compression plate or a radial slip, affect resultant sealability?

Cement:

- What is the likelihood of structural failure of cement under typical pressure loads in shallow depth wells?
- How does cement respond to changes in Young's modulus and Poisson's ratio? This can help not only in designing better cement system but also in estimating the changes in cement performance upon material degradation.
- How does cement sheath height in liner overlap and cement radial width affect cement performance?
- What is the effect of micro-annulus presence on cement performance?
- How does the performance of a pre-stressed cement system compare against conventional systems?
- Which factors affect cement performance the most? This will inform what needs higher while designing?

THIS REPORT WAS INADVERTENTLY DISSEMINATED IN THE PUBLIC DOMAIN/ONLINE SINCE 12/2018 WITHOUT A DISCLAIMER. DISCLAIMER HAS BEEN ADDED – "THIS INFORMATION IS DISTRIBUTED SOLELY FOR THE PURPOSE OF PEER REVIEW UNDER APPLICABLE INFORMATION QUALITY GUIDELINES. IT HAS NOT BEEN FORMALLY DISSEMINATED BY BSEE. IT DOES NOT REPRESENT AND SHOULD NOT BE CONSTRUED TO REPRESENT ANY AGENCY DETERMINATION OR POLICY."

1.3. Objectives

The specific objectives of this study are:

- Identify critical material properties, design parameters, and operational factors that affect the performance of elastomer seal and cement.
- Develop and examine various failure scenarios and evaluate the change in the performance of elastomer seal and cement.
- Generate operating curves, correlations, and rules of thumbs that can predict the performance of elastomer seal and cement.
- Develop guidelines for evaluating seal assembly and cement "fitness for service".

1.4. Research Methodology

To achieve the aforementioned objectives, a comprehensive finite element analysis was conducted. Unlike physical tests, use of computer models helped to examine both barriers (elastomer seal and cement) under close-to-real field conditions in terms of dimensions of components, material properties, and loads.

Elastomer Seal:

An extensive literature review was conducted to identify various parameters that can affect sealability. Finite Element Analysis (FEA) was performed using a three-dimensional computer model consisting of liner, casing, and elastomer seal components. Field scale dimensions and realistic material properties were used to create the models. Seal energizing process similar to normal field operation was simulated. Sealability was examined in terms of the contact stress generated at the casing-seal and liner-seal interfaces.

To generate performance curves, parametric analysis was performed. Various parameters were systematically varied, and contact pressure was examined to understand the behavior of elastomer seal. Several important failure scenarios such as improper seal energization, failure of slips or compression plate, material failure, etc. were evaluated. The severity of each failure scenario was quantified by the amount of reduction in contact pressure. Material failure of the seal was modelled by incorporating material properties obtained from laboratory measurements after exposing elastomers to various gases at different temperatures. To improve the reliability of the simulation data, several techniques of model verification were performed. Additionally, analytical equations were used to validate and bolster the simulation results.

Cement:

A comprehensive literature review was performed to identify the primary modes of mechanical failures in cement and select appropriate models or criteria to be used in evaluating the cement's failure. A three-dimensional FEA model consisting of liner, casing, and cement sheath was developed. The performance of cement sheath was evaluated in terms of mechanical stresses, specifically radial, hoop, and maximum shear stresses that develops because of load application.

Parametric analysis was performed to understand the behaviors of the cement sheath having various material properties and dimensions under different pressure loads. In addition to

THIS REPORT WAS INADVERTENTLY DISSEMINATED IN THE PUBLIC DOMAIN/ONLINE SINCE 12/2018 WITHOUT A DISCLAIMER. DISCLAIMER HAS BEEN ADDED – "THIS INFORMATION IS DISTRIBUTED SOLELY FOR THE PURPOSE OF PEER REVIEW UNDER APPLICABLE INFORMATION QUALITY GUIDELINES. IT HAS NOT BEEN FORMALLY DISSEMINATED BY BSEE. IT DOES NOT REPRESENT AND SHOULD NOT BE CONSTRUED TO REPRESENT ANY AGENCY DETERMINATION OR POLICY."

the several steps of model verification, analytical equations were used to validate the simulation results to improve reliability of the study.

1.5. Scope of Work

The scope of work for the seal assembly and cement models are as follows:

Seal Assembly Model:

The seal assembly model was created based on a conventional liner hanger system in offshore shallow well designs. Specifically, the energization process has been modelled to mimic the setting of the sub-mudline liner hanger. The elastomer component of the seal assembly is the focus of this study. The components such as slips and compression plates have been modelled as boundary conditions. Dimensions and material properties of liner and casing components were kept constant throughout the study.

Since the focus is on offshore shallow well designs, the effect of thermal stresses on sealability is not important and has not been examined. The only effect of temperature that was considered is from the material properties of seals exposed to various gases at high temperatures. For this study, four types of elastomer material were investigated – NBR (Nitrile Butadiene Rubber), EPDM (Ethylene Propylene Diene Monomer), VITON (a synthetic Flouropolymer elastomer), and PTFE (Polytetrafluoroethylen). The elastic modulus of each material was measured and used in the simulation. For all four materials, the elastic modulus was measured after exposure to CH_4, CO_2, H_2S, and mixture of all three gas for 1 day and 7 days at 120°F and 180°F. The data were used in the simulation to examine the resultant effect on sealability. Poisson's ratio of each elastomer was not measured since all elastomer materials typically have a value of 0.49. Nonetheless, the value of Poisson's ratio was varied for each elastomer during simulation to understand the potential effect on sealability.

Besides material properties and failure, the effect of seal dimensions was also examined. Additionally, several operational failure scenarios like insufficient setting load for seal energization, improper centralization, failure in compression plate or slips, wear or erosion of seal element etc. were evaluated for potential effect on sealability.

Cement Model:

The effect of temperature variation i.e. thermal stresses on cement has not been examined since the focus is on shallow well designs. The only loads considered are change in wellbore pressure and change in annulus pressure acting on top of the cement. Dimensions and material properties of liner and casing components were kept constant throughout the study. The focus is on liner overlap therefore, the cement sheath has been modelled only between the liner overlap and casing. Effect of the cement sheath against the formation has not been evaluated.

In the parametric analysis, the effect of seven parameters have been examined – Young's modulus, Poisson's ratio, wellbore pressure, annulus pressure, cement sheath height, cement radial width, and annular fit. The effect of these parameters was examined for three types of cement systems – ductile cement, brittle cement, and cement with moderate Young's modulus and

THIS REPORT WAS INADVERTENTLY DISSEMINATED IN THE PUBLIC DOMAIN/ONLINE SINCE 12/2018 WITHOUT A DISCLAIMER. DISCLAIMER HAS BEEN ADDED – "THIS INFORMATION IS DISTRIBUTED SOLELY FOR THE PURPOSE OF PEER REVIEW UNDER APPLICABLE INFORMATION QUALITY GUIDELINES. IT HAS NOT BEEN FORMALLY DISSEMINATED BY BSEE. IT DOES NOT REPRESENT AND SHOULD NOT BE CONSTRUED TO REPRESENT ANY AGENCY DETERMINATION OR POLICY."

Poisson's ratio. The outcome variables from the simulations are – radial stress, hoop stress, and maximum shear stress developed in cement.

2. LITERATURE REVIEW

2.1. Seal Assembly

2.1.1. Modes of Failure

Below is a summarized list of the most common modes of failure in liner hanger sealing assembly:

- Failure to set or energize the sealing element – often because of the inability to apply desired weight.
- Centralization issues e.g. non-uniform energization (Williford and Smith 2007).
- Faulty equipment or hanger components such as slips or cones.
- Abrasive wear of the seal element.
- Non-uniform pressure distribution can lead to shear and tensile stresses which causes elastomer deformation and possible rupture (Wang et al. 2017). For example, shearing of elastomer seal across an extrusion gap.
- Temperature and chemical degradation.
- Dynamic fatigue under pressure cycles.
- Compression load catastrophic failures.
- Explosive decompression/gasification.

Potential leakage paths through the liner hanger assembly are graphically presented in Figure 2.1. Such failures not only reduce the effectiveness of the applications for which the liners are intended, but they also increase well costs because of the remedial operations that must be undertaken. Furthermore, if such failures go undetected then it can greatly compromise the well's process safety, resulting in loss of well control with greater environmental, safety, and business consequences.

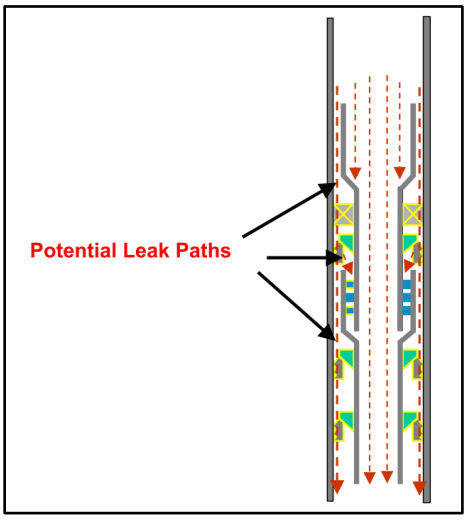

Figure 2.1: Potential leak paths in a liner hanger or liner top packer assembly (Lohoefer et al. 2000)

THIS REPORT WAS INADVERTENTLY DISSEMINATED IN THE PUBLIC DOMAIN/ONLINE SINCE 12/2018 WITHOUT A DISCLAIMER. DISCLAIMER HAS BEEN ADDED – "THIS INFORMATION IS DISTRIBUTED SOLELY FOR THE PURPOSE OF PEER REVIEW UNDER APPLICABLE INFORMATION QUALITY GUIDELINES. IT HAS NOT BEEN FORMALLY DISSEMINATED BY BSEE. IT DOES NOT REPRESENT AND SHOULD NOT BE CONSTRUED TO REPRESENT ANY AGENCY DETERMINATION OR POLICY."

2.1.2. Current Industry Standards

Currently, the industry relies on standards developed for packer equipment - ISO 14310:2008E and API Specification 11D1. They provide guidelines for both manufacturers and end users in the selection, manufacture, design, and laboratory testing of the many types of packers available in today's market.

ISO 14310/API 11D1 for Packer Equipment

These standards establish a minimum set of parameters with which the manufacturer must comply. The International Standard is structured with the requirements for both quality control and design verification in tiered rankings. There are three grades or levels established for quality control and six grades (plus one special grade) for design verification.

The quality standards range from grade Q3 to Q1, with grade Q3 carrying the minimum requirements and Q1 outlining the highest level of inspection and manufacturing verification procedures. Provisions are also established to allow the end user to modify the quality plans to meet the specific application by including additional needs as supplement requirements.

The standard design-validation grades range from V6 to V1. V6 is the lowest grade and V1 represents the highest level of testing. A special grade (V0) was included to meet special acceptance criteria requirements. These six standard validation grades are summarized as follows:

- V6: Supplier/manufacturer-defined
- V5: Liquid test
- V4: Liquid test + axial loads
- V3: Liquid test + axial loads + temperature cycling
- V2: Gas test + axial loads
- V1: Gas test + axial loads + temperature cycling
- Special validation grade:
- V0: Gas test + axial loads + temperature cycling + special acceptance criteria (V1 + zero bubble acceptance criterion)

API 19LH for Liner Hanger

API is currently drafting a standard for liner hanger equipment – API 19LH. This specification will provide requirements for conventional and expandable liner systems including liner hangers, liner packers, liner hanger packers, tieback/polished bore receptacles, seal assemblies, setting adaptors/sleeves, and running/setting tools etc. This specification will also include minimum requirements for the functional specification and technical specification, including design, design verification and validation, materials, quality control, documentation and data control, and repair, shipment, and storage of equipment. The products covered by this specification will be restricted only to applications within a conduit. Installation and field maintenance are outside the scope of this specification.

THIS REPORT WAS INADVERTENTLY DISSEMINATED IN THE PUBLIC DOMAIN/ONLINE SINCE 12/2018 WITHOUT A DISCLAIMER. DISCLAIMER HAS BEEN ADDED – "THIS INFORMATION IS DISTRIBUTED SOLELY FOR THE PURPOSE OF PEER REVIEW UNDER APPLICABLE INFORMATION QUALITY GUIDELINES. IT HAS NOT BEEN FORMALLY DISSEMINATED BY BSEE. IT DOES NOT REPRESENT AND SHOULD NOT BE CONSTRUED TO REPRESENT ANY AGENCY DETERMINATION OR POLICY."

2.1.3. Modelling Studies

Even though conventional liner-hanger assemblies have had frequent sealability failure issues, no dedicated study is available in the public domain that is focused on assessing sealability of elastomer element in conventional liner hangers. However, there are few modelling studies available in the literature that are focused on expandable liner hanger and packer applications. These can provide some useful information for conventional seal assemblies.

Berger (2003) designed, built, and tested a retrievable 7 ¾-in. packer element for high pressure high temperature environment. The objective of the study was to examine various backup systems that provide support during energization. Different systems such as the carbon steel foldback ring, mesh rings, garter springs, and combination of these were evaluated at different temperatures and differential pressures. Sealing performance was tested by conducting ISO 14310 standard liquid and gas tests. A FEA study was also conducted to support the experimental work.

Feng et al. (2010) conducted two-dimensional finite element analysis on packer consisting of two elastomer elements separated by a metal ring. They examined the contact pressure in both seals for various setting loads and observed a relationship that was practically linear (Figure 2.2). The seal on the compression side (upper side in this case) had consistently higher contact pressure than the lower seal.

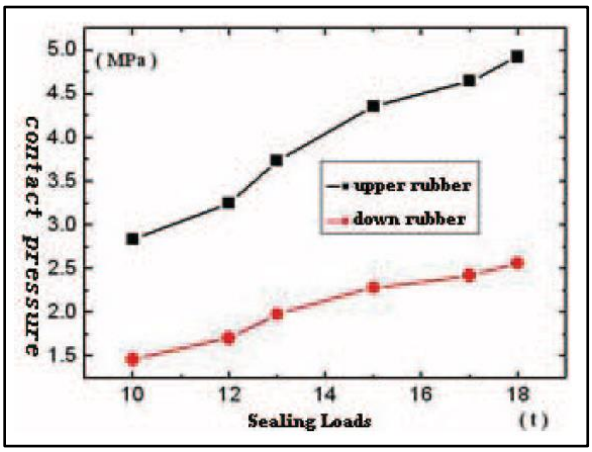

Figure 2.2: Contact pressure as a function of setting load (Feng et al. 2010)

Alzebdeh et al. (2010) conducted finite element simulation of the compression of elastomeric seals in an open hole expandable type liner hanger (Figure 2.3). They modelled the formation in three different forms, as a rigid body, an elastic, and an elastic-plastic material. Two different boundary conditions (fixed-free and fixed-fixed) were employed depending on prevailing practices of oil operators in such applications. The effect of seal length and thickness, compression ratio, and shear resistance at seal-formation interface on the contact pressure were determined. They observed that the rigid formation provides the highest contact pressure, and that a thicker seal with a larger compression ratio yields higher contact stress (Figure 2.4). Furthermore, they observed that contact pressure decreases with increase in seal length up to 200 mm and pressure

THIS REPORT WAS INADVERTENTLY DISSEMINATED IN THE PUBLIC DOMAIN/ONLINE SINCE 12/2018 WITHOUT A DISCLAIMER. DISCLAIMER HAS BEEN ADDED – "THIS INFORMATION IS DISTRIBUTED SOLELY FOR THE PURPOSE OF PEER REVIEW UNDER APPLICABLE INFORMATION QUALITY GUIDELINES. IT HAS NOT BEEN FORMALLY DISSEMINATED BY BSEE. IT DOES NOT REPRESENT AND SHOULD NOT BE CONSTRUED TO REPRESENT ANY AGENCY DETERMINATION OR POLICY."

remains practically constant thereafter. The effect of tubular end conditions was determined to be negligible. No theoretical or experimental validation was provided for the simulation results.

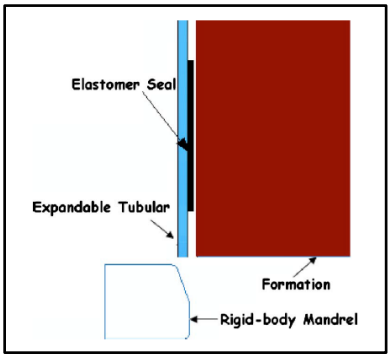

Figure 2.3: 2D axisymmetric finite element model of expandable liner hanger seal (Alzebdeh et al. 2010)

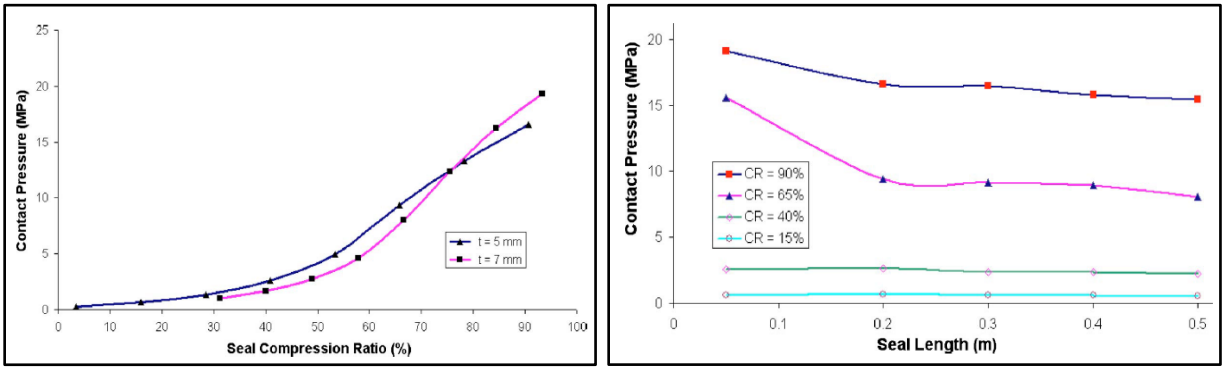

Figure 2.4: Effect of seal compression, seal thickness, and seal length on contact pressure (Alzebdeh et al. 2010)

Guo et al. (2011) used FEA to study a specific design of packer consisting of rubber tube, cone, central pipe, expansion sleeve, and casing pipe. They used nonlinear material properties for the elastomer element and presented contact pressure variation as a function of applied load at different seal thickness. No validation for the FEA results was provided.

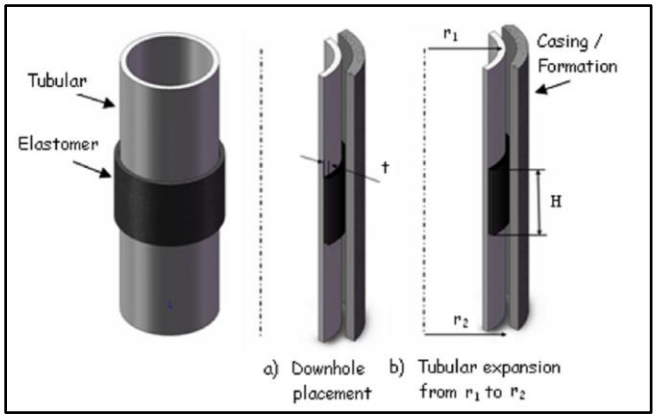

Figure 2.5: Elastomer seal radially confined between metal tubes with fluid pressures in axial direction (Al-Hiddabi et al. 2015)

THIS REPORT WAS INADVERTENTLY DISSEMINATED IN THE PUBLIC DOMAIN/ONLINE SINCE 12/2018 WITHOUT A DISCLAIMER. DISCLAIMER HAS BEEN ADDED – "THIS INFORMATION IS DISTRIBUTED SOLELY FOR THE PURPOSE OF PEER REVIEW UNDER APPLICABLE INFORMATION QUALITY GUIDELINES. IT HAS NOT BEEN FORMALLY DISSEMINATED BY BSEE. IT DOES NOT REPRESENT AND SHOULD NOT BE CONSTRUED TO REPRESENT ANY AGENCY DETERMINATION OR POLICY."

Al-Kharusi et al. (2011) conducted a theoretical analysis on compression of elastomer seals in expandable tubular or liner hangers. They developed an analytical model for elastomer seal assuming linear elastic material property. The model was later refined and presented by Al-Hiddabi et al. (2015). This new model is based on elastomer seal that is radially confined between metal tubes with fluid pressures in axial direction (see Figure 2.5). Originally developed for solid expandable tubular, this model can predict contact pressure along the contact length as a function of seal compression ratio, fluid pressures, and material properties. Besides developing the model, Al-Hiddabi et al. (2015) also performed parametric analysis using the model and investigated the effect of seal thickness, seal length, and compression ratio on contact pressure (Figure 2.6).

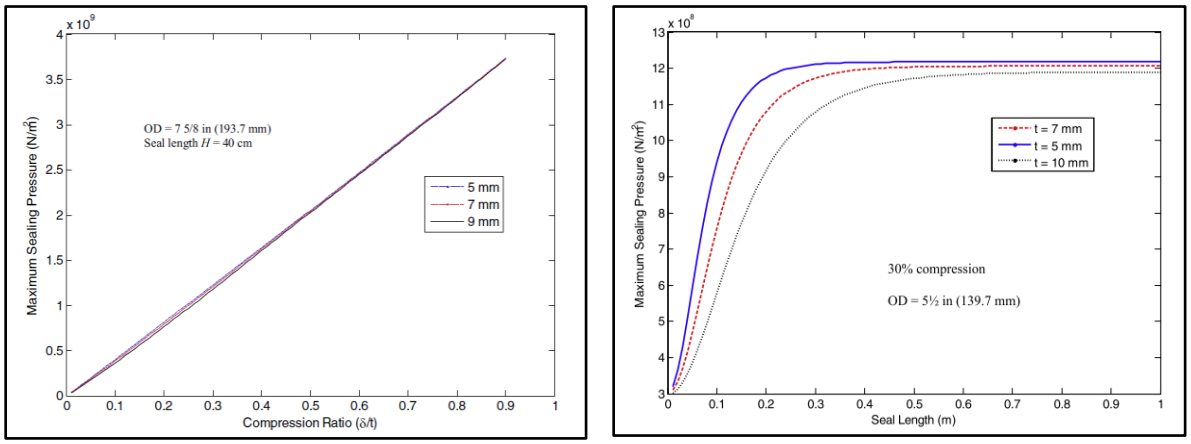

Figure 2.6: Maximum contact pressure as a function of compression ratio and seal length for varying seal thickness for a 7 5/8-in. expandable tubular (Al-Hiddabi et al. 2015)

Guo et al. (2011) performed FEA on packer and studied the maximum stress developed in a casing as a function of the normal contact stiffness factor used in contact formulation.

Lin (2013) conducted finite element structural analysis of slip element in packers. They examined stresses in slip element at different applied loads or setting pressures and observed almost linear correlation (Figure 2.7). They also studied the effect of spacing between the slip tooth on developed maximum stress in slip element. They performed a physical failure test on a slip element and confirmed its consistency with the simulation results.

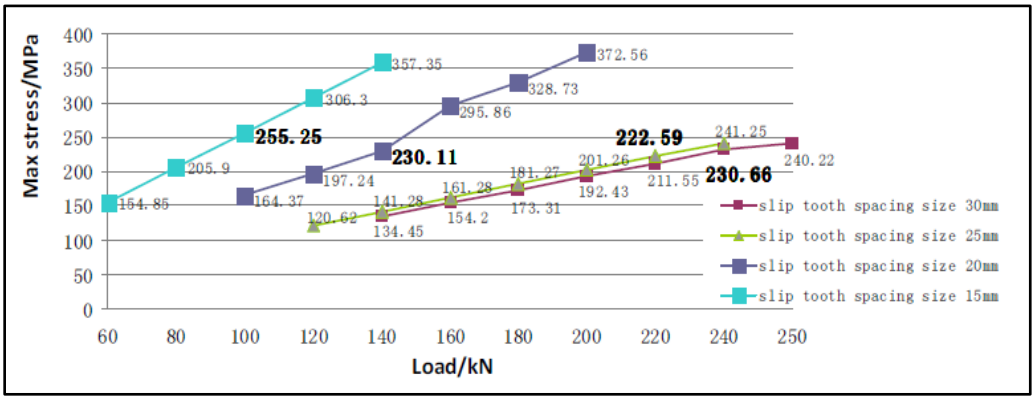

Figure 2.7: Maximum stress in slip element as a function of applied load (Lin 2013)

THIS REPORT WAS INADVERTENTLY DISSEMINATED IN THE PUBLIC DOMAIN/ONLINE SINCE 12/2018 WITHOUT A DISCLAIMER. DISCLAIMER HAS BEEN ADDED – "THIS INFORMATION IS DISTRIBUTED SOLELY FOR THE PURPOSE OF PEER REVIEW UNDER APPLICABLE INFORMATION QUALITY GUIDELINES. IT HAS NOT BEEN FORMALLY DISSEMINATED BY BSEE. IT DOES NOT REPRESENT AND SHOULD NOT BE CONSTRUED TO REPRESENT ANY AGENCY DETERMINATION OR POLICY."

Ma et al. (2014a) examined swellable elastomer packer element using two-dimensional finite element model with non-linear elastomer material properties. They modelled swellability by means of interference between seal thickness and annular space between casing and formation. Under the differential pressure of 20 MPa across the packer, they studied the maximum contact pressure for different seal length, interference thickness, and different formation. They evaluated the sealing performance in terms of sealing safety factors (Z) (see Figure 2.8) which is calculated as contact pressure divided by packer differential pressure. No validation for simulation results is provided. They observed that upper seal element consistently provides higher contact pressures for the same applied load.

In a similar study with two elastomer seal elements, Ma et al. (2014b), investigated effect of different friction coefficient and concluded that contact pressure difference between upper and lower seal element can be manipulated by adjusting friction coefficient.

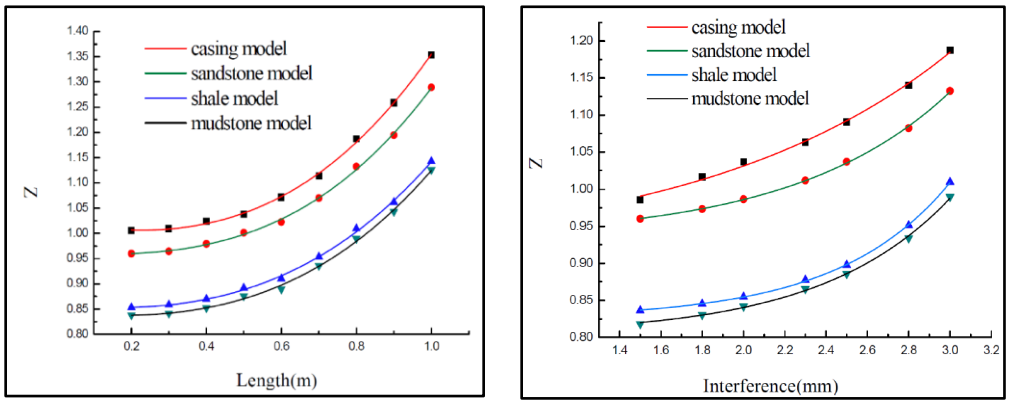

Figure 2.8: Sealing safety factor (contact pressure / operating fluid pressure) stress in slip element as a function of applied (Ma et al. 2014a)

Wang et al. (2015) performed structural FEA of inner tube and setting sleeve of a packer equipment to identify zones of high stress concentration for design optimization. Validation of simulation results was not provided.

Li et al. (2015) performed two dimensional FEA on rubber sealing ring for rotary liner hanger bearing. They studied maximum contact stress as a function of setting pressure at different temperature.

Wang et al. (2017) investigated extrusion, sliding, and rupture type failure modes of elastomer seals for packer application (Figure 2.9). The authors fabricated seals of various parameters in transparent chambers on a desktop, and watched the seals extrude, slide, rupture, and leak. They developed an analytical model that can predict the pressure-extrusion curves using material parameters (elastic modulus, sliding stress, and fracture energy) and geometric parameters (thickness, length, and pre-compression). They also performed experimental validation (Liu et al. 2014; Wang et al. 2017).

THIS REPORT WAS INADVERTENTLY DISSEMINATED IN THE PUBLIC DOMAIN/ONLINE SINCE 12/2018 WITHOUT A DISCLAIMER. DISCLAIMER HAS BEEN ADDED – "THIS INFORMATION IS DISTRIBUTED SOLELY FOR THE PURPOSE OF PEER REVIEW UNDER APPLICABLE INFORMATION QUALITY GUIDELINES. IT HAS NOT BEEN FORMALLY DISSEMINATED BY BSEE. IT DOES NOT REPRESENT AND SHOULD NOT BE CONSTRUED TO REPRESENT ANY AGENCY DETERMINATION OR POLICY."

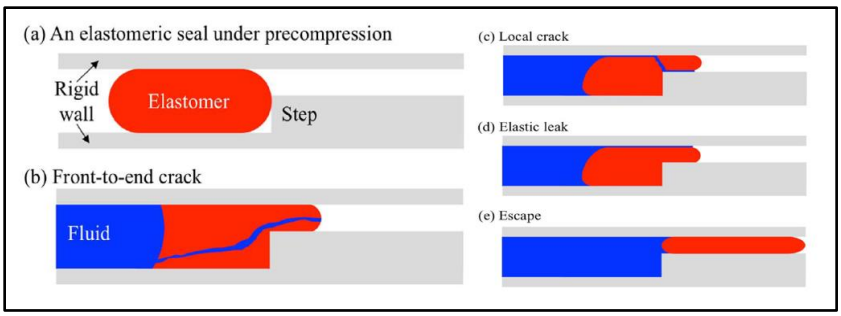

Figure 2.9: Modes of failure of an elastomeric seal investigated (Wang et al. 2017)

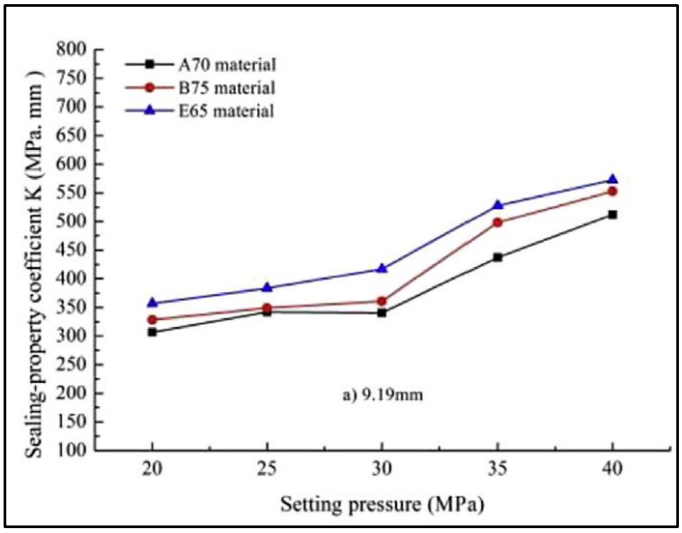

Figure 2.10:Sealing performance of elastomer packer element as a function of setting pressure (Hu et al. 2017)

Hu et al. (2017) studied the effect of elastomer material property on sealing performance of compression packer. They employed three NBR elastomers with different chemical formulation, measured uni-axial tension and compression data, and performed a 3-D finite element analysis with a non-linear material property model. They measured sealing performance in terms of a coefficient K which can be obtained by multiplying the effective contact stress to the effective contact length. They observed that sealing performance increases almost linearly with increase in setting pressure (Figure 2.10). No experimental or analytical validation was provided for contact stress.

Overall, there have been few good studies particularly related to expandable liner hanger and packers that provide useful information. It should be noted that majority of modelling studies discussed were not validated. Still, some of the information from these studies can be extrapolated to be applicable to elastomer seal assembly in conventional liner hanger. These conventional assemblies such as sub mudline liner hanger (Figure 1.1**)** that depend on weight application for seal energization are still widely used. Considering various challenges associated with seal assemblies, there is still a need for a comprehensive modelling as well as experimental study like the one presented in this work that is focused on conventional seal assemblies.

THIS REPORT WAS INADVERTENTLY DISSEMINATED IN THE PUBLIC DOMAIN/ONLINE SINCE 12/2018 WITHOUT A DISCLAIMER. DISCLAIMER HAS BEEN ADDED – "THIS INFORMATION IS DISTRIBUTED SOLELY FOR THE PURPOSE OF PEER REVIEW UNDER APPLICABLE INFORMATION QUALITY GUIDELINES. IT HAS NOT BEEN FORMALLY DISSEMINATED BY BSEE. IT DOES NOT REPRESENT AND SHOULD NOT BE CONSTRUED TO REPRESENT ANY AGENCY DETERMINATION OR POLICY."

2.2. Cement

2.2.1. Stresses in Cement

The liner, set cement, and casing can be considered as a composite hollow cylindrical system. When the set cement is subjected to internal and/or external pressures, it is in the state of tri-axial stresses. As shown in Figure 2.11, the three mutually perpendicular stresses are – radial (σ_r), axial or longitudinal (σ_z), and circumferential or hoop stresses (σ_θ). The radial stress always acts away from or toward the axis of cylinder while the hoop stress acts along the circumference of the cylinder. The axial stress is parallel to the axis of cylinder.

There are two theories for calculating stresses in a hollow cylinder: thin-walled and thick-walled cylinder theory. Thin wall theory assumes that the radial and axial stresses do not vary across the radial width (t) of the cylinder. It also assumes that the magnitude of radial stress is small compared to the other two principle stresses. For a thin-walled cylinder of mean radius r and width w, the hoop and axial stresses under internal pressure P are calculated by:

Hoop Stress: $\sigma_r = \frac{Pr}{w}$ ……………………………………………………………….. (1)

Axial Stress: $\sigma_\theta = \frac{Pr}{2w}$ ……………………...…………………………………………….. (2)

The thin-walled assumption requires that the ratio of wall thickness to inside diameter of the cylinder is less than 1/20 (Hearn 1997). Therefore, this theory is usually not applicable for casing and cement sheath for shallow well completion designs where casings and cement sheath are relatively thicker.

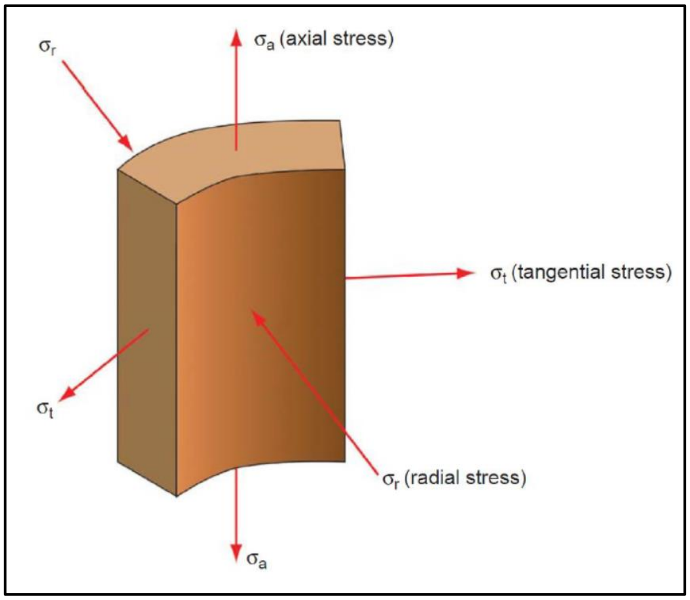

Figure 2.11: Graphical illustration of three principle stresses in set cement – radial, hoop, and axial stresses (Bellarby 2009)

THIS REPORT WAS INADVERTENTLY DISSEMINATED IN THE PUBLIC DOMAIN/ONLINE SINCE 12/2018 WITHOUT A DISCLAIMER. DISCLAIMER HAS BEEN ADDED – "THIS INFORMATION IS DISTRIBUTED SOLELY FOR THE PURPOSE OF PEER REVIEW UNDER APPLICABLE INFORMATION QUALITY GUIDELINES. IT HAS NOT BEEN FORMALLY DISSEMINATED BY BSEE. IT DOES NOT REPRESENT AND SHOULD NOT BE CONSTRUED TO REPRESENT ANY AGENCY DETERMINATION OR POLICY."

For calculating stresses in the thick cement sheath, Lamé's theory is used. According to this theory, radial and hoop stresses vary with the radius as follows:

$$\sigma_r = A - \frac{B}{r^2} \quad \text{..... (3)}$$

$$\sigma_\theta = A + \frac{B}{r^2} \quad \text{..... (4)}$$

Where r is the radial location within the cylinder and A and B are constants dependent on the pressure boundary conditions. The equations can be easily modified for application in liner-cement-casing systems. For the system shown in Figure 2.12**,** the radial and hoop stresses at a particular radius r within the cement can be calculated using the following equations:

$$\sigma_{r-cement} = \frac{b^2 P_{c1} - c^2 P_{c2}}{(c^2 - b^2)} - \frac{(P_{c1} - P_{c2}) b^2 c^2}{(c^2 - b^2) r^2} \quad \text{..... (5)}$$

$$\sigma_{\theta-cement} = \frac{b^2 P_{c1} - c^2 P_{c2}}{(c^2 - b^2)} + \frac{(P_{c1} - P_{c2}) b^2 c^2}{(c^2 - b^2) r^2} \quad \text{..... (6)}$$

Where P_{c1} and P_{c2} are contact pressures at the liner-cement and cement-casing interfaces respectively as shown in Figure 2.12; and b and c are the inner and outer radius of cement sheath respectively. Similar equations can be written for liner and casing components of the system. The radial and hoop stress calculations require contact pressure values. The calculation of P_{c1} and P_{c2} using material properties and boundary conditions is provided in Appendix **A**. The equations will be used later in this work to validate results from the FEA model.

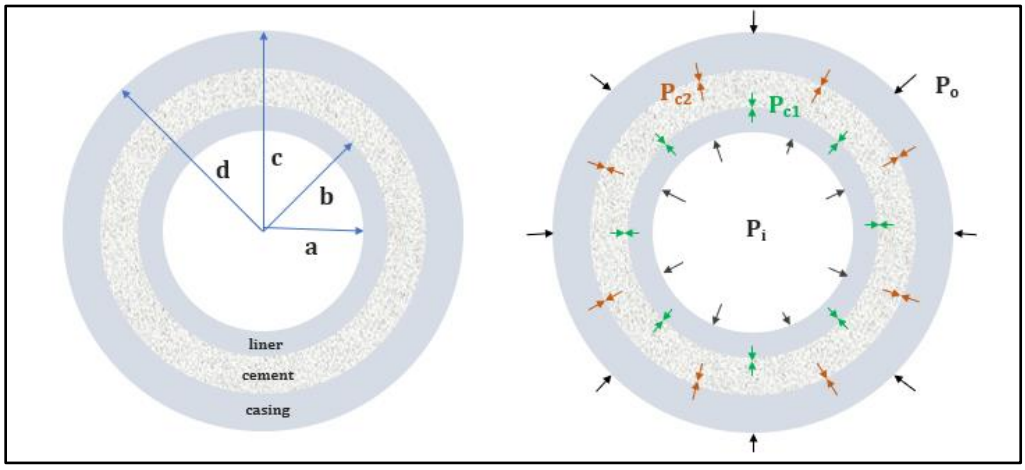

Figure 2.12: Schematic of liner-cement-casing system for analytical equations

2.2.2. Modes of Failure

There are three primary modes of failure for cement – radial debonding, radial cracking, and shear failure (Bustgaard and Nesheim 2016). These failure modes are graphically illustrated in Figure 2.13.

THIS REPORT WAS INADVERTENTLY DISSEMINATED IN THE PUBLIC DOMAIN/ONLINE SINCE 12/2018 WITHOUT A DISCLAIMER. DISCLAIMER HAS BEEN ADDED – "THIS INFORMATION IS DISTRIBUTED SOLELY FOR THE PURPOSE OF PEER REVIEW UNDER APPLICABLE INFORMATION QUALITY GUIDELINES. IT HAS NOT BEEN FORMALLY DISSEMINATED BY BSEE. IT DOES NOT REPRESENT AND SHOULD NOT BE CONSTRUED TO REPRESENT ANY AGENCY DETERMINATION OR POLICY."

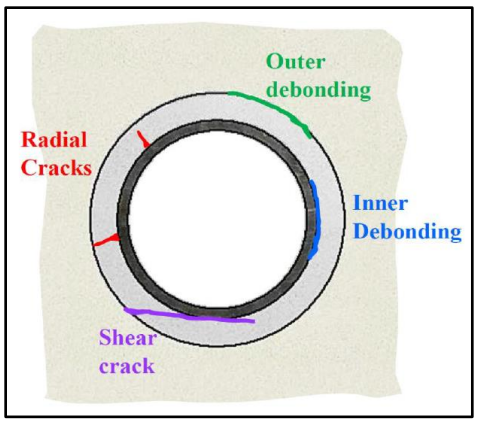

Figure 2.13: Primary modes of failure in a cement sheath (De Andrade and Sangesland 2016)

Debonding depends on the magnitude and direction of radial stress at the interface between cement-formation or cement-casing. The primary reason for development of radial stress is change in internal or wellbore pressure. For example, events such as casing pressure tests, formation integrity tests, increased mud weight for subsequent drilling, perforation or stimulation operation, etc. can lead to increase in wellbore pressure. On the other hand, fluid loss or gas kick while drilling or production of reservoir fluids can reduce the wellbore pressure. Debonding occurs when the magnitude of radial stress exceeds the limiting strength of the cement (Teodoriu et al. 2008).

$$\sigma_r \geq T_0 \quad \text{(Tension)} \qquad (7)$$

$$|\sigma_r| \geq C_0 \quad \text{(Compression)} \qquad (8)$$

where T_0 and C_0 are uniaxial tensile and compressive strengths of cement respectively. In the case of compressional radial stress, the failure is more like stress crushing than debonding (Khandka 2007). The compressive strength of cements is typically higher than the tensile strength, often 10 times more (De Andrade and Sangesland 2016). Therefore, cement is more likely to fail by radial debonding than stress crushing.

The second mode of failure is radial cracking which can occur when the hoop stress exceeds the tensile strength of cement:

$$\sigma_\theta \geq T_0 \quad \text{(Tension)} \qquad (9)$$

The hoop stress can either be tensile or compressive in nature depending on material properties and loading conditions. However, since tensile strength is usually a lower factor, radial cracking is the most likely mode of failure.

Shear failure is another mode of failure in a cement sheath. When the cement undergoes shear failure, it typically results in a complete failure of the sheath (Bustgaard and Nesheim 2016). The shear failure is primarily dependent on difference in magnitude between principle stresses. According to Nelson and Guillot (2006), these effective stresses can rise because of various reasons such as rock subsidence, depletion of the reservoir, vibration from downhole pumps, or

THIS REPORT WAS INADVERTENTLY DISSEMINATED IN THE PUBLIC DOMAIN/ONLINE SINCE 12/2018 WITHOUT A DISCLAIMER. DISCLAIMER HAS BEEN ADDED – "THIS INFORMATION IS DISTRIBUTED SOLELY FOR THE PURPOSE OF PEER REVIEW UNDER APPLICABLE INFORMATION QUALITY GUIDELINES. IT HAS NOT BEEN FORMALLY DISSEMINATED BY BSEE. IT DOES NOT REPRESENT AND SHOULD NOT BE CONSTRUED TO REPRESENT ANY AGENCY DETERMINATION OR POLICY."

ongoing gas lift operations etc. There are several failure criteria for predicting shear failure. The simplest one, which requires minimum information is the Tresca criterion. It is based on a special case of Mohr's stress circle with internal friction angle being zero (Rahimi 2014). According to this criterion, shear failure occurs when the maximum shear stress value exceeds the cohesion of rock. Mathematically it is expressed as:

$$\tau_{max} \geq \varsigma \quad \ldots\ldots (10)$$

$$\tau_{max} = \frac{\sigma_1 - \sigma_3}{2} \quad \ldots\ldots (11)$$

$$\varsigma \approx \frac{C_0}{2} \quad \ldots\ldots (12)$$

where τ_{max} is maximum shear stress, σ_1 is maximum principle stress, σ_3 is minimum principle stress, ς is cohesion or intrinsic shear strength of cement, and C_0 is uniaxial compressive strength of cement.

The failure criteria discussed above are basic - requiring only uniaxial strengths as input parameters. However, they are widely used because of their simplicity and conservative nature. There are several progressively more complex or sophisticated failure criteria developed by researchers, appropriate for different types of cements/rocks and failure conditions. Some of the popular ones are Mohr-Coulomb, Mogi-Coulomb, Von Mises, etc. A comparative review of various failure criteria for rocks/cement was provided by Rahimi (2014).

At this stage there is very little knowledge about cement shear strength. Teodoriu et al. (2018) have shown that cement shear strength is about twice as big than its interfacial shear bond strength.

2.2.3. Current Industry Standards

Current API and ISO standards relevant to cement are summarized as follows –

- *API standard 65 – Part 2* provides best practices for cementing operation. It also contains brief discussion on factors affecting the success of a cement job and post-job evaluation.
- *API RP 10B-2 or ISO 10426-2* contains guidelines, procedures, and information on equipment for testing cement slurries and related materials in laboratory under simulated well conditions.
- *API RP 10B – 4, 5, and 6 or ISO 10426-4, 5 and 6* are for testing foamed cement, shrinkage/expansion of cement slurries, and static gel strength respectively.
- *API SPEC 10A or ISO 10426:2009* provides specific chemical and physical properties requirement for all 8 classes of cement
- API technical reports TR 10TR1-4 contains technical information, principles, and results of research into cement sheath evaluation by logging, cement shrinkage and expansion, temperatures in API well simulation test schedule, and selection of centralizers respectively.

THIS REPORT WAS INADVERTENTLY DISSEMINATED IN THE PUBLIC DOMAIN/ONLINE SINCE 12/2018 WITHOUT A DISCLAIMER. DISCLAIMER HAS BEEN ADDED – "THIS INFORMATION IS DISTRIBUTED SOLELY FOR THE PURPOSE OF PEER REVIEW UNDER APPLICABLE INFORMATION QUALITY GUIDELINES. IT HAS NOT BEEN FORMALLY DISSEMINATED BY BSEE. IT DOES NOT REPRESENT AND SHOULD NOT BE CONSTRUED TO REPRESENT ANY AGENCY DETERMINATION OR POLICY."

Majority of the guidelines, recommendations, or procedures provided in the above standards are primarily focused on cement slurries – their material properties, laboratory testing, consideration during field operation, etc. The current state of regulations or guidelines need improvement in several issues such as - designing cement for shallow depth wells with potential for gas migration, adequacy of pressure test and guidelines for evaluating "fitness for service" of various types of cement systems. They also lack sufficient discussion on selection of appropriate mechanical properties for different conditions, performance curves or response of set cement under various loading conditions, risk assessment of various failure scenarios etc.

2.2.4. Modelling Studies

With the advent of super computing and commercially available software, it has become progressively easier to predict mechanical stresses in cement under various loading conditions. Based on an exhaustive literature review, this section provides an overview of some important cement modelling studies conducted over the past two decades.

Bosma et al. (1999) was one of the earliest studies to conduct basic finite element analysis on a two-dimensional model of cement and formation. The authors examined cement failure at different internal pressures and Young's modulus.

Ravi et al. (2002) analyzed two-dimensional casing-cement-formation systems under different stages of well construction such as drilling, pumping cement, cement volume shrinkage, and hydraulic fracturing.

Khandka (2007) performed a review on fluid leakage behind casing and discussed gas migration mechanisms. The document provides a theoretical description of various factors affecting gas leakage such as volume shrinkage, cyclic pressures, mud buildup, temperature variation, and the bonding between cement and pipe. Using thin-walled approximation for cylinders, the author performed analytical calculation of stresses in cement sheath behind a 9 $^{7}/_{8}$-in. production casing at different wellbore pressures and temperature changes.

Teodoriu et al. (2008) investigated cement failure at HPHT conditions under static and cyclic loading. They used analytically validated a two-dimensional finite element model of casing-cement-formation system to understand failure under cyclic load for different cement and formation properties. They also conducted an experimental investigation on a small-scale cell having a 2-½ in. ID steel pipe cemented between two different sizes of PVC pipes acting as the formations. They used two different class H cement samples and studied failure under cyclic compressive loads of 15,000 psi. They noted that ductile cement performs better under cyclic loading and that high formation pressures help to counteract high internal pressures and improves the performance of the cement sheath.

Bois et al. (2011) presented a comprehensive theoretical mechanistic analysis of micro-annulus formation considering various factors such as cement volume change, heat production

THIS REPORT WAS INADVERTENTLY DISSEMINATED IN THE PUBLIC DOMAIN/ONLINE SINCE 12/2018 WITHOUT A DISCLAIMER. DISCLAIMER HAS BEEN ADDED – "THIS INFORMATION IS DISTRIBUTED SOLELY FOR THE PURPOSE OF PEER REVIEW UNDER APPLICABLE INFORMATION QUALITY GUIDELINES. IT HAS NOT BEEN FORMALLY DISSEMINATED BY BSEE. IT DOES NOT REPRESENT AND SHOULD NOT BE CONSTRUED TO REPRESENT ANY AGENCY DETERMINATION OR POLICY."

during hydration, thermos-poro-elasto-plastic behavior of formation, pressure loads, and the initial stress condition of formation.

Nygaard et al. (2014) examined the effect of dynamic loading on wellbore leakage for CO_2 sequestration wells. They conducted multi-stage simulations (drilling, cementing, casing processes followed by application of dynamic mechanical and thermal loads) and investigated failure near casing-cement and cement-formation interface for different Young's modulus and Poisson's ratio.

Arias (2013) conducted a finite element analysis to examine well cementing in HTHP conditions. A three-dimension model of casing-cement-formation with elastic-plastic material properties was used for the study. The main objective of this FEA was to investigate plastic deformations in set cement and formation after well completion, hydraulic fracturing jobs, and well production. The methodology was to examine the sensitivity of total plastic strain in cement to Young's modulus, Poisson's ratio, and different combinations of cement-formation. The author also performed laboratory measurements of material properties for different cement recipes with various additives and examined their suitability for specific applications in three Colombian oil fields. The study showed that hydraulic fracturing jobs are the main cause of plastic deformation in set cements during the life of a well. The plastic deformation was observed to be more in hard rock relative to soft rock.

Chu et al. (2015) presented a theoretical model based on Mohr-Coulomb yield criterion for plastic deformation to estimate the size of the micro-annulus, considering the interaction among casing, cement sheath, and formation. They also showed agreement between model predictions and experimental observations.

Feng et al. (2016) used finite element analysis to simulate debonding and fracture propagation at cement interfaces. The model was used to quantify the length, width, and circumferential coverage of fractures. They reported the dependence of debonding fracture width and circumferential coverage on in-situ stress conditions, initial cracks around the casing shoe, and cement and formation properties.

De Andrade and Sangesland (2016) conducted a finite element study with the aim of assessing the relevance of casing-cement-formation material properties, geometric parameters, and characteristic of well-loading events. They emphasized more on thermal loads and also performed a transient analysis on well heating/cooling to assess its effect on the cement sheath.

Bustgaard and Nesheim (2016) examined failure of cement between a 9 5/8-in. production casing and formation at about 10,000 ft. They used axisymmetric thick-walled cylinder theory and performed plane strain analysis to calculate radial, hoop, and axial stresses in cement. They incorporated equation of linear thermal expansion in the analytical equations to account for thermal stresses. They investigated cement failure in form of debonding, radial crack, and shear cracking and presented safety factors for a typical brittle cement system at different pressure and temperature changes. For the same load cases, they also studied for burst or collapse failure of

THIS REPORT WAS INADVERTENTLY DISSEMINATED IN THE PUBLIC DOMAIN/ONLINE SINCE 12/2018 WITHOUT A DISCLAIMER. DISCLAIMER HAS BEEN ADDED – "THIS INFORMATION IS DISTRIBUTED SOLELY FOR THE PURPOSE OF PEER REVIEW UNDER APPLICABLE INFORMATION QUALITY GUIDELINES. IT HAS NOT BEEN FORMALLY DISSEMINATED BY BSEE. IT DOES NOT REPRESENT AND SHOULD NOT BE CONSTRUED TO REPRESENT ANY AGENCY DETERMINATION OR POLICY."

casing to determine whether casing or cement sheath fails first. For the specific cases investigated, they did not observe any effect of Poisson's ratio and thermal expansion coefficient on cement failure. Interestingly, they observed potential failure in the cement system for pressure test load of 5800 psi.

Zhang et al. (2017) studied cement sheath integrity in underground gas storage wells. They analyzed casing-cement-rock as multi-layered cylinders using thermoelastic, elasto-plastic, and poro-elastic theory under cyclic loading and unloading. The analytical model was validated using finite element model simulations. They investigated the effects of temperature, pore pressure, far-field in-situ stresses, casing pressure, and cement material properties.

3. MODEL DESCRIPTION

This section discusses the process of setting up FEA models of seal assembly and cement. This includes descriptions of models' dimensions, material properties, boundary conditions, meshing, contact formulation, and model verification.

3.1. Seal Assembly Model

The schematic of the model is provided in Figure 3.1. This simplified geometry consists of a 18 in. surface liner, an elastomeric packer seal, and a 22 in. conductor casing. The diameter of each component is based on an actual well design of one of the wells with a well control incident (BSEE, 2014). To avoid end-effects, the overall length of the model was kept more than 8 times greater than the inner diameter. Considering the symmetrical nature of the model, only $^{1}/_{8}^{th}$ segment of the wellbore cross section has been modelled. This helped to minimize computational requirement without losing accuracy.

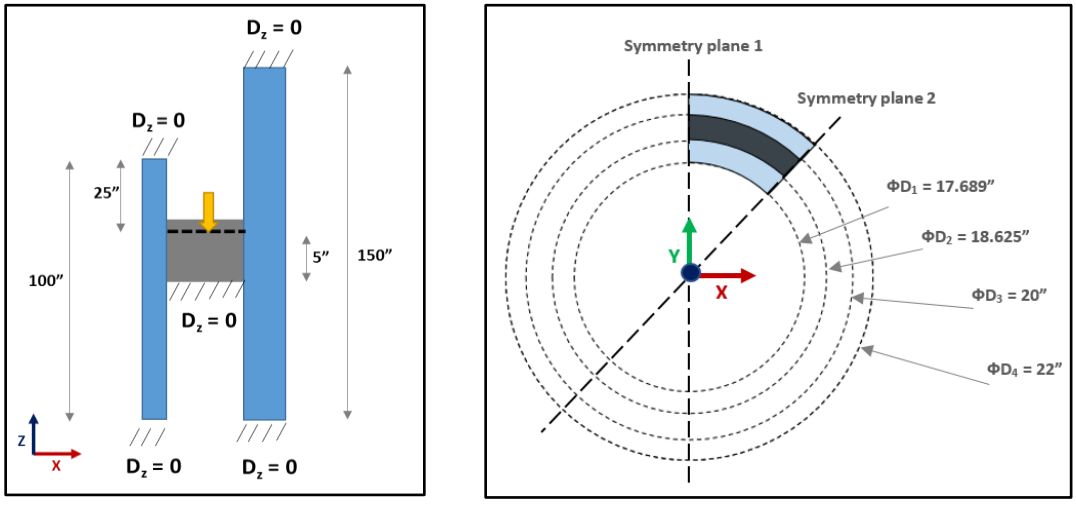

(a) (b)

Figure 3.1: Schematic of elastomer seal model (a) 2-D schematic in XZ plane. (b) top view of the model in XY plane

THIS REPORT WAS INADVERTENTLY DISSEMINATED IN THE PUBLIC DOMAIN/ONLINE SINCE 12/2018 WITHOUT A DISCLAIMER. DISCLAIMER HAS BEEN ADDED – "THIS INFORMATION IS DISTRIBUTED SOLELY FOR THE PURPOSE OF PEER REVIEW UNDER APPLICABLE INFORMATION QUALITY GUIDELINES. IT HAS NOT BEEN FORMALLY DISSEMINATED BY BSEE. IT DOES NOT REPRESENT AND SHOULD NOT BE CONSTRUED TO REPRESENT ANY AGENCY DETERMINATION OR POLICY."

3.1.1. Material Properties

The liner and casing components were modelled as isotropic linear elastic material and their material properties are provided in Table 3.1**.** The elastomer seals were also assumed to exhibit isotropic linear elastic behavior with low Elastic modulus and Poisson's ratio of 0.49 (Table 3.2). This assumption is valid for low shear strains as exhibited by the linear shear stress vs shear strain behavior (see Figure 3.2) observed during the uni-axial compression tests performed on four different types of elastomer materials. Moreover, the elastomer material used in packers or plug applications are often very stiff and do not exhibit high non-linear behavior. It is not uncommon to model them as linear elastic material (Bosma et al. 2000). Besides, linear elastic behavior is a conservative approach and is often used in design work. Modelling elastomer seal as hyper-elastic material would require model calibration with experimental data from few material properties tests such as uniaxial tension, uniaxial compression, biaxial tension etc. which would be beyond the scope of the study.

Table 3.1: Material properties used for casing and liner in the model

Property	P110 Liner	X80 Casing
Young's Modulus, psi	29 x 10^6 psi	29 x 10^6 psi
Poisson's ratio	0.3	0.3
Yield Strength, psi	110,000 psi	80,000 psi
Tensile Strength, psi	125,000 psi	90,000 psi

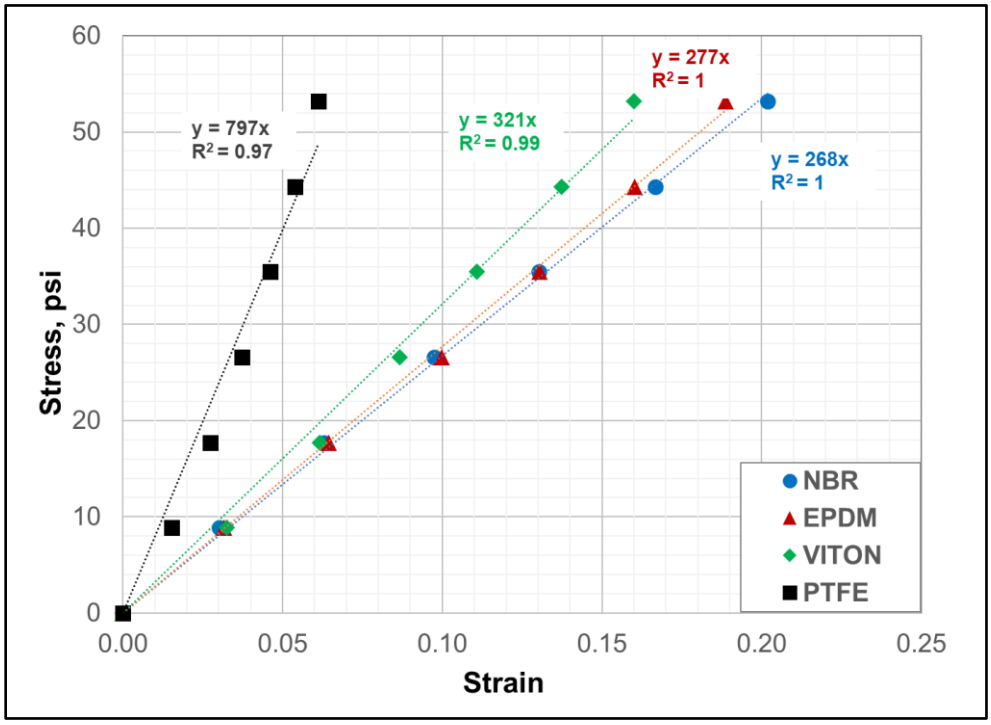

Figure 3.2: Uni-axial compression data for different elastomers

THIS REPORT WAS INADVERTENTLY DISSEMINATED IN THE PUBLIC DOMAIN/ONLINE SINCE 12/2018 WITHOUT A DISCLAIMER. DISCLAIMER HAS BEEN ADDED – "THIS INFORMATION IS DISTRIBUTED SOLELY FOR THE PURPOSE OF PEER REVIEW UNDER APPLICABLE INFORMATION QUALITY GUIDELINES. IT HAS NOT BEEN FORMALLY DISSEMINATED BY BSEE. IT DOES NOT REPRESENT AND SHOULD NOT BE CONSTRUED TO REPRESENT ANY AGENCY DETERMINATION OR POLICY."

3.1.2. Boundary Conditions

The top and bottom ends of liner and casing were restrained from any movement in z direction by assigning a zero displacement boundary condition. As shown in Figure 3.1, the bottom of the seal is fixed in the z (vertical) direction. To energize the seal, the top boundary of the seal is displaced in the negative z direction by a specified amount. Elastomer will be compressed and exert contact pressure on both liner and casing interfaces (see Figure 3.3**)**. This process is similar to how sub-mudline liner hanger seal assembly is set.

Table 3.2:Material properties used for seal element in the model

Elastomer	Elastic Modulus (E), psi	Poisson's Ratio (ν)
NBR	268	0.49
EPDM	277	0.49
VITON	321	0.49
PTFE	797	0.49

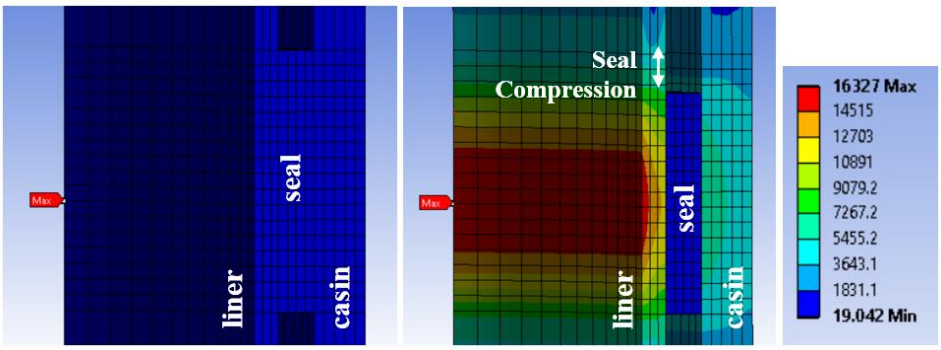

Figure 3.3: Equivalent (von-Mises) stress before (a) and after (b) the seal energization by displacement

There are two reasons for selecting a displacement boundary condition instead of specifying a compressive load condition to energize the seal. First, displacement boundary conditions tend to provide faster and more controlled numerical convergence. Second reason is that it is less susceptible to failure than the load type boundary conditions.

3.1.3. Mesh

All the bodies of the model were discretized into small elements using hexahedral meshing (see Figure 3.4). Hexahedral mesh was selected mainly because of its regular shape and near orthogonality of grids. From the physical point of view, it is sensible to have structured grids that follow the direction of boundaries as well as stresses within. Unlike tetrahedral or pyramidal elements, hex grids remain fairly normal to the wall boundaries and doesn't exhibit large face

THIS REPORT WAS INADVERTENTLY DISSEMINATED IN THE PUBLIC DOMAIN/ONLINE SINCE 12/2018 WITHOUT A DISCLAIMER. DISCLAIMER HAS BEEN ADDED – "THIS INFORMATION IS DISTRIBUTED SOLELY FOR THE PURPOSE OF PEER REVIEW UNDER APPLICABLE INFORMATION QUALITY GUIDELINES. IT HAS NOT BEEN FORMALLY DISSEMINATED BY BSEE. IT DOES NOT REPRESENT AND SHOULD NOT BE CONSTRUED TO REPRESENT ANY AGENCY DETERMINATION OR POLICY."

skewness. Besides, hexahedral mesh typically exhibits higher numerical and computational efficiency than the other types of mesh.

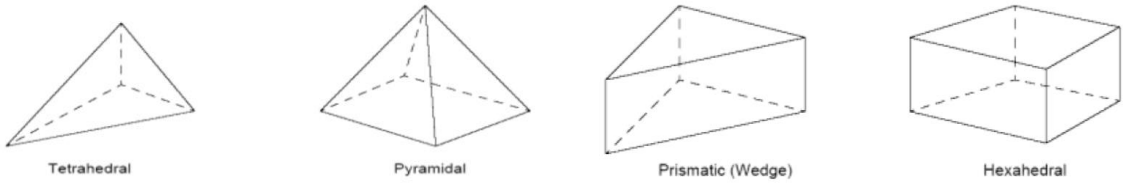

Figure 3.4: Comparison of hexahedral type mesh element with other shapes of mesh (ANSYS 2017)

3.1.4. Contact Formulation

Contact is a changing status nonlinearity and its formulation can significantly affect simulation results. Therefore, it is the most critical aspect of this model. There are two contact surfaces in the model: seal-liner and the seal-casing interface. These contacting bodies can transmit compressive normal force and tangential frictional force but not tensile normal force. Realistically, the contacting bodies do not penetrate each other. In finite element modelling, various contact formulations are available that enforce this contact compatibility to various degrees.

The most common contact formulations are pure penalty and augmented Lagrange. As shown in Figure 3.5**,** a contact stiffness (similar to spring constant) is assigned to the contact surfaces. The higher the contact stiffness, the lower the penetration. Ideally, for an infinite contact stiffness, one would get zero penetration. This is not numerically possible, but as long as penetration is small or negligible, the solution results will be accurate. Because of the additional parameter λ, the augmented Lagrange method is less sensitive to the stiffness constant. Normal Lagrange formulation adds an extra degree of freedom in the form of contact pressure to satisfy the contact compatibility. This eliminated the need for contact stiffness. This method provides excellent penetration control but takes a longer time to converge.

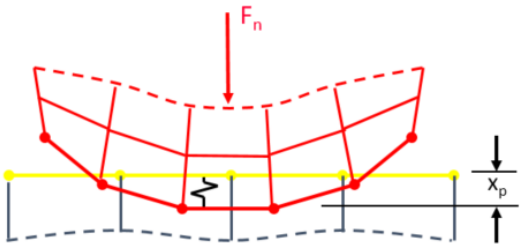

Pure Penalty: $F_{normal} = k_{normal} x_{penetration}$

Augmented Lagrange: $F_{normal} = k_{normal} x_{penetration + \lambda}$

Figure 3.5: Pure penalty or augmented Lagrange contact formulation

Various contact formulation and their pros and cons were carefully considered. Detailed description of contact formulation is out of the scope of this report. However, a summary of options used in contact modelling are as follows:

- Both contact surfaces (seal-liner and seal-casing) have been considered as frictionless.

THIS REPORT WAS INADVERTENTLY DISSEMINATED IN THE PUBLIC DOMAIN/ONLINE SINCE 12/2018 WITHOUT A DISCLAIMER. DISCLAIMER HAS BEEN ADDED – "THIS INFORMATION IS DISTRIBUTED SOLELY FOR THE PURPOSE OF PEER REVIEW UNDER APPLICABLE INFORMATION QUALITY GUIDELINES. IT HAS NOT BEEN FORMALLY DISSEMINATED BY BSEE. IT DOES NOT REPRESENT AND SHOULD NOT BE CONSTRUED TO REPRESENT ANY AGENCY DETERMINATION OR POLICY."

- Because of significant difference between material properties of seal and casing/liner, asymmetric contact behavior has been selected. Based on general guidelines, seal has been selected as contact body and the liner and casing as target bodies.
- Either Augmented Lagrange with an optimized stiffness factor or a normal Lagrange is often selected as the contact formulation in this work.
- The nodal normal detection method has been selected as preferred method for contact detection as it provides less penetrations, particularly at the corners and edges.
- Pinball radius is a sphere surrounding each contact detection point within which the solver considers all nodes to be "near" contact and monitors the relationship. Its value is ensured to be sufficiently larger than seal interference or displacement.
- To ensure maximum accuracy, contact trimming - used for faster convergence, has been turned off. "Trim Contact" automatically reduces the number of contact elements generated within each pair, thereby speeding up processer time.

3.1.5. Model Verification and Reliability

To improve reliability of the contact pressures simulated by the model, it is important to perform model verification and validation. Model verification is the process of confirming whether the finite element tool is solving the model correctly or not. Model validation is the process of confirming whether the model assumptions are true, and the results are representative of the reality.

Two steps were taken to verify the model. First, it was checked whether the displacement boundary conditions applied are indeed being observed in the simulation results. The second step was to perform a mesh sensitivity analysis. As mesh becomes finer, the numerical error reduces. However, it also increases computational requirements. To confirm that the results obtained in this study are independent of mesh, contact pressures were examined as a function of mesh element size as shown in Figure 3.6.

THIS REPORT WAS INADVERTENTLY DISSEMINATED IN THE PUBLIC DOMAIN/ONLINE SINCE 12/2018 WITHOUT A DISCLAIMER. DISCLAIMER HAS BEEN ADDED – "THIS INFORMATION IS DISTRIBUTED SOLELY FOR THE PURPOSE OF PEER REVIEW UNDER APPLICABLE INFORMATION QUALITY GUIDELINES. IT HAS NOT BEEN FORMALLY DISSEMINATED BY BSEE. IT DOES NOT REPRESENT AND SHOULD NOT BE CONSTRUED TO REPRESENT ANY AGENCY DETERMINATION OR POLICY."

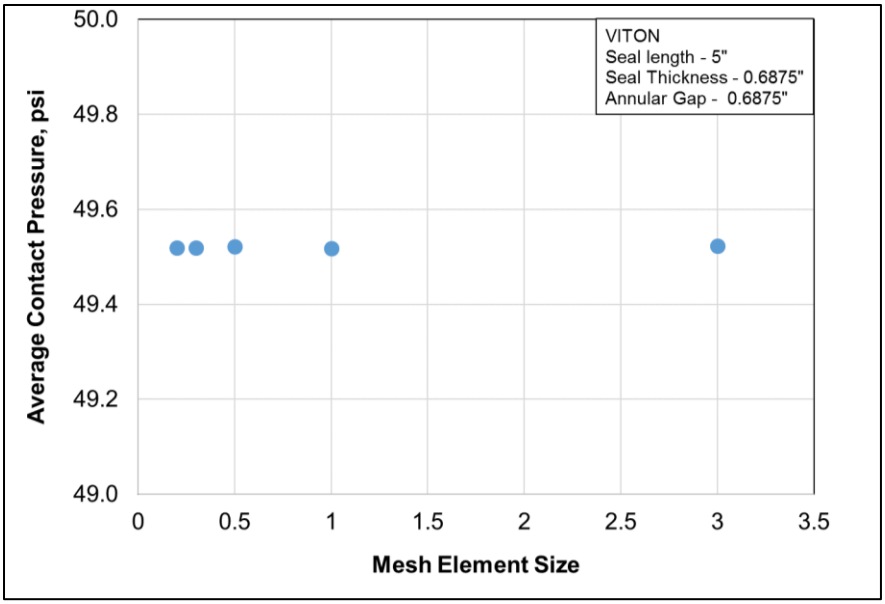

Figure 3.6:Average contact pressure on casing-seal and liner-seal interface as a function of mesh element size

The most crucial verification is that of contact pressure as it is the target output property from the simulations. One way to increase the accuracy and reliability of contact pressure is to minimize penetration as much as possible by increasing the contact stiffness index. As shown in Figure 3.7, the stiffness index was varied from 0.1 to 1000. Penetration decreased 100-fold over this range. Contact pressure values plateaued near 90 psi at a higher stiffness index. Residual penetration of the order of 10^{-4} in. is practically negligible. Moreover, normal Lagrange method independently yielded contact pressure of 91 psi at significantly low penetration of the order of 10^{-7} in. Thus, it can be estimated with reasonable certainty that contact pressure is approximately 90 psi. This provides further validation of model results.

THIS REPORT WAS INADVERTENTLY DISSEMINATED IN THE PUBLIC DOMAIN/ONLINE SINCE 12/2018 WITHOUT A DISCLAIMER. DISCLAIMER HAS BEEN ADDED – "THIS INFORMATION IS DISTRIBUTED SOLELY FOR THE PURPOSE OF PEER REVIEW UNDER APPLICABLE INFORMATION QUALITY GUIDELINES. IT HAS NOT BEEN FORMALLY DISSEMINATED BY BSEE. IT DOES NOT REPRESENT AND SHOULD NOT BE CONSTRUED TO REPRESENT ANY AGENCY DETERMINATION OR POLICY."

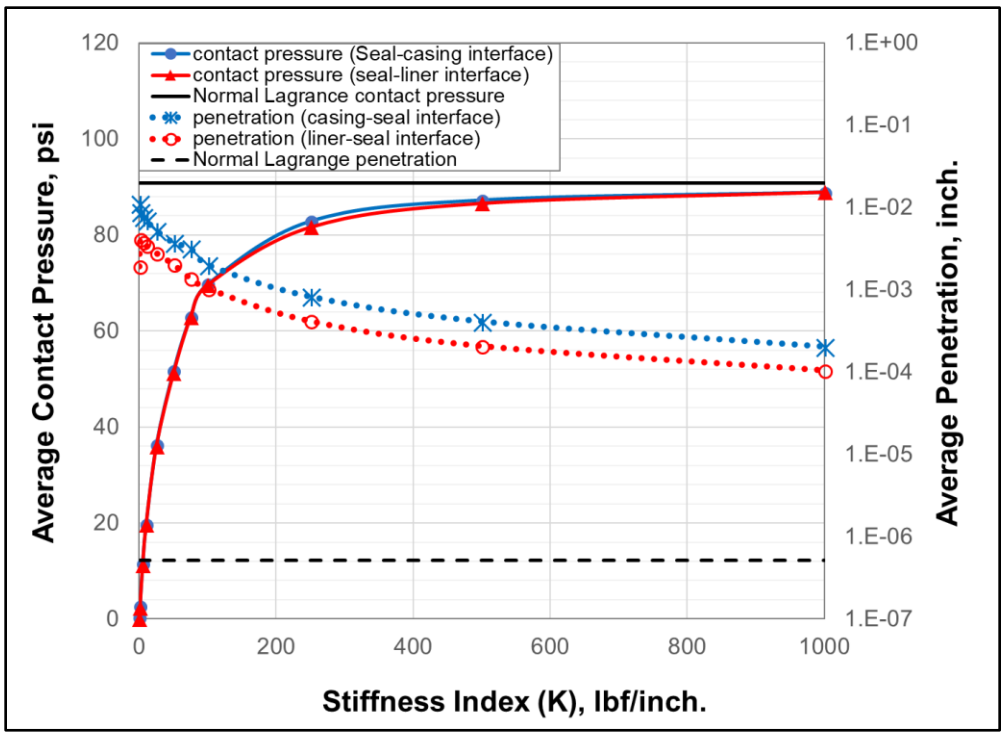

Figure 3.7: Sensitivity of contact pressure and residual penetration to stiffness index. Both augmented Lagrange and Normal Lagrange method independently predicts contact pressure of about 90 psi.

It should be noted that increasing the stiffness index increased the time required for the solution to converge. Normal Lagrange was the most computationally intensive formulation as it has the most stringent requirement for contact penetration.

In summary, various model verification techniques discussed in this section indicate that the model is setup correctly and should produce reliable results.

3.2. Cement Model

The 2-D schematic of the FEA model of cement sheath is provided in Figure 3.8**.** This is similar to the seal assembly model with the replacement of seal by cement. The liner and casing dimensions and their material properties are the same as the seal assembly model. The symmetry planes are also the same and only an $^{1}/_{8}^{th}$ segment of the wellbore cross section was modelled to minimize computational requirement.

3.2.1. Material Properties

The material model and properties for liner and casing components are the same as the seal assembly model (see Table 3.1). The cement sheath has been modeled as isotropic linear elastic behavior. Three types of cement systems were selected for simulations – (i) a ductile cement system with low Young's modulus and high Poisson's ratio (Sample A), (ii) cement system with moderate Young's modulus and moderate Poisson's ratio (Sample B), and (iii) a brittle cement system with high Young's modulus and low Poisson's ratio (Sample C). The material properties

THIS REPORT WAS INADVERTENTLY DISSEMINATED IN THE PUBLIC DOMAIN/ONLINE SINCE 12/2018 WITHOUT A DISCLAIMER. DISCLAIMER HAS BEEN ADDED – "THIS INFORMATION IS DISTRIBUTED SOLELY FOR THE PURPOSE OF PEER REVIEW UNDER APPLICABLE INFORMATION QUALITY GUIDELINES. IT HAS NOT BEEN FORMALLY DISSEMINATED BY BSEE. IT DOES NOT REPRESENT AND SHOULD NOT BE CONSTRUED TO REPRESENT ANY AGENCY DETERMINATION OR POLICY."

for the cement systems (Table 3.3) were selected based on typical values found in the literature (Teodoriu et al. 2008).

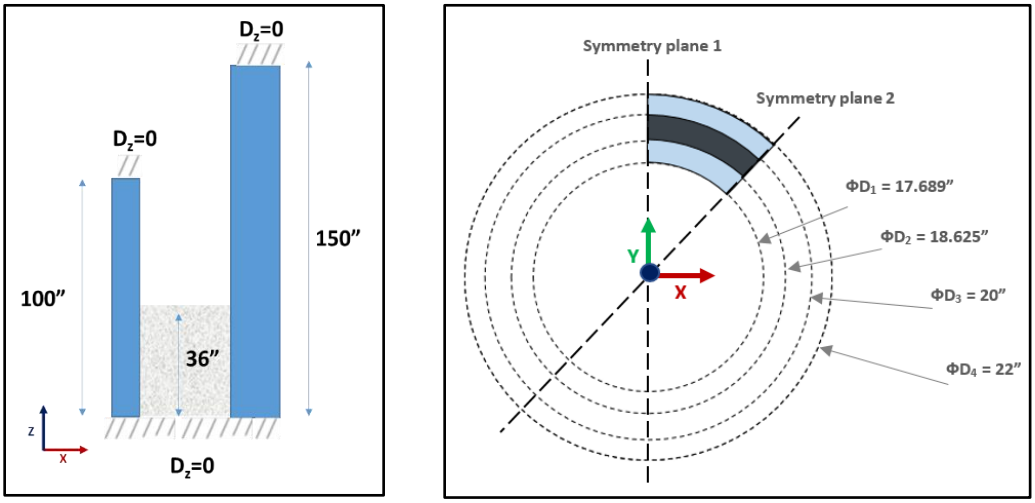

(a) (b)

Figure 3.8: Schematic of cement sheath model (a) 23-D schematic in XZ plane. (b) top view of the model in XY plane

Table 3.3: Material properties of the cement systems selected

Property	Sample A	Sample B	Sample C
Young's Modulus, psi	6.9 x 105 psi	1.0 x 10^6 psi	2.4 x 10^6 psi
Poisson's ratio	0.4	0.25	0.1
Tensile Strength, psi	1000 psi	1500 psi	3000 psi
Compressive Strength, psi	3000 psi	4500 psi	9500 psi
Cohesive Strength, psi	1500 psi	2250 psi	4750 psi

3.2.2. Boundary Conditions

The top and bottom ends of the liner and casing were restrained from any movement in the z direction by assigning zero displacement boundary condition. As shown in Figure 3.8, the bottom of cement sheath was also constrained from any movement in the axial z direction.

3.2.3. Mesh

The mesh selection was similar to the seal assembly model. All the bodies of the model were discretized into small elements using hexahedral meshing (see Figure 3.4).

THIS REPORT WAS INADVERTENTLY DISSEMINATED IN THE PUBLIC DOMAIN/ONLINE SINCE 12/2018 WITHOUT A DISCLAIMER. DISCLAIMER HAS BEEN ADDED – "THIS INFORMATION IS DISTRIBUTED SOLELY FOR THE PURPOSE OF PEER REVIEW UNDER APPLICABLE INFORMATION QUALITY GUIDELINES. IT HAS NOT BEEN FORMALLY DISSEMINATED BY BSEE. IT DOES NOT REPRESENT AND SHOULD NOT BE CONSTRUED TO REPRESENT ANY AGENCY DETERMINATION OR POLICY."

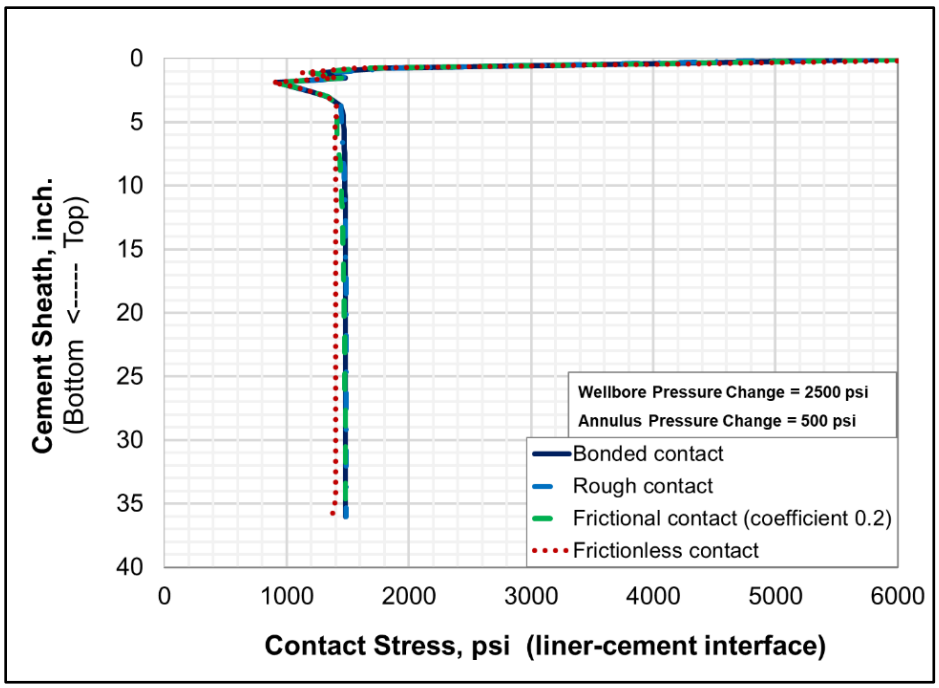

Figure 3.9: Sensitivity of contact pressure to contact formulation

3.2.4. Contact Formulation

There are two contact surfaces in the model: cement-liner and cement-casing interface. When the cement sets, it forms a bonding with the pipe surface. Unlike elastomer seal in hanger assembly, the cement, once set, cannot slide along the pipe surface. Among all the available contact types, only the 'bonded' and 'rough' types meet this condition. In addition to 'no sliding', cement does not separate from the pipe unless the radial stress developed at the interface under a certain load exceeds the bond strength. The 'rough' type of contact would permit separation as soon as the radial stress becomes positive i.e. tensile. Therefore, the only logical contact type that is closest to reality is the 'bonded' type contact which never permits separation of contacting bodies. The separation of cement i.e. debonding from liner or casing can be manually predicted by checking whether simulated radial stress is higher or lower than the cement's bond strength.

The contact formulation, contact detection method, contact behavior etc. parameters were kept similar to the contact formulation in the seal assembly model.

3.2.5. Model Verification and Reliability

Similar to the seal assembly model, to confirm whether the model is correctly setup or not, three model verification steps were performed. First, it was checked whether the displacement boundary conditions applied were indeed being observed in the simulation results. Second, the model's sensitivity to mesh size and selection of symmetry planes was examined. The results were found not to vary with the mesh size and symmetry planes. The third step of model verification was to setup different contact formulations and confirm that the results are independent of it. As shown in Figure 3.9**,** the contact stress values were found to be fairly independent of contact formulation.

THIS REPORT WAS INADVERTENTLY DISSEMINATED IN THE PUBLIC DOMAIN/ONLINE SINCE 12/2018 WITHOUT A DISCLAIMER. DISCLAIMER HAS BEEN ADDED – "THIS INFORMATION IS DISTRIBUTED SOLELY FOR THE PURPOSE OF PEER REVIEW UNDER APPLICABLE INFORMATION QUALITY GUIDELINES. IT HAS NOT BEEN FORMALLY DISSEMINATED BY BSEE. IT DOES NOT REPRESENT AND SHOULD NOT BE CONSTRUED TO REPRESENT ANY AGENCY DETERMINATION OR POLICY."

4. SIMULATION RESULTS

4.1. Seal Assembly Model

Using the verified model, a parametric analysis was performed. This will provide insight into the behavior of elastomer seal by examining the contact pressure as various parameters are systematically varied. In addition to design parameters such as material properties and seal dimensions, few important seal failure scenarios have also been examined. Unless otherwise mentioned, the base case parameter values are listed in Table 4.1.

Table 4.1: Base simulation case for parametric analysis of seal assembly

Parameter	Value
Seal elastic modulus	321 psi (VITON)
Seal Poisson's Ratio	0.49
Seal length	5 in.
Seal radial thickness	0.6875 in.
Annular gap between liner and casing	0.6875 in.
Compression Ratio	1%
Seal energization process	No fault in compression and support
Simulated average contact pressure for the base case	51 psi

This model behavior analysis will facilitate identification of the most critical parameters affecting sealability of the liner hanger. Additionally, the simulation results have been used to develop correlation and guidelines for estimating contact pressure in any condition.

4.1.1. Compression Ratio and Elastic Modulus

The first in the series of simulation studies was to examine the effect of the elastic modulus of seal material on contact pressure. Contact pressures were simulated at various amounts of seal energization for four types of elastomer materials – NBR, EPDM, VITON, and PTFE. The seal energization has been quantified by a term defined as compression ratio δ which is calculated as:

$$\text{compression ratio } (\delta) = \frac{\text{change in seal height due to compression}}{\text{original seal height}} \times 100\% \quad \ldots\ldots\ldots\ldots (13)$$

THIS REPORT WAS INADVERTENTLY DISSEMINATED IN THE PUBLIC DOMAIN/ONLINE SINCE 12/2018 WITHOUT A DISCLAIMER. DISCLAIMER HAS BEEN ADDED – "THIS INFORMATION IS DISTRIBUTED SOLELY FOR THE PURPOSE OF PEER REVIEW UNDER APPLICABLE INFORMATION QUALITY GUIDELINES. IT HAS NOT BEEN FORMALLY DISSEMINATED BY BSEE. IT DOES NOT REPRESENT AND SHOULD NOT BE CONSTRUED TO REPRESENT ANY AGENCY DETERMINATION OR POLICY."

Two parameters - elastic modulus (E) and compression ratio (δ) were varied. The remaining parameters were the same as the base case described in Table 4.1. Model predictions of contact pressure are graphically presented as a function of E and δ in Figure 4.1 and Figure 4.2. Each data point represents one simulation run. The contact pressure variation on both the casing-seal interface and liner-seal interface were minor and hence, their values were averaged to obtain a single representative value.

It is clear from the results that the contact pressure is linearly correlated with both the elastic modulus and the compression ratio. This behavior was anticipated because of the assumption of linear elastic material properties.

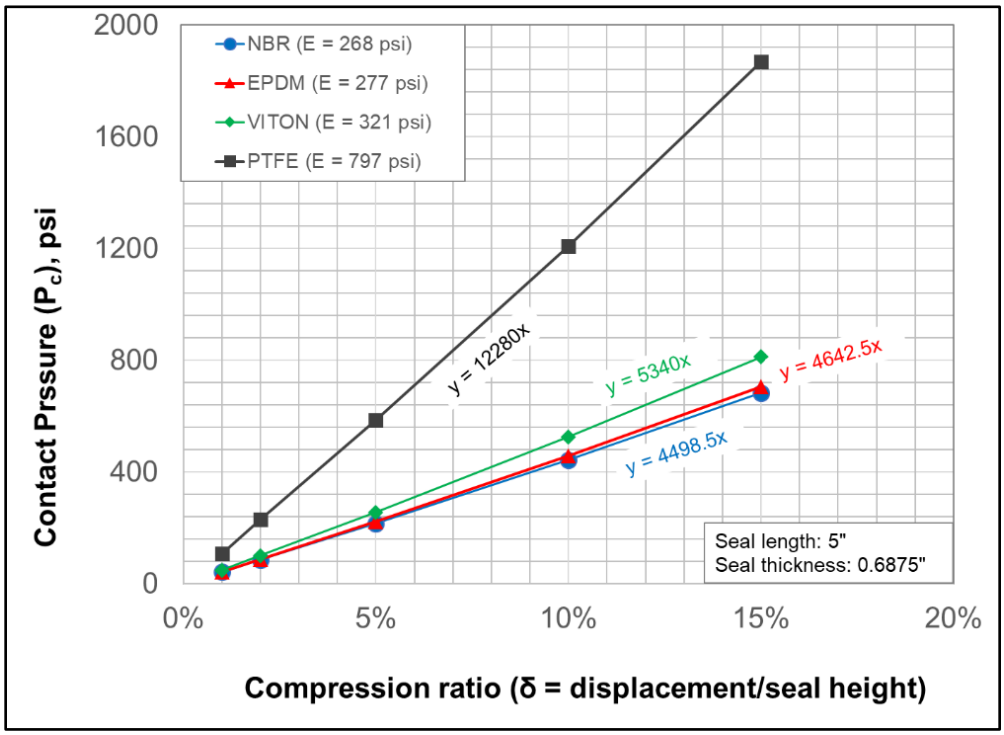

Figure 4.1: Contact pressure as a function of compression ratio at different elastic modulus

THIS REPORT WAS INADVERTENTLY DISSEMINATED IN THE PUBLIC DOMAIN/ONLINE SINCE 12/2018 WITHOUT A DISCLAIMER. DISCLAIMER HAS BEEN ADDED – "THIS INFORMATION IS DISTRIBUTED SOLELY FOR THE PURPOSE OF PEER REVIEW UNDER APPLICABLE INFORMATION QUALITY GUIDELINES. IT HAS NOT BEEN FORMALLY DISSEMINATED BY BSEE. IT DOES NOT REPRESENT AND SHOULD NOT BE CONSTRUED TO REPRESENT ANY AGENCY DETERMINATION OR POLICY."

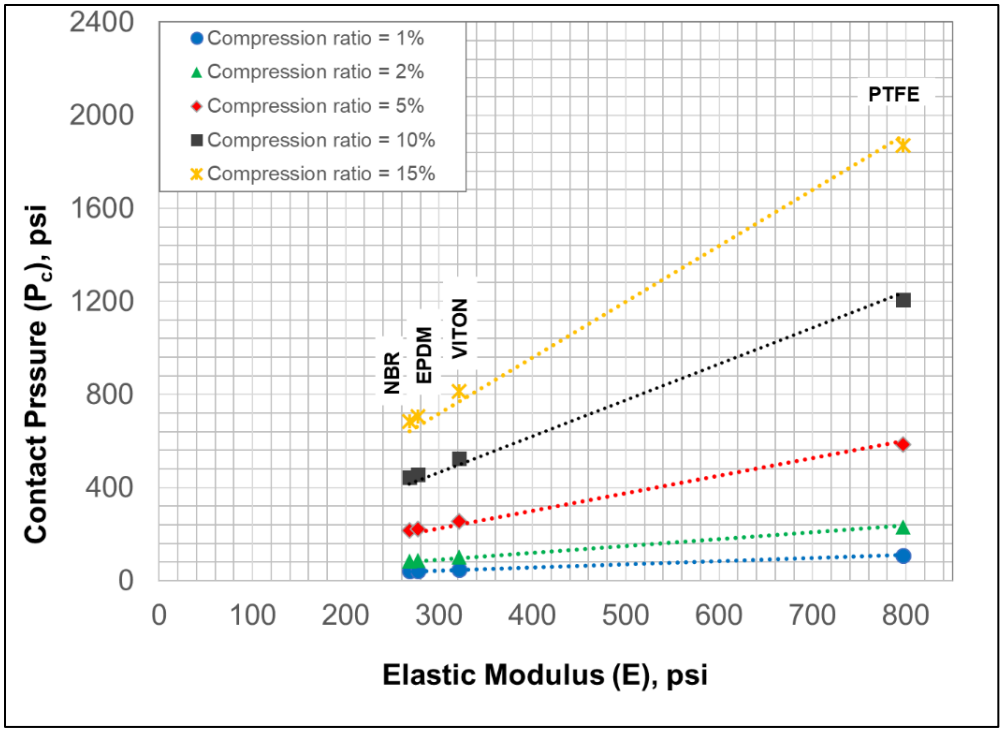

Figure 4.2: Contact pressure as a function of elastic modulus at different compression ratio

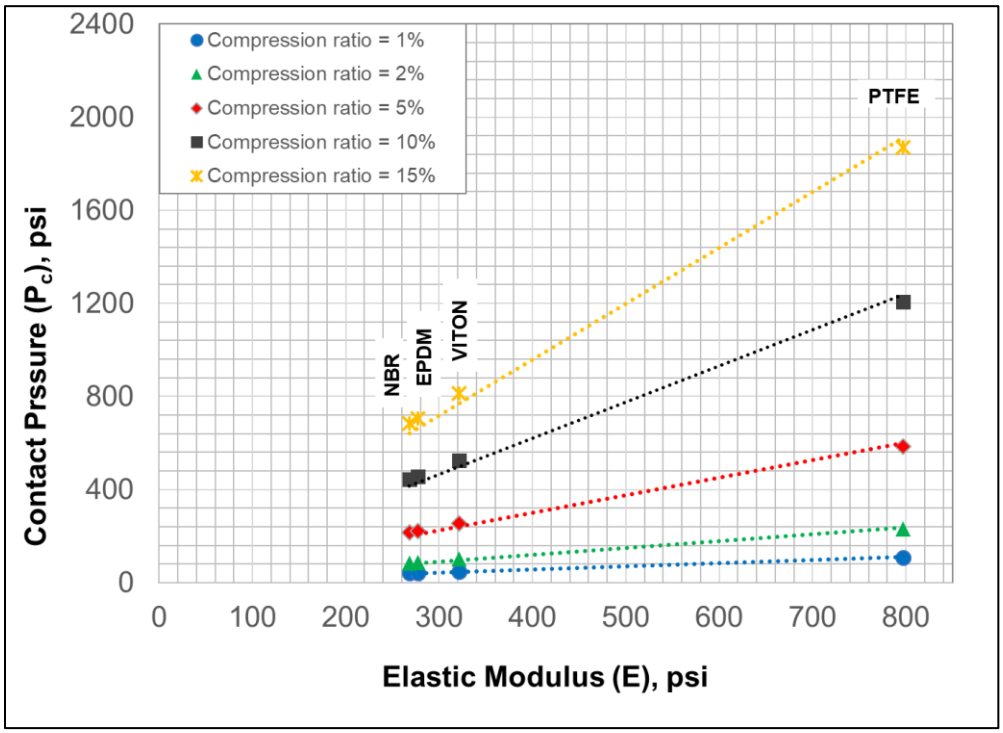

Figure 4.3: Pressure required to achieve certain compression ratio at various elastic modulus

THIS REPORT WAS INADVERTENTLY DISSEMINATED IN THE PUBLIC DOMAIN/ONLINE SINCE 12/2018 WITHOUT A DISCLAIMER. DISCLAIMER HAS BEEN ADDED – "THIS INFORMATION IS DISTRIBUTED SOLELY FOR THE PURPOSE OF PEER REVIEW UNDER APPLICABLE INFORMATION QUALITY GUIDELINES. IT HAS NOT BEEN FORMALLY DISSEMINATED BY BSEE. IT DOES NOT REPRESENT AND SHOULD NOT BE CONSTRUED TO REPRESENT ANY AGENCY DETERMINATION OR POLICY."

A linear regression was performed to obtain the following correlation for estimating contact pressure,

$$\text{Contact Pressure } (P_c, \text{psi}) = 15.78\, E\, \delta \qquad (\text{for } \nu = 0.49) \quad \ldots\ldots\ldots\ldots\ldots\ldots \; (14)$$

The liner hanger should be able to provide hydraulic sealing up to the value of contact pressure generated at the casing-seal interface. Therefore, the higher the elastic modulus or seal energization, the higher the sealability will be. However, the pressure required to energize the seal was also determined to be linearly related to the elastic modulus and the compression ratio (see Figure 4.3**)**. Thus, sealability will be limited by the amount of weight that can be safely exerted on the seal for energization. The following correlation was derived for calculating the pressure required to achieve a certain compression ratio for a specific elastomer material.

$$\text{Pressure Required } (P) = 15.78\, E\, \delta \qquad (\text{for } \nu = 0.49) \quad \ldots\ldots\ldots\ldots\ldots\ldots \; (15)$$

4.1.2. Poisson's Ratio

For elastomer material, Poisson's ratio of 0.49 is common. However, considering the possibility that in oil field applications, stiffer elastomer materials may be used, it was decided to examine effects of lower Poisson's ratio on sealability. Contact pressure as a function of Poisson's ratio for different elastomer materials at a 2% compression ratio is plotted in Figure 4.4. Each data point represents the averaged contact pressure value from an independent simulation run.

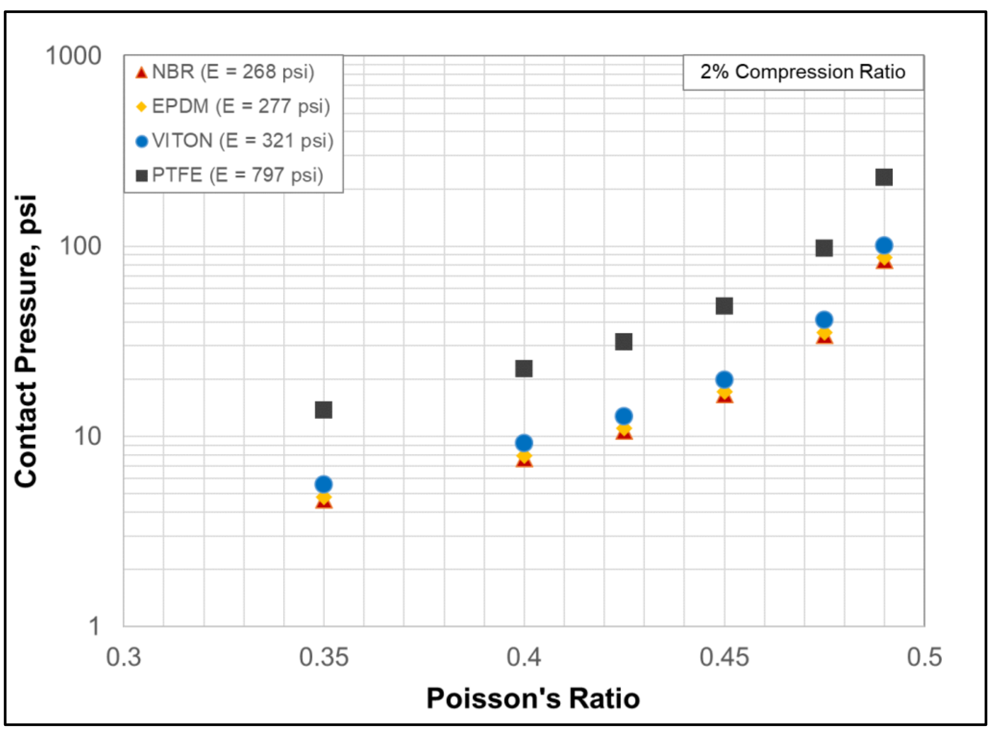

Figure 4.4: Effect of Poisson's ratio on contact pressure

THIS REPORT WAS INADVERTENTLY DISSEMINATED IN THE PUBLIC DOMAIN/ONLINE SINCE 12/2018 WITHOUT A DISCLAIMER. DISCLAIMER HAS BEEN ADDED – "THIS INFORMATION IS DISTRIBUTED SOLELY FOR THE PURPOSE OF PEER REVIEW UNDER APPLICABLE INFORMATION QUALITY GUIDELINES. IT HAS NOT BEEN FORMALLY DISSEMINATED BY BSEE. IT DOES NOT REPRESENT AND SHOULD NOT BE CONSTRUED TO REPRESENT ANY AGENCY DETERMINATION OR POLICY."

At the lower end, metallic elements typically have Poisson's ratio of about 0.3 to 0.35. The theoretical upper limit for Poisson's ratio is 0.5. As shown in Figure 4.4, contact pressure increases gradually for less than 0.425 Poisson's ratio, beyond which it increases exponentially and even faster.

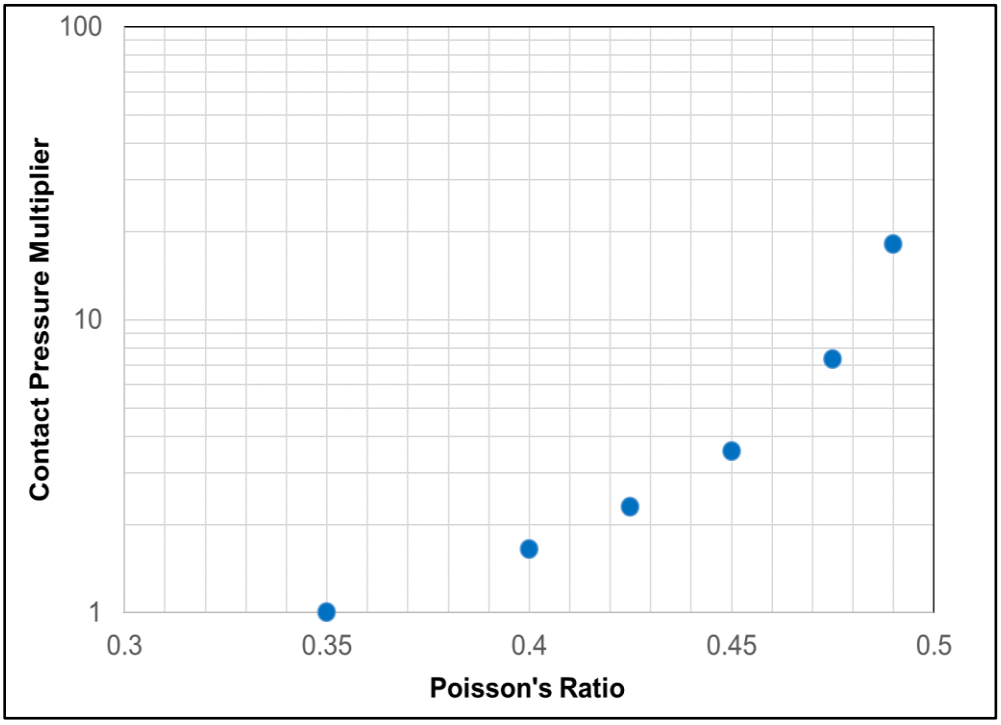

Figure 4.5: Incremental contact pressure with increase in Poisson's ratio remains approximately the same for all the elastomers and compression ratios

Table 4.2: Contact pressure adjustment based on Poisson's ratio

Poisson's Ratio	Contact Pressure Multiplier	Contact Pressure Value
0.49	18.0	18x
0.475	7.3	7.3x
0.45	3.6	3.6x
0.425	2.3	2.3x
0.40	1.6	1.6x
0.35	1.0	x

Considering contact pressure at $\nu = 0.35$ as reference value, the incremental contact pressure or contact pressure multiplier remains approximately the same for all elastomer and compression ratios (See Figure 4.5). In other words, the contact pressure value as predicated by equation (15**)** which can be downscaled or upscaled as shown in Table 4.2 to adjust for change in

THIS REPORT WAS INADVERTENTLY DISSEMINATED IN THE PUBLIC DOMAIN/ONLINE SINCE 12/2018 WITHOUT A DISCLAIMER. DISCLAIMER HAS BEEN ADDED – "THIS INFORMATION IS DISTRIBUTED SOLELY FOR THE PURPOSE OF PEER REVIEW UNDER APPLICABLE INFORMATION QUALITY GUIDELINES. IT HAS NOT BEEN FORMALLY DISSEMINATED BY BSEE. IT DOES NOT REPRESENT AND SHOULD NOT BE CONSTRUED TO REPRESENT ANY AGENCY DETERMINATION OR POLICY."

Poisson's ratio. For example, estimating the contact pressure for 2% compression of VITON having elastic modulus of 321 psi and Poisson's ratio of 0.45,

$$P_c = [15.78\ E\ \delta\ (\text{at } \nu = 0.49)] \times \left[\frac{P_c \text{ multiplier at } \nu = 0.45}{P_c \text{ multiplier at } \nu = 0.49}\right] \ldots\ldots\ldots\ldots\ldots\ldots\ldots\ldots \quad (16)$$

$$P_c = [15.78 \times 321 \times 0.02] \times \left[\frac{3.6}{18}\right]$$

$$P_c = 20.26\ psi$$

The value was confirmed by performing a simulation.

4.1.3. Seal length

For the same elastomer and compression ratio, seal length does not have a significant effect on contact pressure. Three seal lengths – 0.75-, 2.5-, and 5- in. were examined, and it was observed that contact pressure slightly decreases with increase in seal length (see Figure 4.6) but the reduction is only about 2-3%. So, for practical purposes, it can be considered insignificant.

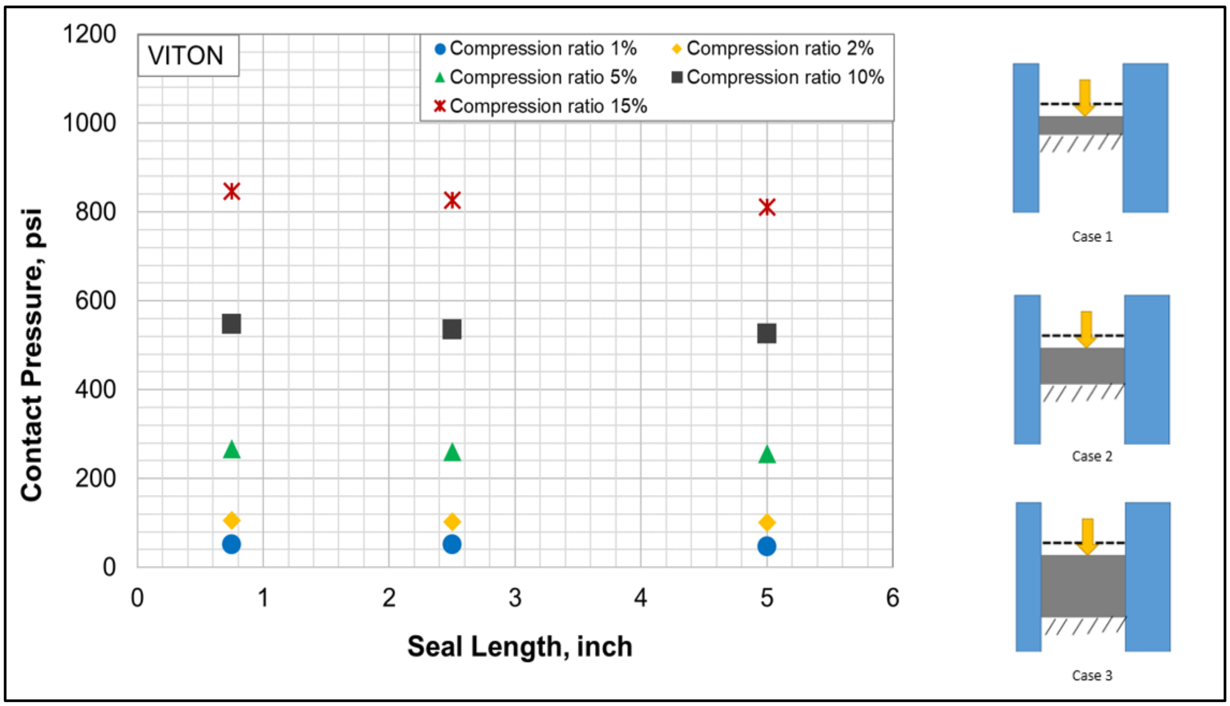

Figure 4.6: Effect of seal length on contact pressure

4.1.4. Seal Thickness

Seal thickness in the radial direction depends on the annular gap between the liner and previous casing. The seal thickness was varied from 0.25 to 1 in. This amounts to approximately -60% to +50% change, considering 0.6875 in. thickness as the base case. The liner and casing thicknesses were kept constant. As shown in Figure 4.7, increasing the seal thickness results in higher contact

THIS REPORT WAS INADVERTENTLY DISSEMINATED IN THE PUBLIC DOMAIN/ONLINE SINCE 12/2018 WITHOUT A DISCLAIMER. DISCLAIMER HAS BEEN ADDED – "THIS INFORMATION IS DISTRIBUTED SOLELY FOR THE PURPOSE OF PEER REVIEW UNDER APPLICABLE INFORMATION QUALITY GUIDELINES. IT HAS NOT BEEN FORMALLY DISSEMINATED BY BSEE. IT DOES NOT REPRESENT AND SHOULD NOT BE CONSTRUED TO REPRESENT ANY AGENCY DETERMINATION OR POLICY."

pressures for the same seal length and compression ratio. The effect was more prominent in the case of a longer seal (5 in. seal length) compared to a shorter seal (0.75 in. length). Overall, change in contact pressure was not significant (mostly < 2%) even for larger changes (±40%) in thickness.

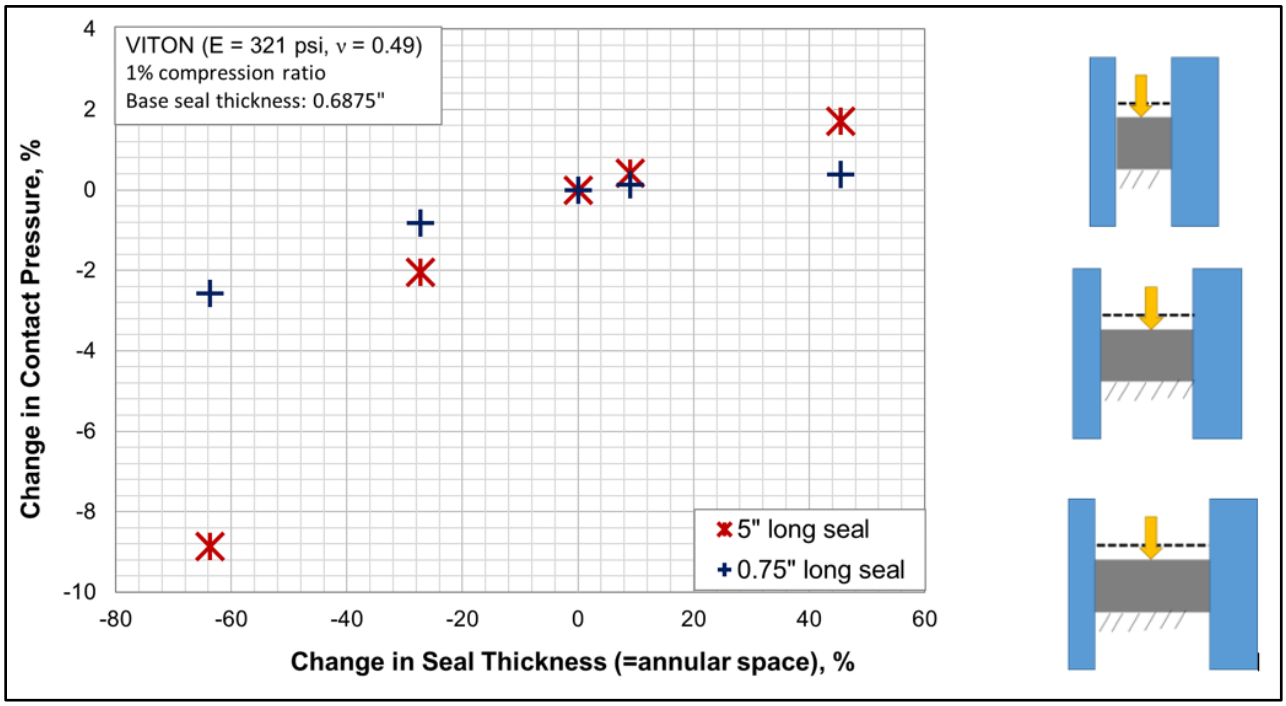

Figure 4.7: Effect of seal thickness on contact pressure

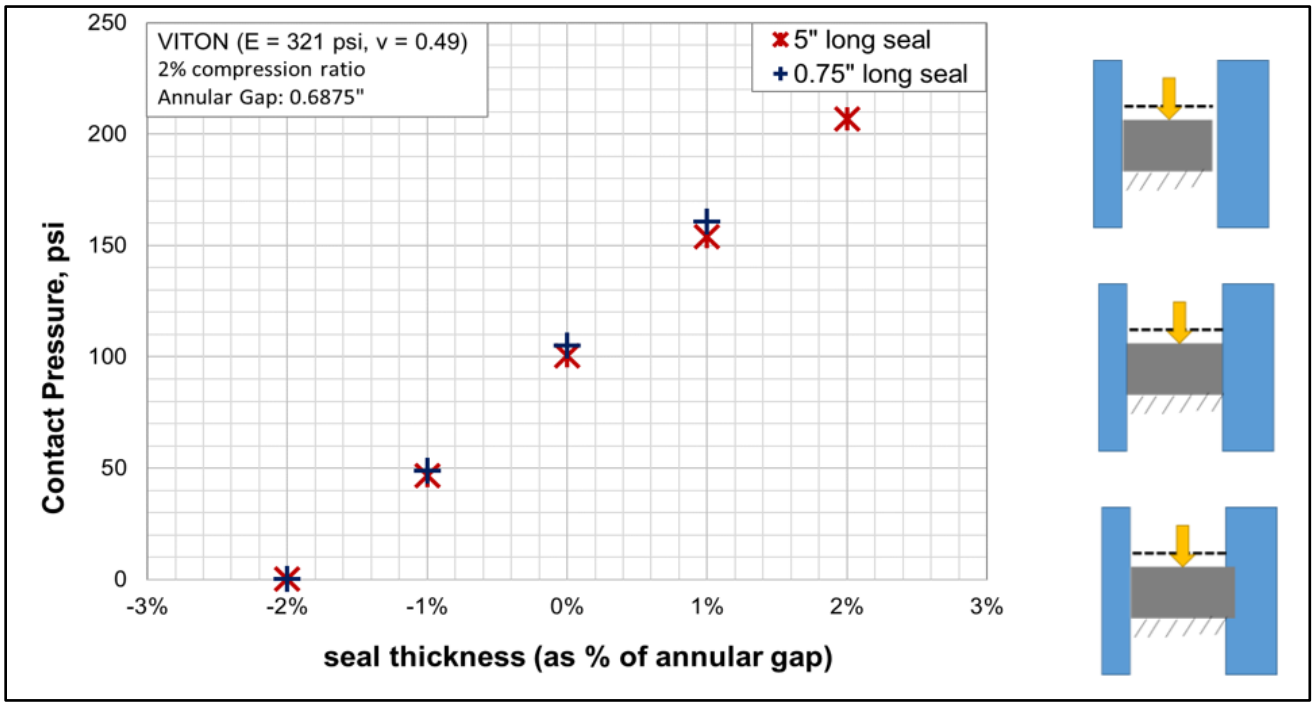

Figure 4.8: Effect of annular fit of seal on contact pressure

THIS REPORT WAS INADVERTENTLY DISSEMINATED IN THE PUBLIC DOMAIN/ONLINE SINCE 12/2018 WITHOUT A DISCLAIMER. DISCLAIMER HAS BEEN ADDED – "THIS INFORMATION IS DISTRIBUTED SOLELY FOR THE PURPOSE OF PEER REVIEW UNDER APPLICABLE INFORMATION QUALITY GUIDELINES. IT HAS NOT BEEN FORMALLY DISSEMINATED BY BSEE. IT DOES NOT REPRESENT AND SHOULD NOT BE CONSTRUED TO REPRESENT ANY AGENCY DETERMINATION OR POLICY."

4.1.5. Annular fit/gap

Typically, the seal element in liner hanger assembly would have a drift diameter smaller than the casing internal diameter so that the seal does not get damaged while running in. Moreover, dimensional tolerances during manufacturing of casing, liner, and seal elements also make it impossible to achieve 100% fit. Hence, this analysis was performed to investigate the effect of sealability in scenarios where seal thickness is not equal to the annular gap between the liner hanger and casing. This would help to optimize the dimensions in the design and manufacturing of seal elements.

Figure 4.8 presents contact pressure for 5 in. and 0.75 in. long VITON seal for various annular fit. The annular gap was fixed at 0.6875 in. and seal thickness was varied from 98% to 102% of annular clearance. 100% being the perfect seal fit. In each case 2% compression ratio was used to energize the seal.

It can be observed from the Figure 4.8 that contact pressure is highly sensitive to the seal's annular fit tolerance. As expected, if the seal is 1% and 2% thicker than the annulus, the contact pressures would be almost 50% and 100% higher respectively than the base case. However, in this case, running the liner hanger inside the casing would be challenging and also damage the seal. If the seal is 1% and 2% thinner than the annular space, which is a more likely happen in an actual field scenario, then contact pressure reduces from the base case by approximately 50% and 100% respectively. This is because some portion of compression applied will be wasted in achieving a contact between the seal and casing. Overall, from various simulation runs, it was observed that if the seal is thinner than the annulus by -x%, then it would require +x% more compression ratio to compensate for the gap and vice versa to achieve the same contact pressure as a 100% fit seal (see Table 4.3 for example).

Table 4.3: Contact pressure adjustment based on seal annular fit tolerance

Annular Fit %	2% Compression Ratio	3% Compression Ratio
98%	0	51
99%	47	101
100%	101	152
101%	154	203
102%	207	253

4.1.6. Material Failure by Gas Exposure

To examine seal material failure, four types of elastomer samples were exposed to CH_4, CO_2, H_2S, and a mixture of all gases for 1 and 7 days at 120°F and 180°F. After aging, the uniaxial compression data was acquired for each elastomer sample. The stress-strain data in the measured range was still practically linear; hence, new elastic moduli were calculated. Using these new elastic modulus values, contact pressures were simulated at various compression ratio.

THIS REPORT WAS INADVERTENTLY DISSEMINATED IN THE PUBLIC DOMAIN/ONLINE SINCE 12/2018 WITHOUT A DISCLAIMER. DISCLAIMER HAS BEEN ADDED – "THIS INFORMATION IS DISTRIBUTED SOLELY FOR THE PURPOSE OF PEER REVIEW UNDER APPLICABLE INFORMATION QUALITY GUIDELINES. IT HAS NOT BEEN FORMALLY DISSEMINATED BY BSEE. IT DOES NOT REPRESENT AND SHOULD NOT BE CONSTRUED TO REPRESENT ANY AGENCY DETERMINATION OR POLICY."

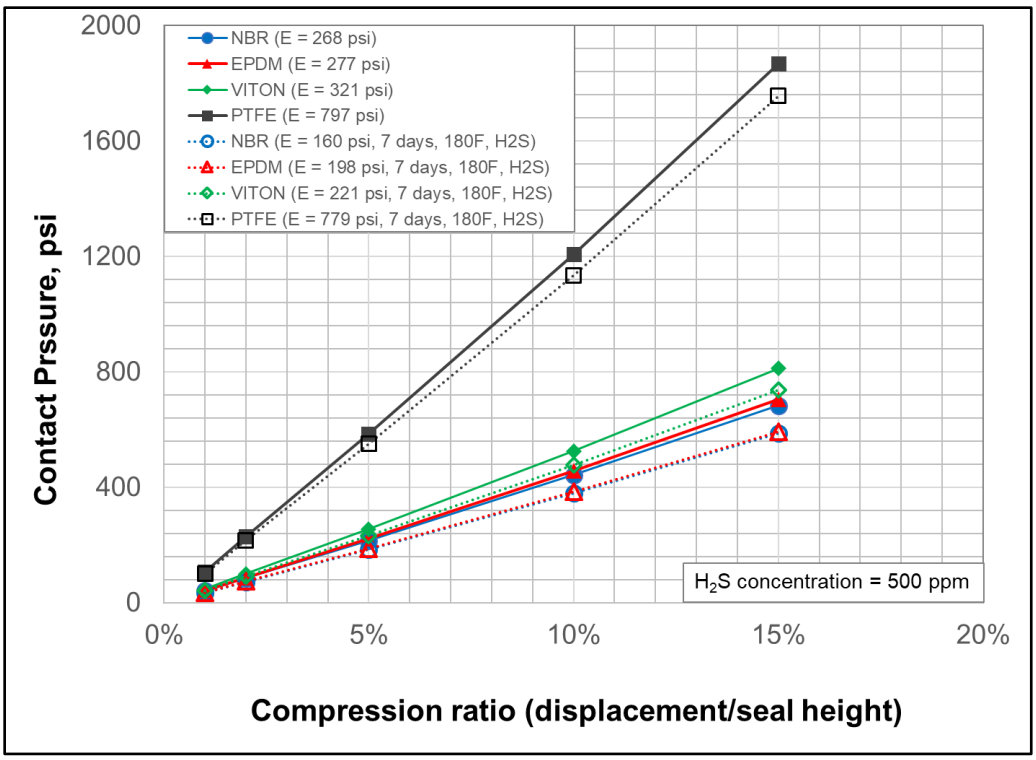

Figure 4.9: Seal energization plots for un-aged elastomer samples compared with samples that were exposed to CO_2 (7 days at 180°F)

Table 4.4: Average reduction in contact pressure (as predicted by eq. 1) after exposure to various gas

Elastomer Type	All gases (50% CH_4 with 500 ppm H_2S + 50% CO_2)								CH_4 (100%)		CO_2 (998,000 ppm)		H_2S (500 ppm in methane carrier)	
	1 day, 120°F		7 days, 120°F		1 day, 180°F		7 days, 180°F		7 days, 180°F		7 days, 180°F		7 days, 180°F	
	Vapor phase	Brine phase	Vapor phase	Brine phase	Vapor phase	Brine phase	Vapor phase	Brine phase	Vapor phase	Brine phase	Vapor phase	Brine phase	Vapor phase	Brine phase
NBR	-41	-38	-36	-35	-36	-31	-30	-29	-16	-13	-40	-38	-14	-11
EPDM	-26	-21	-24	-21	-19	-17	-25	-22	-10	-4	-29	-27	-16	-8
VITON	-22	-14	-20	-13	-14	-7	-17	-11	-4	-6	-31	-28	-9	-6
PTFE	-5	-4	-6	-3	-10	-3	-5	-1	-3	-2	-2	-5	-6	-1

THIS REPORT WAS INADVERTENTLY DISSEMINATED IN THE PUBLIC DOMAIN/ONLINE SINCE 12/2018 WITHOUT A DISCLAIMER. DISCLAIMER HAS BEEN ADDED – "THIS INFORMATION IS DISTRIBUTED SOLELY FOR THE PURPOSE OF PEER REVIEW UNDER APPLICABLE INFORMATION QUALITY GUIDELINES. IT HAS NOT BEEN FORMALLY DISSEMINATED BY BSEE. IT DOES NOT REPRESENT AND SHOULD NOT BE CONSTRUED TO REPRESENT ANY AGENCY DETERMINATION OR POLICY."

As shown in Figure 4.9**,** the contact pressures were observed to be linearly dependent on the compression ratio. The average % reduction in contact pressures and the slope of energization plot after CO_2 exposure was approximately the same as the reduction in the elastic modulus. Reduction in elastic modulus of elastomer samples after exposure to various gases are listed in Table 4.4. The worst case is 7 days exposure to CO_2 at 180°F. It resulted in sealability reduction of NBR (40%), EPDM (29%), VITON (9%), and theoretical PTFE elastomer (2%).

4.1.7. Faulty Support

The liner hanger assembly typically relies on compression plates and slips for providing the support while the seal element is being compressed by the application of weight. If this support is not uniform in radial and/or circumferential direction, then operating contact pressure will be lesser than the designed one and such low contact pressure points along the seal may serve as an initiation point for hydraulic penetration. To investigate the effect of partial support on contact pressure, this study was conducted. A total of six simulation cases were run, depending on the location of the support failure and amount of areal support provided (Figure 4.10).

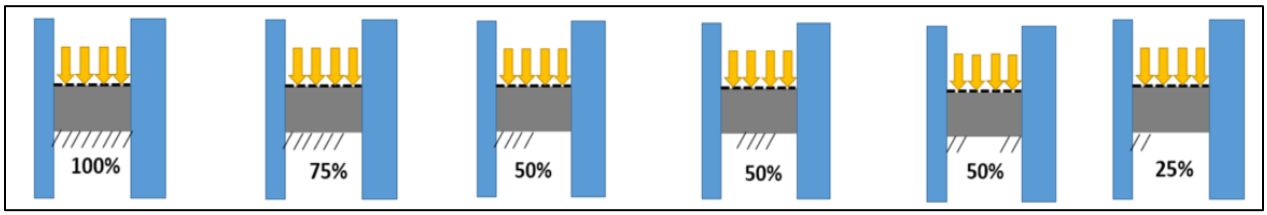

Figure 4.10: Simulation cases of full and various faulty support

Results from the simulation run are graphically presented in Figure 4.11 and Figure 4.12**.** Unlike previous analyses, contact pressures were not averaged to a single value because observing and comparing contact pressure profile along the seal length is important in this case. In the plots, the support side of the seal is at the bottom and the compression is being applied from the top. Interestingly, the contact pressure slightly increased towards the support, reached a peak and then steeply decreased to zero at the support. This can easily permit fluid to penetrate; thus, increasing the risk of leakage. The profiles for casing-seal and liner-seal interfaces are almost opposite to each other.

For a 5 in. long seal (Figure 4.11), the average reduction in contact pressure because of partial support ranged from **13% to 68%** for 75% to 25% support respectively. For shorter seal (Figure 4.12) on the other hand, the loss in sealability was **51% to 95%** for 75% to 25% support respectively. This indicates that the effect of faulty support becomes more detrimental in the case of a shorter seal.

THIS REPORT WAS INADVERTENTLY DISSEMINATED IN THE PUBLIC DOMAIN/ONLINE SINCE 12/2018 WITHOUT A DISCLAIMER. DISCLAIMER HAS BEEN ADDED – "THIS INFORMATION IS DISTRIBUTED SOLELY FOR THE PURPOSE OF PEER REVIEW UNDER APPLICABLE INFORMATION QUALITY GUIDELINES. IT HAS NOT BEEN FORMALLY DISSEMINATED BY BSEE. IT DOES NOT REPRESENT AND SHOULD NOT BE CONSTRUED TO REPRESENT ANY AGENCY DETERMINATION OR POLICY."

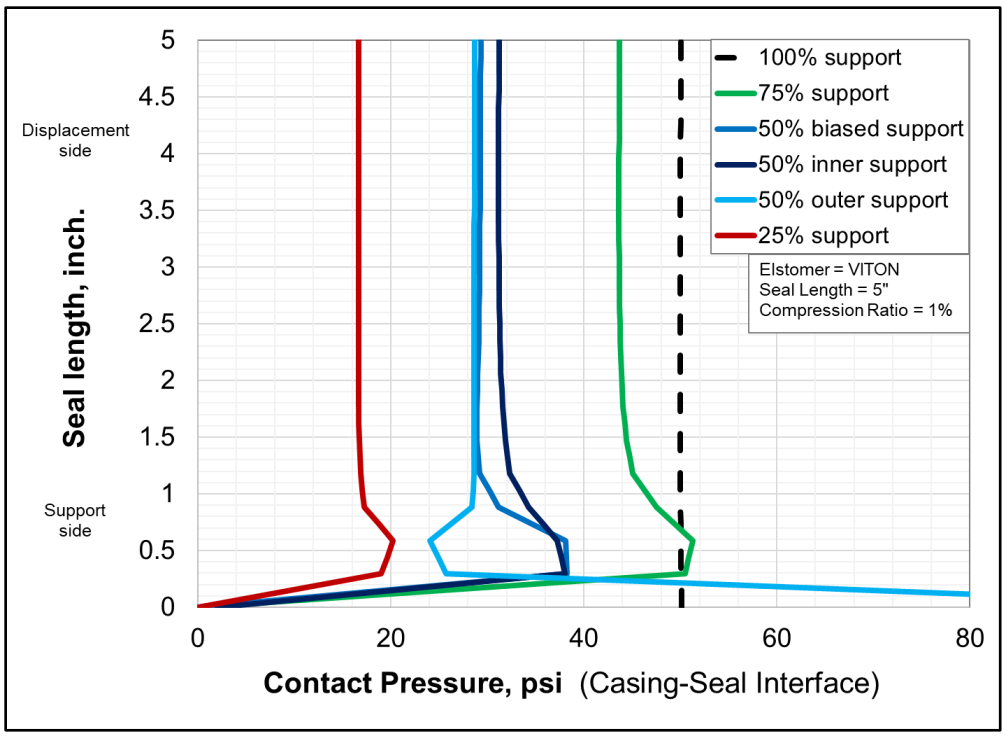

(a)

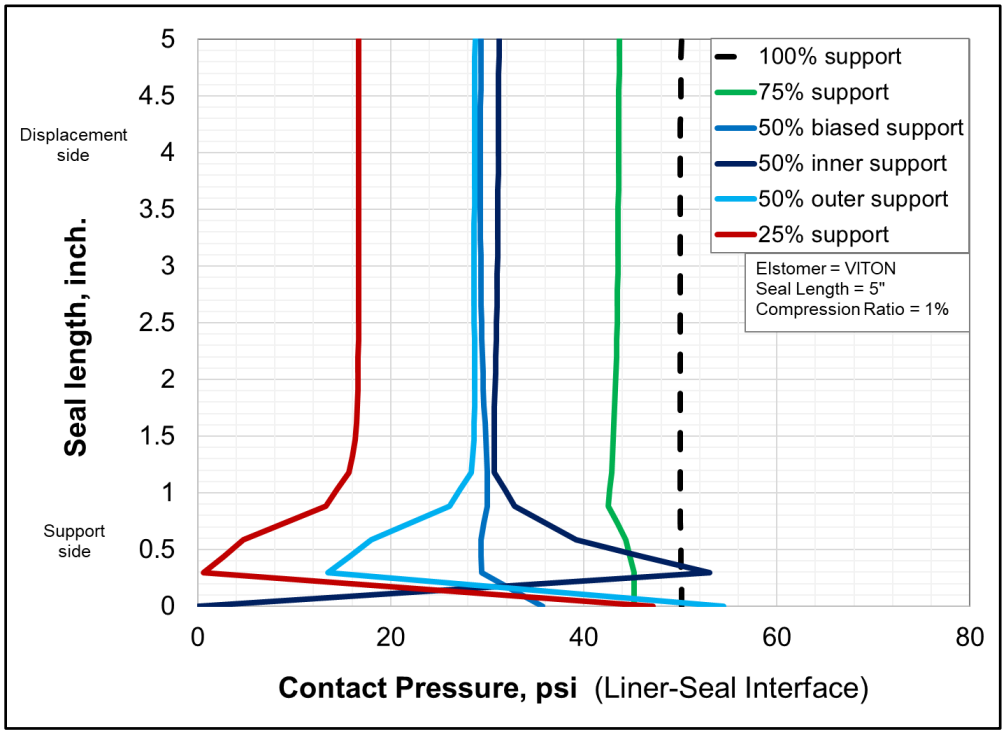

(b)

Figure 4.11: 5 in. long VITON seal with partial support: contact pressure profile along the seal length in z direction at (a) casing-seal interface, and (b) liner-seal interface

THIS REPORT WAS INADVERTENTLY DISSEMINATED IN THE PUBLIC DOMAIN/ONLINE SINCE 12/2018 WITHOUT A DISCLAIMER. DISCLAIMER HAS BEEN ADDED – "THIS INFORMATION IS DISTRIBUTED SOLELY FOR THE PURPOSE OF PEER REVIEW UNDER APPLICABLE INFORMATION QUALITY GUIDELINES. IT HAS NOT BEEN FORMALLY DISSEMINATED BY BSEE. IT DOES NOT REPRESENT AND SHOULD NOT BE CONSTRUED TO REPRESENT ANY AGENCY DETERMINATION OR POLICY."

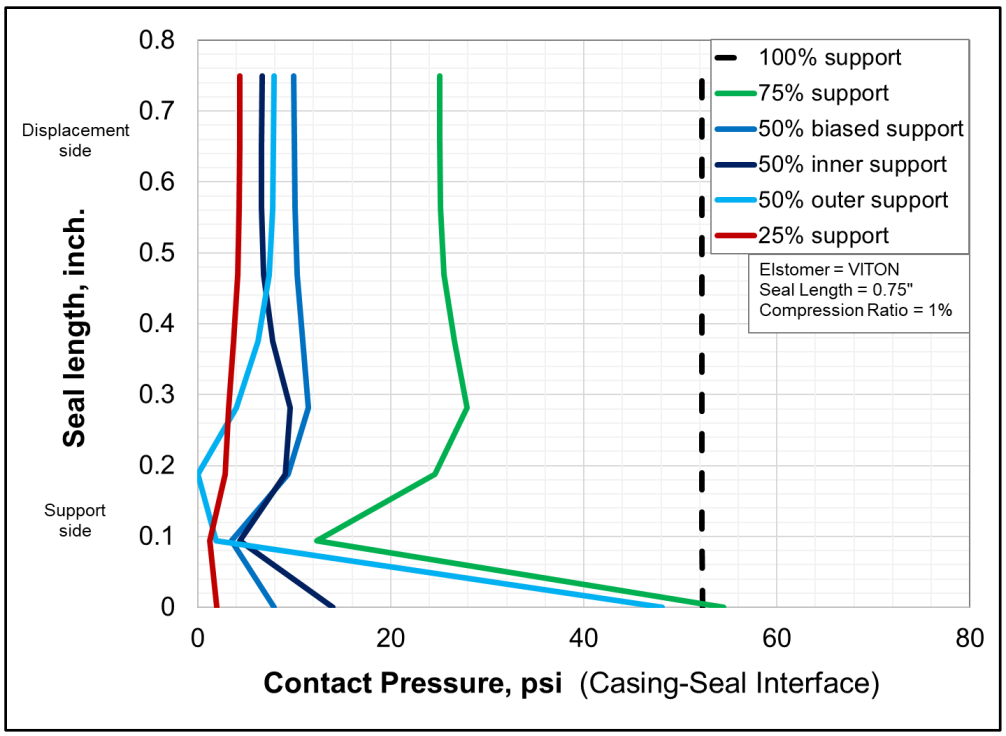

(a)

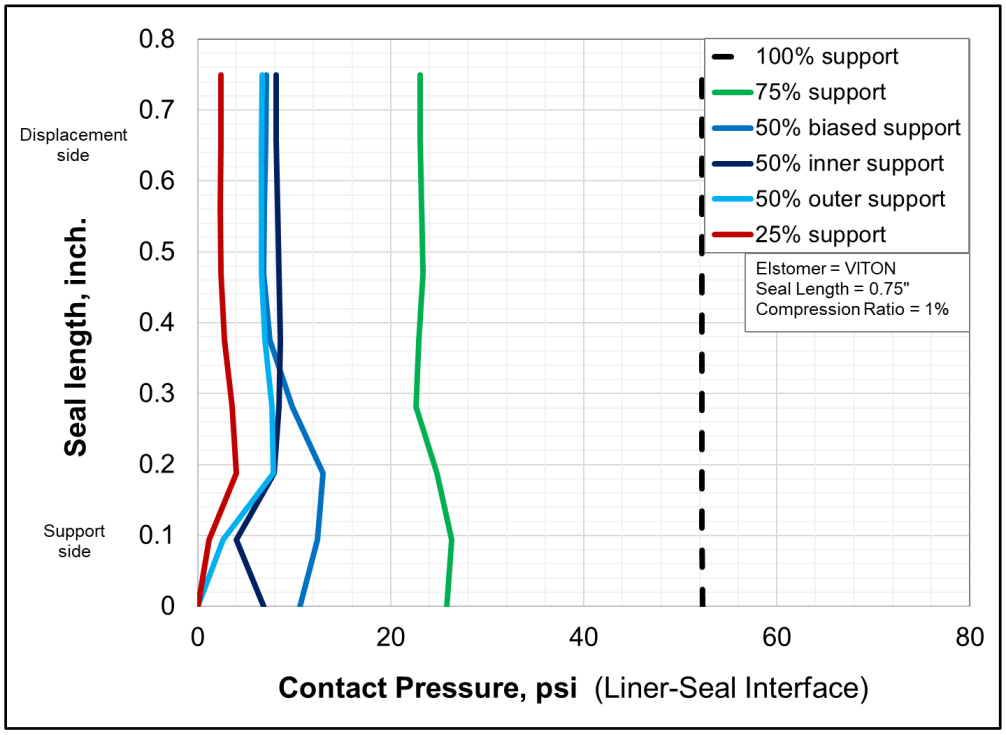

(b)

Figure 4.12: 0.75 in. long VITON seal with partial support: contact pressure profile along the seal length in z direction at (a) casing-seal interface, and (b) liner-seal interface

THIS REPORT WAS INADVERTENTLY DISSEMINATED IN THE PUBLIC DOMAIN/ONLINE SINCE 12/2018 WITHOUT A DISCLAIMER. DISCLAIMER HAS BEEN ADDED – "THIS INFORMATION IS DISTRIBUTED SOLELY FOR THE PURPOSE OF PEER REVIEW UNDER APPLICABLE INFORMATION QUALITY GUIDELINES. IT HAS NOT BEEN FORMALLY DISSEMINATED BY BSEE. IT DOES NOT REPRESENT AND SHOULD NOT BE CONSTRUED TO REPRESENT ANY AGENCY DETERMINATION OR POLICY."

4.1.8. Non-uniform Seal Energization

To achieve good sealability, setting forces up to 100,000 lbf are often required. In certain conditions such as shallow liner installation or deviated wells, it is often not possible to apply the required force. Moreover, the weight applied may not be uniformly distributed over the seal in the radial and circumferential direction. This can lead to the operating contact pressure being lesser than the designed one. To examine the effect of non-uniform compression, seven cases were simulated (Figure 4.13). The seal was supported from the bottom and the displacement boundary condition at the top of seal was varied in terms of location and area coverage.

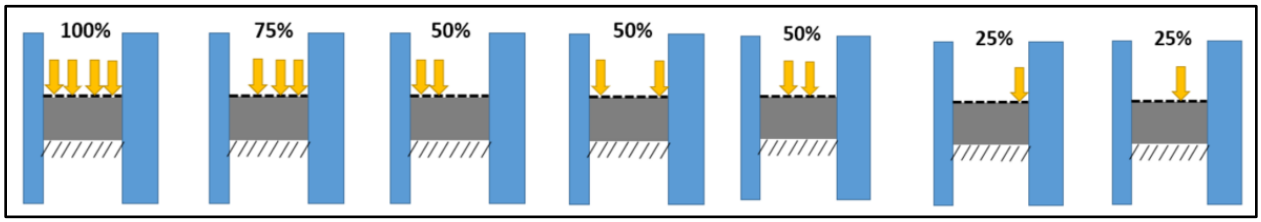

Figure 4.13: Simulation cases of full and different faulty seal energizations

The results from the simulation run are graphically presented in Figure 4.14 and Figure 4.15**.** In the plots, the support side of the seal is at the bottom and compression is applied from the top. Pressure curves and the interpretations are similar to the faulty support case.

For a 5 in. long seal (Figure 4.14), the average reduction in contact pressure due to non-uniform compression ranged from **13% to 80%** for 75% to 25% compression area respectively. For shorter seal (Figure 4.15) on the other hand, the loss in sealability was **53% to 95%** for 75% to 25% support respectively. Similar to the faulty support case, the effect of faulty compression becomes more detrimental for a shorter seal. Overall, the faulty support and faulty compression case results are similar in percentage reduction of contact pressure. However, it should be noted that improper compression is a more likely scenario in the field.

4.1.9. Summary of Parametric Analysis

The results from the simulation study are summarized as follows:

- Contact pressure is linearly dependent on the elastic modulus and the compression ratio.
- Contact pressure increases gradually with the increase in Poisson's ratio up to 0.425, beyond which it increases exponentially and even faster. Considering contact pressure at $\nu = 0.35$ as reference value, the incremental contact pressure or contact pressure multiplier remains approximately the same for all elastomer and compression ratios.
- Contact pressure reduces only by 2-3% even with approximately a 5 times increase in seal length (0.75 in. to 5 in.). For all practical purposes, it can be considered insignificant.
- Change in contact pressure was not significant (< 2%) even for large changes (±40%) in seal thickness.

THIS REPORT WAS INADVERTENTLY DISSEMINATED IN THE PUBLIC DOMAIN/ONLINE SINCE 12/2018 WITHOUT A DISCLAIMER. DISCLAIMER HAS BEEN ADDED – "THIS INFORMATION IS DISTRIBUTED SOLELY FOR THE PURPOSE OF PEER REVIEW UNDER APPLICABLE INFORMATION QUALITY GUIDELINES. IT HAS NOT BEEN FORMALLY DISSEMINATED BY BSEE. IT DOES NOT REPRESENT AND SHOULD NOT BE CONSTRUED TO REPRESENT ANY AGENCY DETERMINATION OR POLICY."

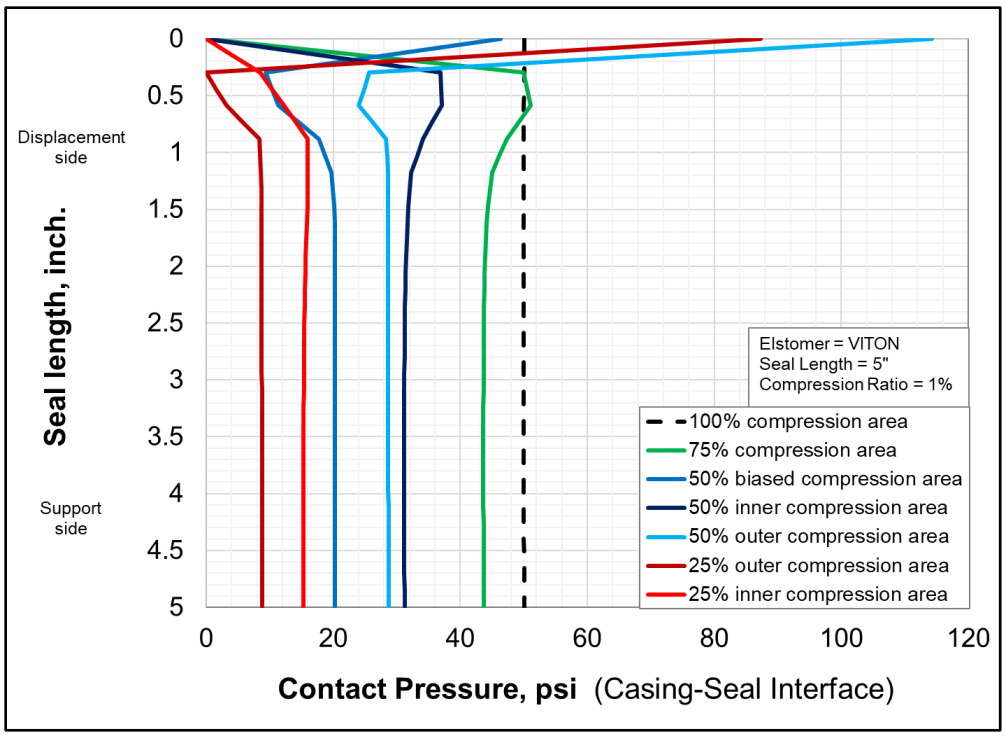

(a)

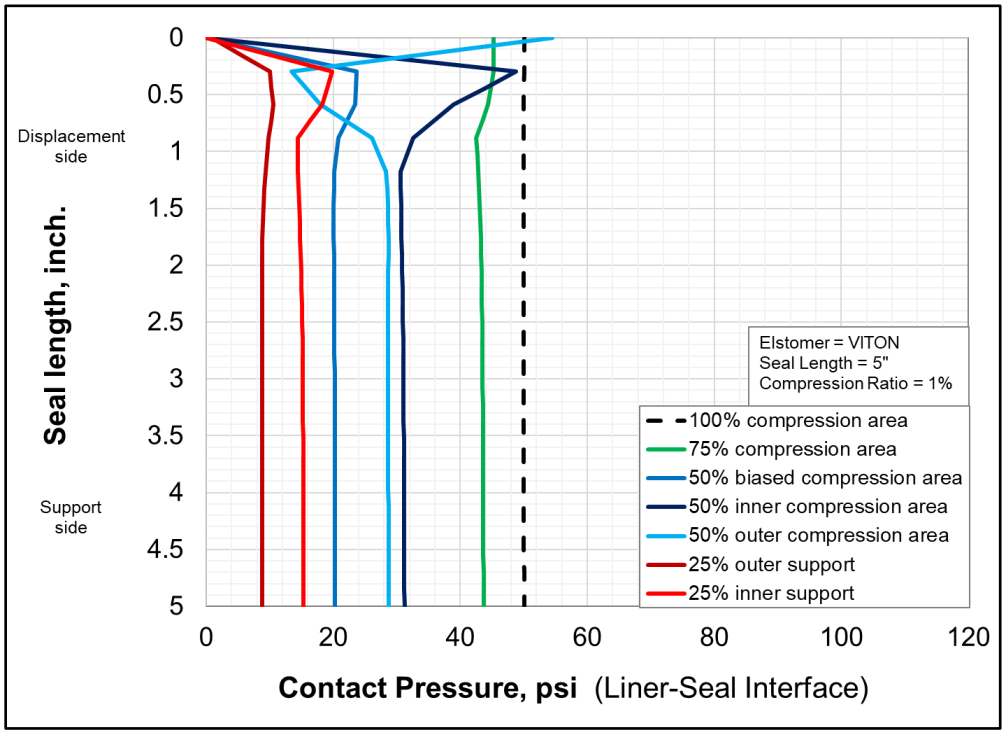

(b)

Figure 4.14: 5 in. long VITON seal with partial compression: contact pressure profile along the seal length in z direction at (a) casing-seal interface, and (b) liner-seal interface

THIS REPORT WAS INADVERTENTLY DISSEMINATED IN THE PUBLIC DOMAIN/ONLINE SINCE 12/2018 WITHOUT A DISCLAIMER. DISCLAIMER HAS BEEN ADDED – "THIS INFORMATION IS DISTRIBUTED SOLELY FOR THE PURPOSE OF PEER REVIEW UNDER APPLICABLE INFORMATION QUALITY GUIDELINES. IT HAS NOT BEEN FORMALLY DISSEMINATED BY BSEE. IT DOES NOT REPRESENT AND SHOULD NOT BE CONSTRUED TO REPRESENT ANY AGENCY DETERMINATION OR POLICY."

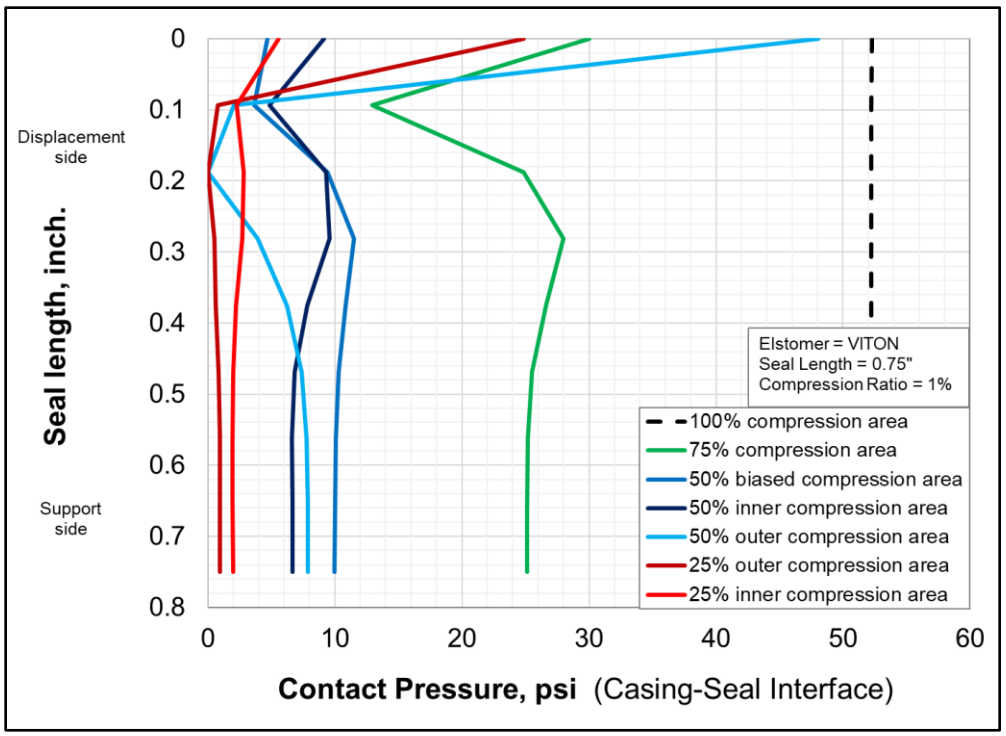

(a)

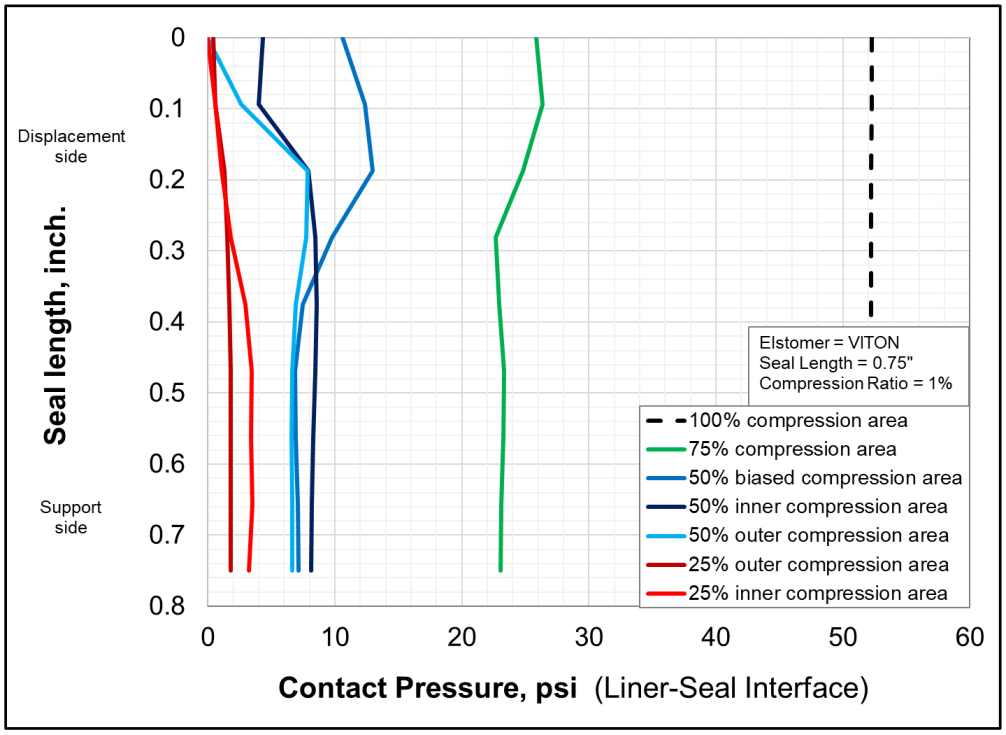

(b)

Figure 4.15: 0.75 in. long VITON seal with partial compression: contact pressure profile along the seal length in z direction at (a) casing-seal interface, and (b) liner-seal interface

THIS REPORT WAS INADVERTENTLY DISSEMINATED IN THE PUBLIC DOMAIN/ONLINE SINCE 12/2018 WITHOUT A DISCLAIMER. DISCLAIMER HAS BEEN ADDED – "THIS INFORMATION IS DISTRIBUTED SOLELY FOR THE PURPOSE OF PEER REVIEW UNDER APPLICABLE INFORMATION QUALITY GUIDELINES. IT HAS NOT BEEN FORMALLY DISSEMINATED BY BSEE. IT DOES NOT REPRESENT AND SHOULD NOT BE CONSTRUED TO REPRESENT ANY AGENCY DETERMINATION OR POLICY."

- Contact pressure is highly sensitive to the annular fit of seal. For a fixed annular space, each ± x% change in seal thickness would require ∓ x% compression ratio to compensate for that change and achieve the same contact pressure as 100% fit seal. In other words, if the radial gap between the seal and casing is x% higher than anticipated, then it can effectively reduce compression by x% and vice versa. A radial gap of 1% higher than the designed value can reduce the effective contact pressure by an amount approximately equal to 16 times the elastic modulus of the seal.
- The average % reduction in contact pressures due to gas exposure is practically equal to the % reduction in the elastic modulus.
- The loss in sealability due to faulty support can range from 13% to 68% in a long seal (5 in.) and 51% to 95% in a short seal (2.5 in.) depending on severity. In the case of non-uniform compression, the loss can range from 13% to 80% in a longer seal (5 in.) and 53% to 95% in a shorter seal (2.5 in.) depending on the severity. Overall, the loss is more pronounced and detrimental for a shorter seal.

All these results can be combined into the following comprehensive correlation for estimating contact pressure.

$$\text{Contact Pressure } (P_c) = 15.78\ E\ (\delta - \lambda) \left[\frac{P_c \text{ multiplier at desired } \nu}{P_c \text{ multiplier at } \nu = 0.49}\right] \quad \ldots\ldots\ldots\ldots\ldots\ldots\ldots\ldots\ldots\ldots \quad (17)$$

where,

E is the elastic modulus, δ is the compression ratio in fraction, λ is the annular gap between seal and pipe in fraction, and Pc multiplier is a constant which can be obtained from the Table 4.2. P_c and E are in consistent units. The effects of seal length and seal thickness can be ignored with ±2% error in the estimate. Material failure can be incorporated simply in form of change in elastic modulus and Poison's ratio.

4.1.10. Analytical Validation

The simulated contact pressure values are the most important items that require validation. The contact pressure values were validated using two different analytical equations.

First, the contact pressures can be verified using the simple analytical relationship between volumetric strain, bulk modulus, and pressure,

$$\frac{\Delta V}{V} = -\frac{P}{K} \quad \ldots\ldots\ldots\ldots\ldots\ldots\ldots\ldots\ldots\ldots\ldots\ldots\ldots\ldots\ldots\ldots\ldots\ldots\ldots\ldots\ldots\ldots\ldots\ldots \quad (18)$$

$$K = \frac{E}{3(1-2\nu)} \quad \ldots\ldots\ldots\ldots\ldots\ldots\ldots\ldots\ldots\ldots\ldots\ldots\ldots\ldots\ldots\ldots\ldots\ldots\ldots\ldots\ldots\ldots\ldots\ldots \quad (19)$$

THIS REPORT WAS INADVERTENTLY DISSEMINATED IN THE PUBLIC DOMAIN/ONLINE SINCE 12/2018 WITHOUT A DISCLAIMER. DISCLAIMER HAS BEEN ADDED – "THIS INFORMATION IS DISTRIBUTED SOLELY FOR THE PURPOSE OF PEER REVIEW UNDER APPLICABLE INFORMATION QUALITY GUIDELINES. IT HAS NOT BEEN FORMALLY DISSEMINATED BY BSEE. IT DOES NOT REPRESENT AND SHOULD NOT BE CONSTRUED TO REPRESENT ANY AGENCY DETERMINATION OR POLICY."

where P is pressure, K is bulk modulus, ν is Poisson's ratio, V is the original volume of elastomer seal, and ΔV is change in volume as shown in Figure 4.16. All variables have consistent unit.

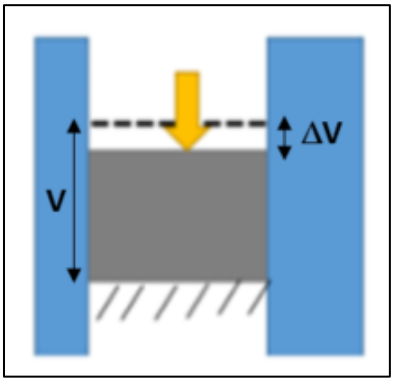

Figure 4.16: Use of analytical equation of bulk modulus to validate contact pressure

The second analytical equation that was used for validation was based on model developed by Al-Hiddabi et al. (2015) for predicting contact pressure in expandable liner hanger seals. This model is based on an elastomer seal that is radially confined between metal tubes with fluid pressures in an axial direction (see Figure 4.17). Originally developed for a solid expandable tubular, this model assumes linear elastic material property and can predict contact pressure along the contact length as a function of the seal compression ratio, fluid pressures, and material properties.

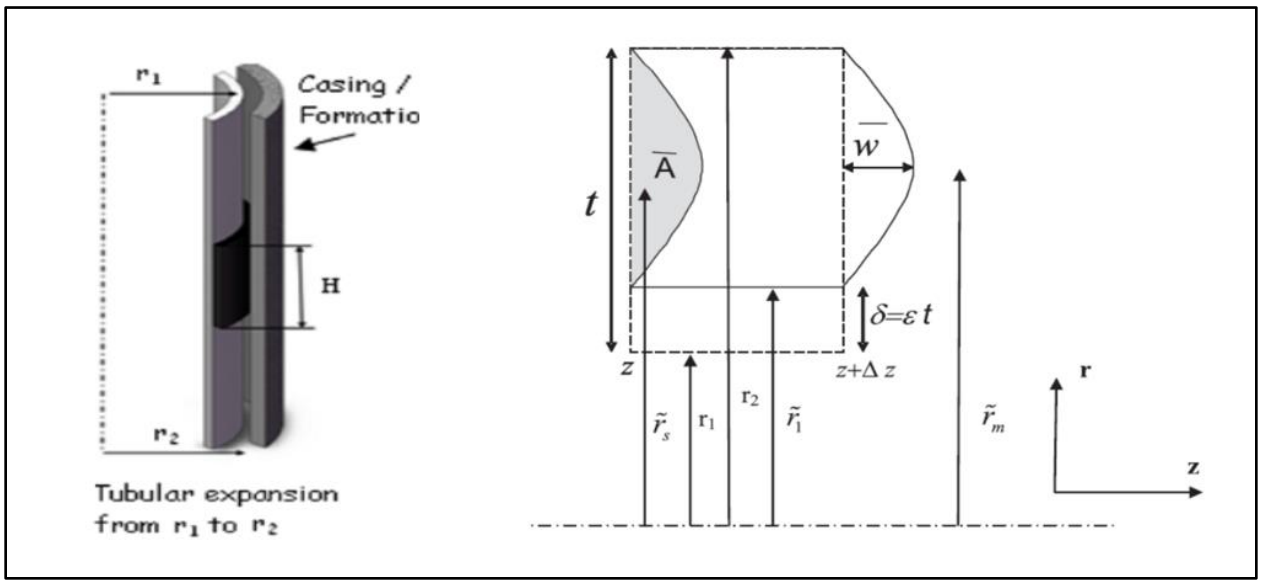

Figure 4.17: Elastomer seal radially confined between metal tubes (Al-Hiddabi et al. 2015)

THIS REPORT WAS INADVERTENTLY DISSEMINATED IN THE PUBLIC DOMAIN/ONLINE SINCE 12/2018 WITHOUT A DISCLAIMER. DISCLAIMER HAS BEEN ADDED – "THIS INFORMATION IS DISTRIBUTED SOLELY FOR THE PURPOSE OF PEER REVIEW UNDER APPLICABLE INFORMATION QUALITY GUIDELINES. IT HAS NOT BEEN FORMALLY DISSEMINATED BY BSEE. IT DOES NOT REPRESENT AND SHOULD NOT BE CONSTRUED TO REPRESENT ANY AGENCY DETERMINATION OR POLICY."

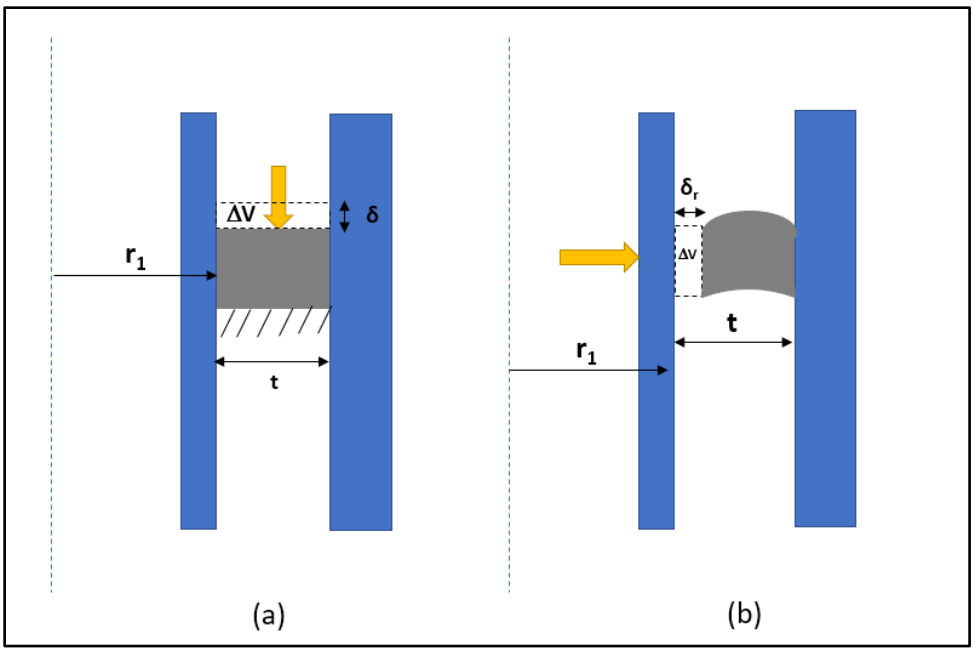

Figure 4.18: Comparison between the FEA model prepared in the present work (a) and the analytical model of Al-Hiddabi et al. (2015) (b)

As shown in Figure 4.18, the geometry and boundary conditions for analytical model developed by Al-Hiddabi et al. (2015) has some similarities to the FEA model developed in this report. Hence, the original contact pressure equation provided in the reference (Al-Hiddabi et al. 2015) can be modified and used to provide approximate validation of contact pressures simulated in this work. After adjusting relevant input parameters, the maximum contact pressure in our model can be estimated by,

$$P_{max} = \frac{(2\bar{r}_1+\bar{\delta}_r)\bar{\delta}_r K}{(2\bar{r}_1+1)} \quad \text{..... (20)}$$

where

$$\bar{r}_1 = \frac{r_1}{t}\ ,\ \bar{\delta}_r = \frac{\delta_r}{t}\ ,\quad and \quad K = \frac{E}{3(1-2\nu)}$$

In the above equations, P_{max} is the maximum contact pressure, K is bulk modulus, and ν is Poisson's ratio. As shown in Figure 4.18, r_1 is the outer radius of the liner, t is the radial width of the seal, and δ_r is radial compression. δ_r is such that the change in volume is equivalent to the change in volume caused by the compression ratio δ in our FEA model. P_{max} and K are in consistent units.

Next, contact pressures calculated from analytical equations (18) and (20) were compared with the values simulated by the FEA model. Both analytical equations yielded similar values. The comparison between analytical and FEA contact pressure values for different elastomers, at various compression ratio, and different Poisson's ratio is provided in Figure 4.19 and Figure 4.20.

THIS REPORT WAS INADVERTENTLY DISSEMINATED IN THE PUBLIC DOMAIN/ONLINE SINCE 12/2018 WITHOUT A DISCLAIMER. DISCLAIMER HAS BEEN ADDED – "THIS INFORMATION IS DISTRIBUTED SOLELY FOR THE PURPOSE OF PEER REVIEW UNDER APPLICABLE INFORMATION QUALITY GUIDELINES. IT HAS NOT BEEN FORMALLY DISSEMINATED BY BSEE. IT DOES NOT REPRESENT AND SHOULD NOT BE CONSTRUED TO REPRESENT ANY AGENCY DETERMINATION OR POLICY."

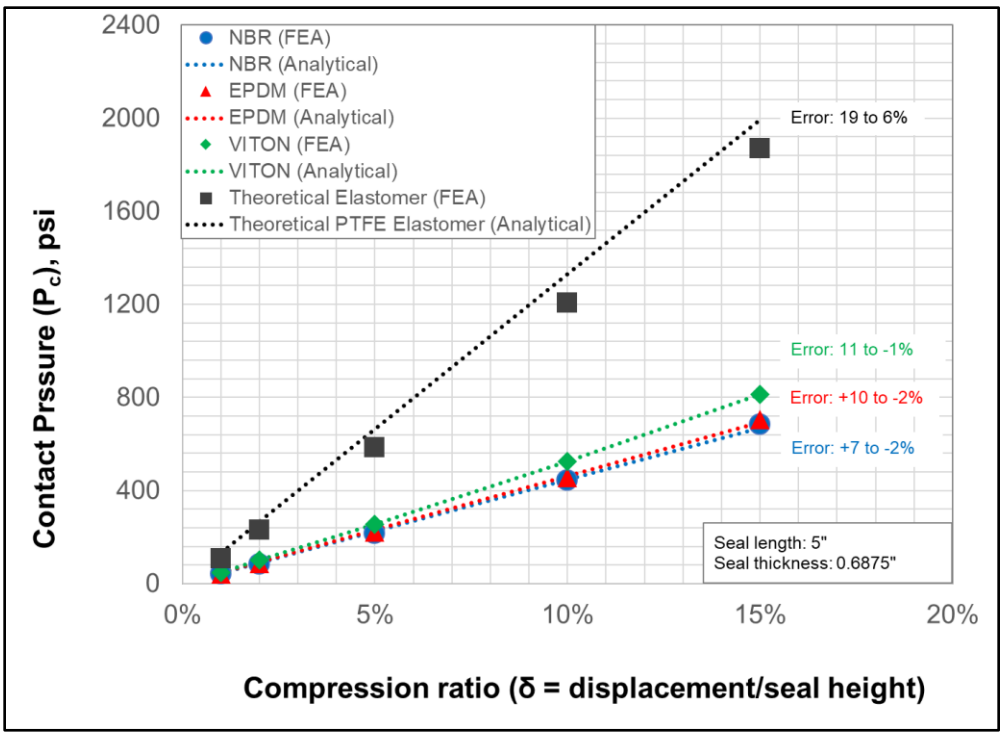

Figure 4.19: Comparison between FEA simulated and analytical contact pressure values for different elastomers at various compression ratios

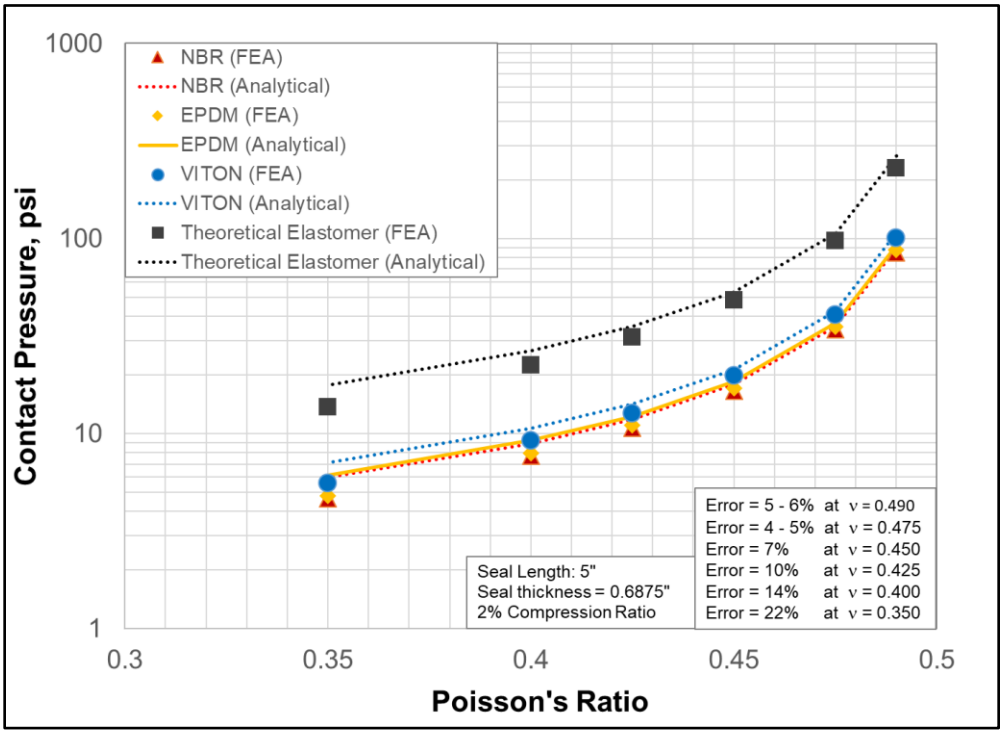

Figure 4.20: Comparison between FEA simulated and analytical contact pressure values for different elastomers at different Poisson's ratio

THIS REPORT WAS INADVERTENTLY DISSEMINATED IN THE PUBLIC DOMAIN/ONLINE SINCE 12/2018 WITHOUT A DISCLAIMER. DISCLAIMER HAS BEEN ADDED – "THIS INFORMATION IS DISTRIBUTED SOLELY FOR THE PURPOSE OF PEER REVIEW UNDER APPLICABLE INFORMATION QUALITY GUIDELINES. IT HAS NOT BEEN FORMALLY DISSEMINATED BY BSEE. IT DOES NOT REPRESENT AND SHOULD NOT BE CONSTRUED TO REPRESENT ANY AGENCY DETERMINATION OR POLICY."

It is clear from the Figures that the FEA results match reasonably well with the analytical solution. The error ranged from 7-22% at the lowest contact pressure values (low compression and Poisson's ratio) to 1-6% at high contact pressure values (high compression and Poisson's ratio). It should be noted that the analytical equations used are approximate and do not represent the exact compression mechanism and boundary conditions. Nonetheless, these results combined with the analytical validation of stresses in casing and liner certainly establish confidence in the FEA results.

4.1.11. FEA Model of Setup - 2

A special FEA model was prepared to confirm the experimental results obtained using setup – II of the project. The schematic of the model with dimensions and boundary conditions is provided in Figure 4.21. The actual setup II has two elastomer ring seals and three aluminum plates. Modelling that exact configuration would have resulted in too many contact regions and led to convergence issues. To mitigate the convergence issues, only one seal between two plates was used for the FEA model. This also helped to reduce the simulation time.

As shown in the Figure 4.21, seal energization was performed by applying displacement boundary conditions to the top of the aluminum plate. The displacement values used in the simulation were obtained from the setup II by measuring the approximate displacement using the scales attached to the pipe. Figure 4.22 is a graphical representation of the FEA before and after seal energization. The model setup and contact formulation were kept the same as discussed in section **3.1.** Material properties used to represent cast acrylic pipe and aluminum plate are listed in Table 4.5. The elastomer material properties are in Table 3.2 of section **3.1**.

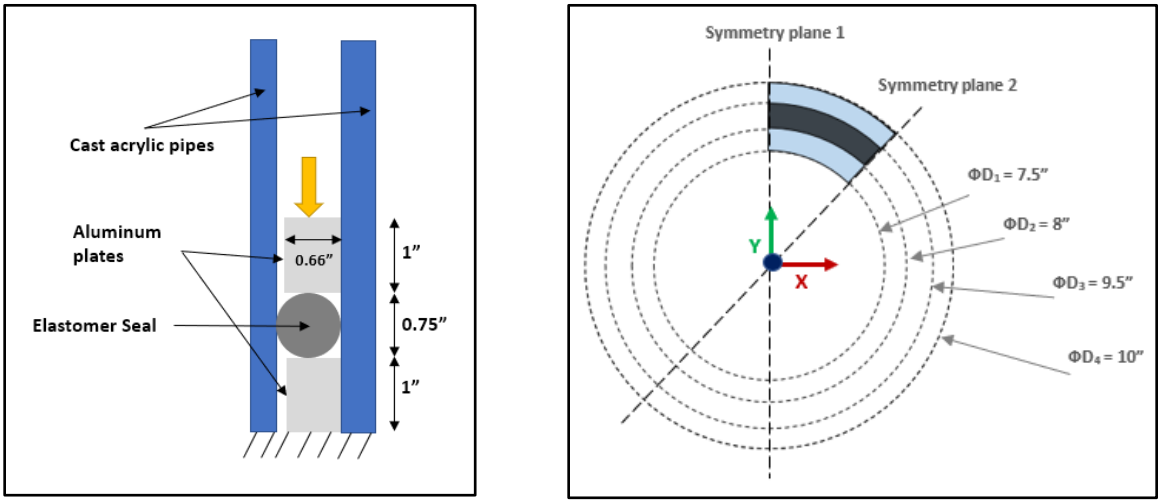

(a) **(b)**

Figure 4.21: Schematic and dimension of FEA model of setup II (a) 2D schematic in XZ plane. (b) top view of the model in XY plane

THIS REPORT WAS INADVERTENTLY DISSEMINATED IN THE PUBLIC DOMAIN/ONLINE SINCE 12/2018 WITHOUT A DISCLAIMER. DISCLAIMER HAS BEEN ADDED – "THIS INFORMATION IS DISTRIBUTED SOLELY FOR THE PURPOSE OF PEER REVIEW UNDER APPLICABLE INFORMATION QUALITY GUIDELINES. IT HAS NOT BEEN FORMALLY DISSEMINATED BY BSEE. IT DOES NOT REPRESENT AND SHOULD NOT BE CONSTRUED TO REPRESENT ANY AGENCY DETERMINATION OR POLICY."

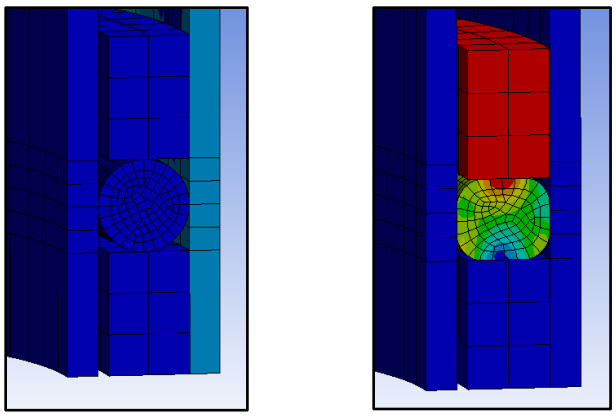

(a) (b)

Figure 4.22: Graphical representation of FEA model of setup II before (a) and after (b) seal energization

Table 4.5: Material properties for cast acrylic pipe and aluminum alloy plate used in FEA model of setup II

	Cast Acrylic Casing and Liner	Aluminum Alloy NL Plates
Young's Modulus	0.4 x 10^6 psi	10.29 X 10^6 psi
Poisson's ratio	0.37	0.33

For the EPDM elastomer seal, the effect of compression or displacement on contact pressure is graphically presented in Figure 4.23. It should be noted that there are four contact interfaces with the seal – two with aluminum plates and one each with liner and casing. The X- axis in the Figure 4.23, represents the location on seal in terms of degree angle 0°, 90°, 180°, 270°, and 360° which corresponds to seal-casing, seal-bottom plate, seal-liner, and seal-upper plate interfaces respectively. The Y-axis represents the corresponding contact pressure.

Contact pressure molded EPDM elastomer rings used in setup II were identified to have diameter approximately 1 mm greater than the annulus gap. Hence, the effect of seal interference or seal annular fit on contact pressure was examined. The summary of maximum contact pressure generated as a function of seal interference and externally applied displacement/compression is graphically presented in Figure 4.24. As expected, contact pressure is linearly correlated to displacement amount. The presence of interference leads to pre-stress condition and results in an intercept value at zero displacement.

The molded EPDM seal used in conducting tests on setup II had a diameter of 1 mm greater than the annular space. Inserting the seal into the setup led to a pre-stress condition and the system was observed to be gas tight when a 40 psig pressure injection test was performed in the absence of an external displacement application via bolts. This is confirmed by the FEA model which predicts contact pressure of 48 psi for the EPDM seal with 1 mm interference and 0 mm displacement application (See Figure 4.24).

THIS REPORT WAS INADVERTENTLY DISSEMINATED IN THE PUBLIC DOMAIN/ONLINE SINCE 12/2018 WITHOUT A DISCLAIMER. DISCLAIMER HAS BEEN ADDED – "THIS INFORMATION IS DISTRIBUTED SOLELY FOR THE PURPOSE OF PEER REVIEW UNDER APPLICABLE INFORMATION QUALITY GUIDELINES. IT HAS NOT BEEN FORMALLY DISSEMINATED BY BSEE. IT DOES NOT REPRESENT AND SHOULD NOT BE CONSTRUED TO REPRESENT ANY AGENCY DETERMINATION OR POLICY."

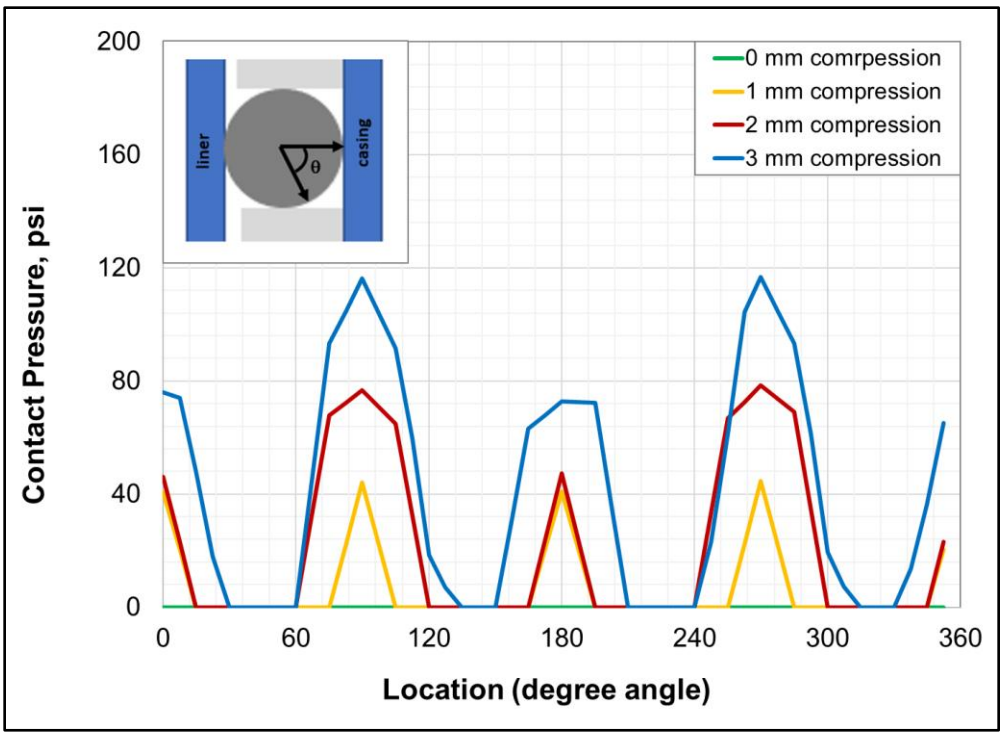

Figure 4.23: Contact pressure distribution ring along circular cross section for EPDM seal at various amount of compression

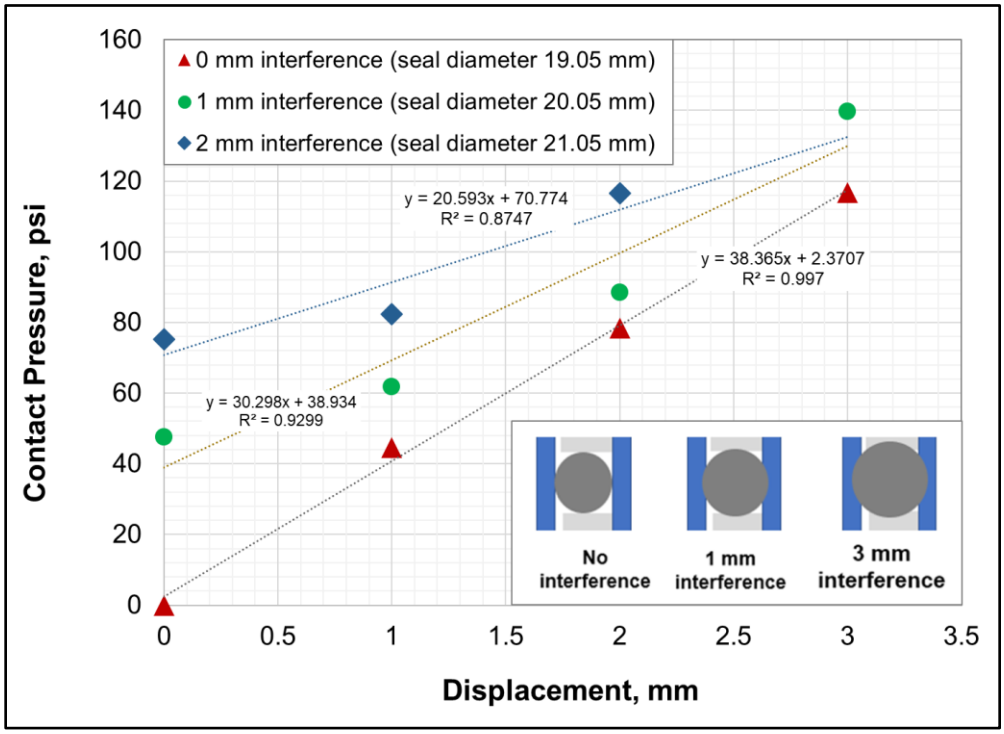

Figure 4.24: Effect of compression and interference on contact pressure at the seal – pipe interface for EPDM seal

THIS REPORT WAS INADVERTENTLY DISSEMINATED IN THE PUBLIC DOMAIN/ONLINE SINCE 12/2018 WITHOUT A DISCLAIMER. DISCLAIMER HAS BEEN ADDED – "THIS INFORMATION IS DISTRIBUTED SOLELY FOR THE PURPOSE OF PEER REVIEW UNDER APPLICABLE INFORMATION QUALITY GUIDELINES. IT HAS NOT BEEN FORMALLY DISSEMINATED BY BSEE. IT DOES NOT REPRESENT AND SHOULD NOT BE CONSTRUED TO REPRESENT ANY AGENCY DETERMINATION OR POLICY."

4.2. Cement Model

Unlike seal assembly, it is difficult to quantify sealability of cement and it is not sufficient to only examine the contact pressure at cement-pipe interface. To assess "fitness for service" of cement, it is important to evaluate the likelihood of radial debonding, radial crack, and shear failure. This was accomplished by performing a parametric analysis and examining the effect of various operational and design parameters on radial stress, hoop stress, and maximum shear stress at cement-liner interface.

Considering the scope of work and based on the literature review, it was decided to investigate the effect of 7 operational and design parameters – wellbore pressure, annulus pressure, height of cement sheath in liner overlap, radial width of set cement, 'annular fit' (i.e. radial width of set cement relative to annular gap), Young's modulus, and Poisson's ratio. Since the study is focused on offshore shallow depth wells, the effect of thermal stresses is not critical and temperature variation was not examined. The material properties of liner and casing were kept constant and are provided in section **3.1.1**.

Based on the analytical model discussed in section **2.1.1** and Appendix **A**, it is expected that in the presence of only internal pressure, the stresses generated at the cement-inner pipe interface are typically higher in magnitude than at cement-outer pipe interface. In our case, this means that the cement sheath is likely to fail at the cement-liner interface before the cement-casing interface. This trend was also observed in all the simulation runs in this study. Therefore, all the results discussed in the subsequent sections are based on the stresses generated at cement-liner interface. Moreover, to avoid end effects and also maintain consistency, each value of radial, hoop, and maximum shear stresses reported henceforth were observed at the middle of cement column at the cement-liner interface. Negative and positive sign represents compressive and tensile stress respectively.

4.2.1. Wellbore Pressure

Wellbore pressure or internal pipe pressure is the dominant load for a set cement in a shallow depth well. Once the cement sets, any change in wellbore pressure can induce stresses in the cement sheath. There are several possible reasons for change in wellbore pressure. For example, events such as a casing pressure test, formation integrity test, increased mud weight for subsequent drilling, perforation or stimulation operation etc. can lead to increase in wellbore pressure. On the other hand, fluid loss, gas kick while drilling, or production can reduce the wellbore pressure. The effect of change in wellbore pressure on radial, hoop, and maximum shear stresses for three different types of cement samples is presented in Figure 4.25**,** Figure 4.26**,** and Figure 4.27 respectively.

THIS REPORT WAS INADVERTENTLY DISSEMINATED IN THE PUBLIC DOMAIN/ONLINE SINCE 12/2018 WITHOUT A DISCLAIMER. DISCLAIMER HAS BEEN ADDED – "THIS INFORMATION IS DISTRIBUTED SOLELY FOR THE PURPOSE OF PEER REVIEW UNDER APPLICABLE INFORMATION QUALITY GUIDELINES. IT HAS NOT BEEN FORMALLY DISSEMINATED BY BSEE. IT DOES NOT REPRESENT AND SHOULD NOT BE CONSTRUED TO REPRESENT ANY AGENCY DETERMINATION OR POLICY."

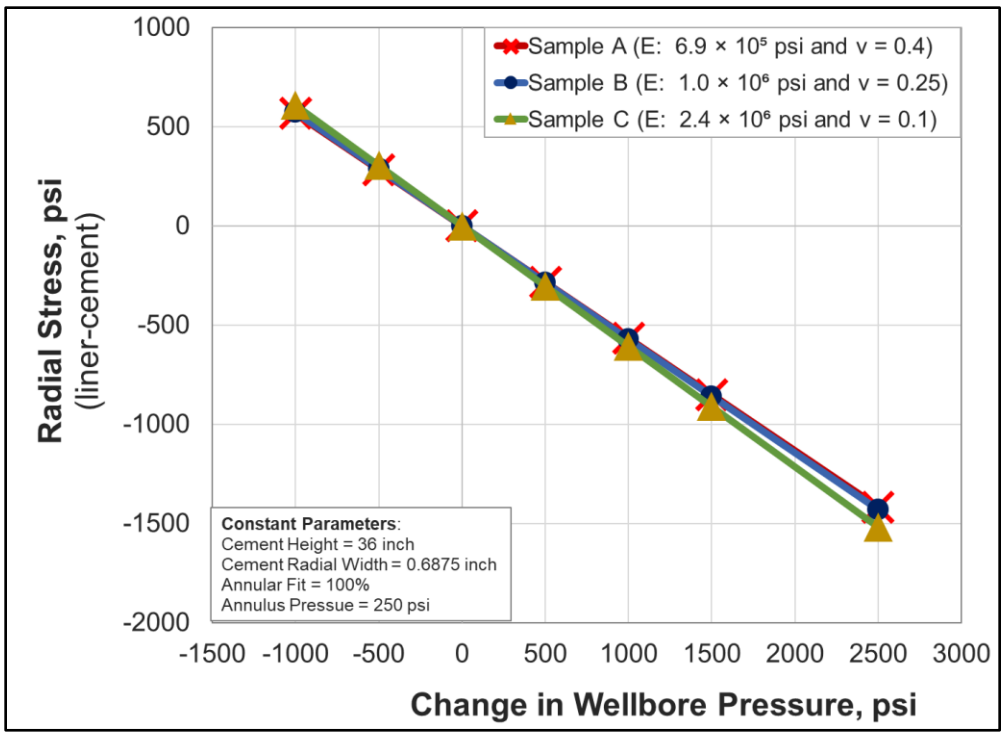

Figure 4.25: Effect of change in wellbore pressure on radial stress in cement at liner-cement interface

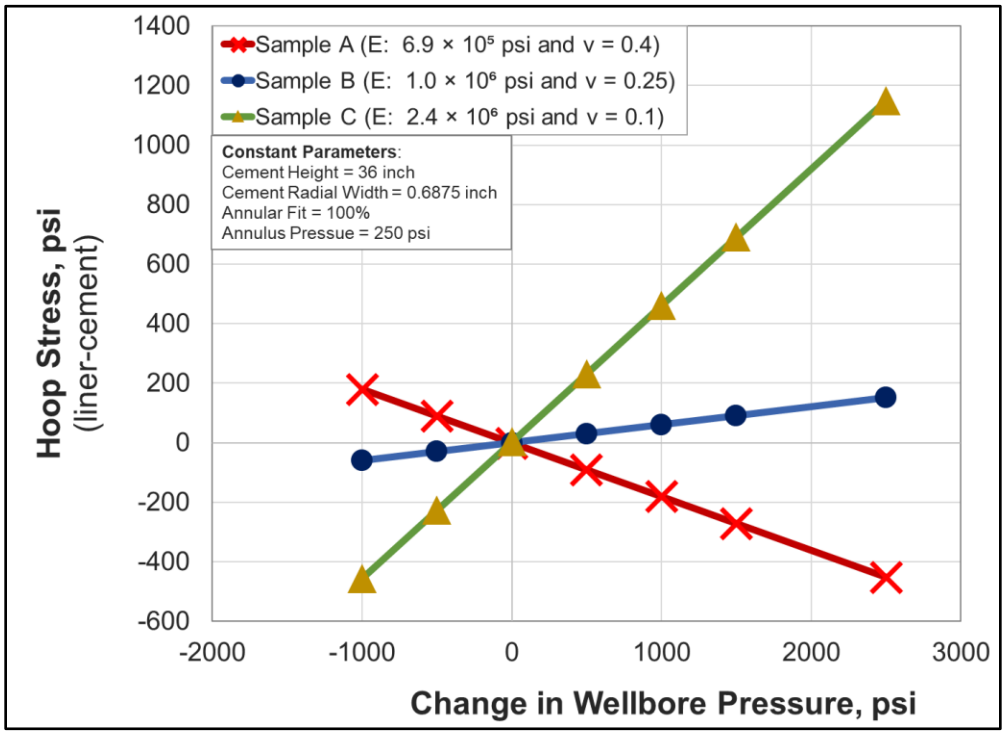

Figure 4.26: Effect of change in wellbore pressure on hoop stress in cement at liner-cement interface

THIS REPORT WAS INADVERTENTLY DISSEMINATED IN THE PUBLIC DOMAIN/ONLINE SINCE 12/2018 WITHOUT A DISCLAIMER. DISCLAIMER HAS BEEN ADDED – "THIS INFORMATION IS DISTRIBUTED SOLELY FOR THE PURPOSE OF PEER REVIEW UNDER APPLICABLE INFORMATION QUALITY GUIDELINES. IT HAS NOT BEEN FORMALLY DISSEMINATED BY BSEE. IT DOES NOT REPRESENT AND SHOULD NOT BE CONSTRUED TO REPRESENT ANY AGENCY DETERMINATION OR POLICY."

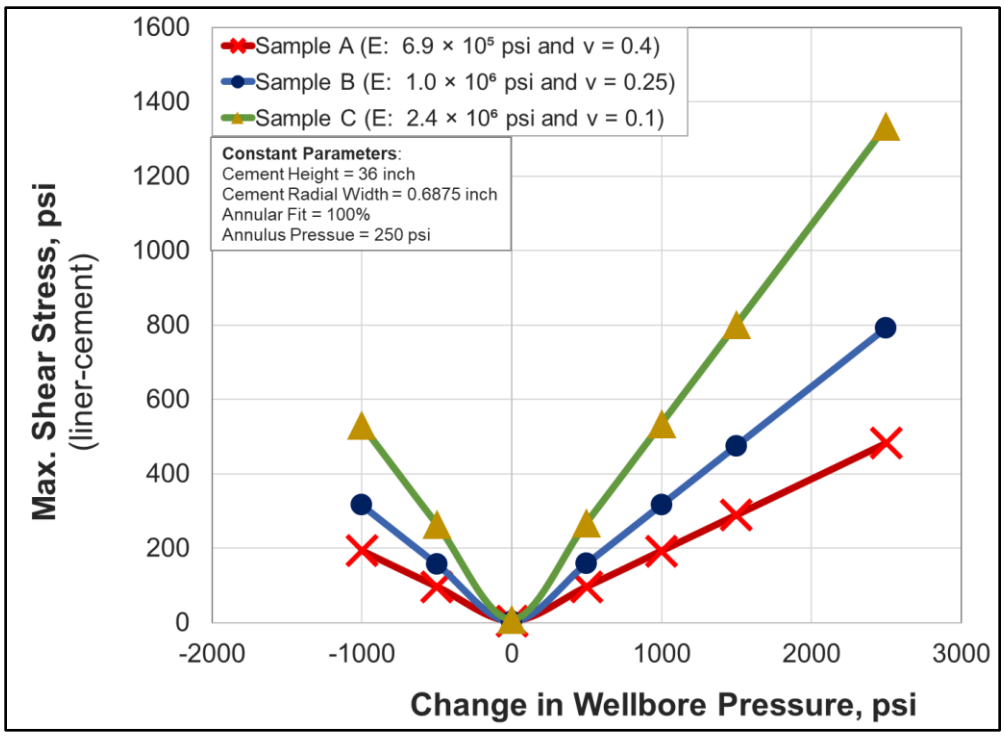

Figure 4.27: Effect of change in wellbore pressure on maximum shear stress in cement at liner-cement interface

Radial Stress

As shown in Figure 4.25, change in wellbore pressure is linearly correlated to radial stress. Any increase in wellbore pressure after the cement sets, causes development of compressive (negative) radial stress at the liner-cement interface. The magnitude increases linearly with further increase in pressure. This eliminates the risk of debonding but introduces risk of failure by compressive or stress crushing with a likelihood that depends on compressive strength of the cement. Any decrease in pressure however, introduces tensile radial stress at the interface. If the pressure reduction is large enough to cause radial stress higher than the tensile strength of the cement, then it can lead to radial debonding.

Upon closer inspection, the effect of wellbore pressure on radial stress is high in case of brittle cement (Sample C) and low for more ductile cement (Sample A). The difference among three samples is however not huge for low pressure variations.

Hoop Stress

Similar to radial stress, hoop stress is linearly correlated with changes in wellbore pressure. Sample B has the highest robustness to change in wellbore pressure followed by sample A and then Sample C. Interestingly, the direction of resultant hoop stress is dependent on cement material properties. Under the condition of increasing wellbore pressure, only samples B and C are susceptible to radial

THIS REPORT WAS INADVERTENTLY DISSEMINATED IN THE PUBLIC DOMAIN/ONLINE SINCE 12/2018 WITHOUT A DISCLAIMER. DISCLAIMER HAS BEEN ADDED – "THIS INFORMATION IS DISTRIBUTED SOLELY FOR THE PURPOSE OF PEER REVIEW UNDER APPLICABLE INFORMATION QUALITY GUIDELINES. IT HAS NOT BEEN FORMALLY DISSEMINATED BY BSEE. IT DOES NOT REPRESENT AND SHOULD NOT BE CONSTRUED TO REPRESENT ANY AGENCY DETERMINATION OR POLICY."

cracking if hoop stress exceeds their tensile strength limit. The ductile cement (sample A) is prone to radial cracking only under the condition of decreasing wellbore pressure.

This opposite effect can be attributed to Poisson's ratio. Sample A has high Poisson's ratio of 0.4 and the applied radial pressure results in high axial deformation which dominates hoop stress and is compressive in nature due to zero displacement boundary conditions applied to the ends of the cement and pipes. For the same wellbore pressure and a low Poisson's ratio of 0.1 (Sample C), the axial deformation is very low and tensile hoop stress is still dominant. Sample B has near optimum material properties and it shows the highest robustness to wellbore pressure compared to the other two samples.

Maximum Shear Stress

Shear failure occurs when the maximum shear stress exceeds the critical value or shear strength of cement. As shown in Figure 4.27, the maximum shear stress is also linearly correlated with change in wellbore pressure. It should be noted that its value does not depend on the direction of pressure change. It is clearly indicated in the figure that as cement becomes more brittle (Sample A to Sample C), the robustness of maximum shear stress to wellbore pressure decreases. This is because the shear modulus decreases from Sample A towards Sample C. In other words, the sample with low Poisson's ratio, has a higher difference between maximum principle and minimum principle stress compared to a sample with higher Poisson's ratio.

The effect of change in wellbore pressure on radial, hoop, and maximum shear stresses can be quantified in terms of change in stress value per unit change in pressure. The summary of all the three stresses discussed above is provided in Table 4.6,

Table 4.6: Effect of change in wellbore pressure on radial, hoop, and maximum shear stress at liner-cement interface

Cement Sample	$\Delta\sigma_r/\Delta P_{wellbore}$	$\Delta\sigma_\theta/\Delta P_{wellbore}$	$\Delta\tau_{max}/\lvert\Delta P_{wellbore}\rvert$
Sample A (E: 6.9×10^5 psi and $\nu = 0.4$)	-0.5667	-0.1805	0.1918
Sample B (E: 1.0×10^6 psi and $\nu = 0.25$)	-0.5727	0.0608	0.3158
Sample C (E: 2.4×10^6 psi and $\nu = 0.1$)	- 0.6075	0.4586	0.5310

This table provides valuable information. The ductile cement has the least sensitivity to wellbore pressure in radial and shear stress. This means that hypothetically, if all three cement samples had same tensile, compressive, and shear strengths, then the ductile cement (Sample A) would have the least likelihood of radial (debonding/stress crushing) and shear failure. Sample B (cement with

THIS REPORT WAS INADVERTENTLY DISSEMINATED IN THE PUBLIC DOMAIN/ONLINE SINCE 12/2018 WITHOUT A DISCLAIMER. DISCLAIMER HAS BEEN ADDED – "THIS INFORMATION IS DISTRIBUTED SOLELY FOR THE PURPOSE OF PEER REVIEW UNDER APPLICABLE INFORMATION QUALITY GUIDELINES. IT HAS NOT BEEN FORMALLY DISSEMINATED BY BSEE. IT DOES NOT REPRESENT AND SHOULD NOT BE CONSTRUED TO REPRESENT ANY AGENCY DETERMINATION OR POLICY."

low Young's modulus and low Poisson's ratio) exhibits the least sensitivity to pressure change when it comes to hoop stress and might be preferred.

Even though it seems like ductile cement should be the preferred choice, it should be noted that, in reality, uniaxial strengths usually tend to be smaller for ductile cement and higher for brittle cement. Hence, selection should be based on specific situations.

The Table 4.6 can be useful in examining the likelihood of failure under a specific loading condition. For increasing wellbore pressure of 1000 psi, the hoop stress in brittle cement system is 459 psi. For example, this is more than the tensile strength (429 psi) of a neat class H cement - a brittle cement with similar material properties (Iverson et al. 2008). Wellbore pressure increase of 1000 psi is not huge and is not unusual for a positive pressure test.

Consider two example loading conditions –(i) pressure increase of 2500 psi and (ii) pressure decrease of 2500 psi and compare likelihood of failure in the cement samples by calculating safety factor. The tensile and compressive strength of the cement samples used is provided in Table 3.3. For shear failure, the simplest form of Tresca criteria will be used (section **2.2.2**). The calculated safety factors are provided in Table 4.7.

It is clear from the Table 4.7 that, the ductile cement (Sample A) would fail by radial debonding when wellbore pressure reduces by 2500 psi. Sample B would fail next. Overall, reduction in wellbore pressure is more detrimental than increasing pressure when it comes to radial debonding. Shear failure is not dependent on the direction of pressure change. In the case of radial cracking, increment in pressure is more detrimental for brittle cement and pressure reduction is more detrimental for ductile cement.

Table 4.7: Comparison of likelihood of cement failure for wellbore pressure change of 2500 psi

Cement	$\Delta P_{wellbore}$ = 2500 psi			$\Delta P_{wellbore}$ = - 2500 psi		
	$SF_{debonding}$	$SF_{radial\ cracking}$	SF_{shear}	$SF_{debonding}$	$SF_{radial\ cracking}$	SF_{shear}
Sample A	2.1	6.6	3.1	0.7	2.2	3.1
Sample B	3.1	9.9	2.8	1.0	29.6	2.8
Sample C	6.3	2.6	3.6	2.0	8.3	3.6

4.2.2. Annulus Pressure

Annulus pressure in the liner overlap (between the liner and casing) is exerted by the completion fluid or pre-flush fluid circulated before cementing and lying on top of the set cement column. The annulus pressure is usually less than the wellbore pressure and should not change unless under

THIS REPORT WAS INADVERTENTLY DISSEMINATED IN THE PUBLIC DOMAIN/ONLINE SINCE 12/2018 WITHOUT A DISCLAIMER. DISCLAIMER HAS BEEN ADDED – "THIS INFORMATION IS DISTRIBUTED SOLELY FOR THE PURPOSE OF PEER REVIEW UNDER APPLICABLE INFORMATION QUALITY GUIDELINES. IT HAS NOT BEEN FORMALLY DISSEMINATED BY BSEE. IT DOES NOT REPRESENT AND SHOULD NOT BE CONSTRUED TO REPRESENT ANY AGENCY DETERMINATION OR POLICY."

some special circumstances such as significant gravity segregation of solid particles in the fluid column or fluid influx from the top through the seal assembly. The effect of change in annulus pressure on radial, hoop, and maximum shear stresses for three different types of cement samples is presented in Figure 4.28, Figure 4.29**,** and Figure 4.30 respectively**.**

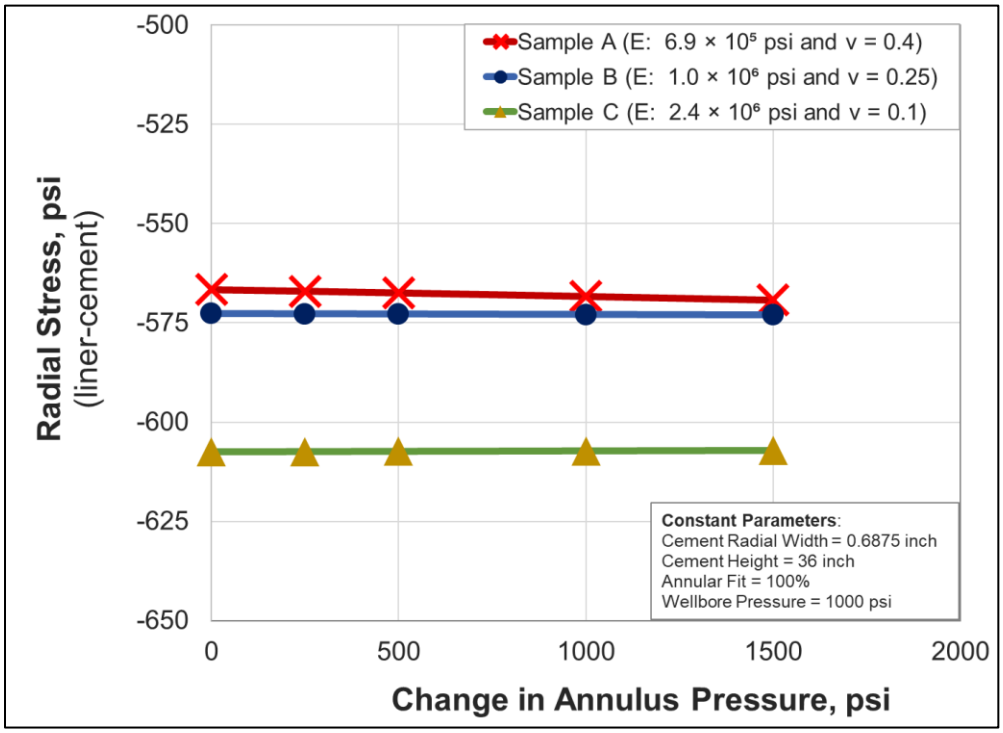

Figure 4.28: Effect of change in annulus pressure on radial stress in cement at liner-cement interface

THIS REPORT WAS INADVERTENTLY DISSEMINATED IN THE PUBLIC DOMAIN/ONLINE SINCE 12/2018 WITHOUT A DISCLAIMER. DISCLAIMER HAS BEEN ADDED – "THIS INFORMATION IS DISTRIBUTED SOLELY FOR THE PURPOSE OF PEER REVIEW UNDER APPLICABLE INFORMATION QUALITY GUIDELINES. IT HAS NOT BEEN FORMALLY DISSEMINATED BY BSEE. IT DOES NOT REPRESENT AND SHOULD NOT BE CONSTRUED TO REPRESENT ANY AGENCY DETERMINATION OR POLICY."

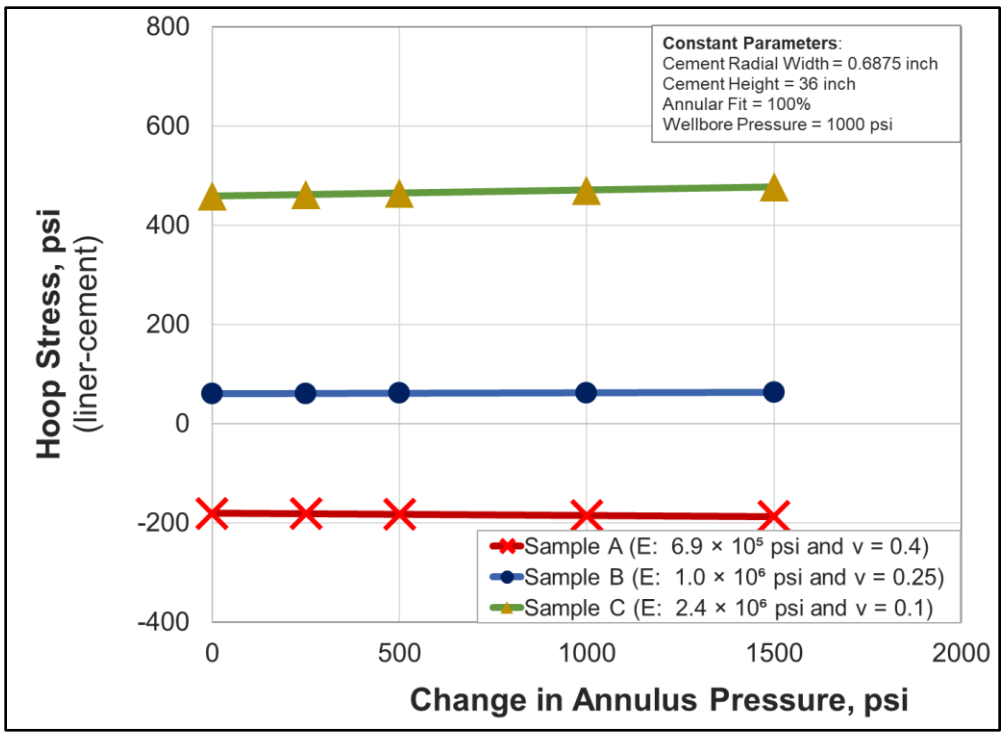

Figure 4.29: Effect of change in annulus pressure on hoop stress in cement at liner-cement interface

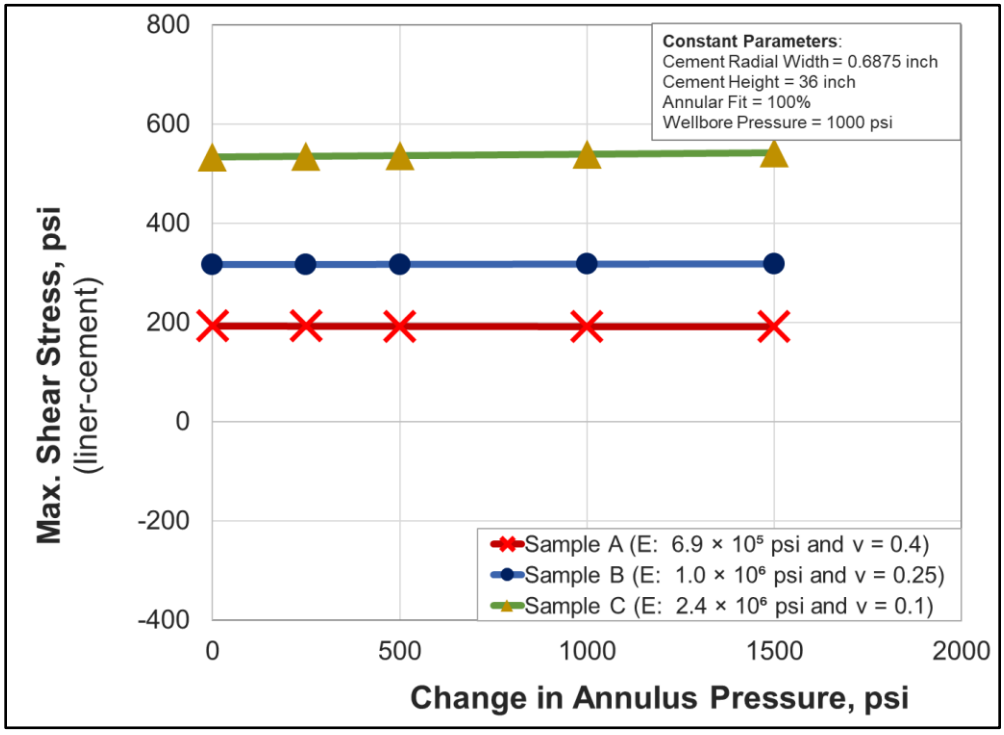

Figure 4.30: Effect of change in annulus pressure on maximum shear stress in cement at liner-cement interface

THIS REPORT WAS INADVERTENTLY DISSEMINATED IN THE PUBLIC DOMAIN/ONLINE SINCE 12/2018 WITHOUT A DISCLAIMER. DISCLAIMER HAS BEEN ADDED – "THIS INFORMATION IS DISTRIBUTED SOLELY FOR THE PURPOSE OF PEER REVIEW UNDER APPLICABLE INFORMATION QUALITY GUIDELINES. IT HAS NOT BEEN FORMALLY DISSEMINATED BY BSEE. IT DOES NOT REPRESENT AND SHOULD NOT BE CONSTRUED TO REPRESENT ANY AGENCY DETERMINATION OR POLICY."

The results indicate that there is practically no effect of changes in annulus pressure on radial, hoop, and maximum shear stresses. This is not surprising because the cement sheath is modelled to be bonded with both liner and casing which does not permit sliding or separation and there is restriction on axial displacement. Moreover, the annulus pressure is not high enough to cause a ballooning of annulus, push liner and casing apart, and develop radial stresses at contact interfaces. These results were also confirmed by modelling contacts as the 'rough' type which allows them to separate.

4.2.3. Cement Sheath Height

Often, the liner overlap is not cemented all the way to the top of liner. It is logical that having more of a cement column in the annulus is beneficial as it increases the length of permeable path within the cement and help resist or delay fluid flow. Nonetheless, the purpose of varying height of cement column was to examine whether it affects mechanical stresses and consequently structural failure within the cement. The effect of changes in the cement sheath height on radial, hoop, and maximum shear stresses for three different types of cement samples is presented in Figure 4.31, Figure 4.32, and Figure 4.33 respectively.

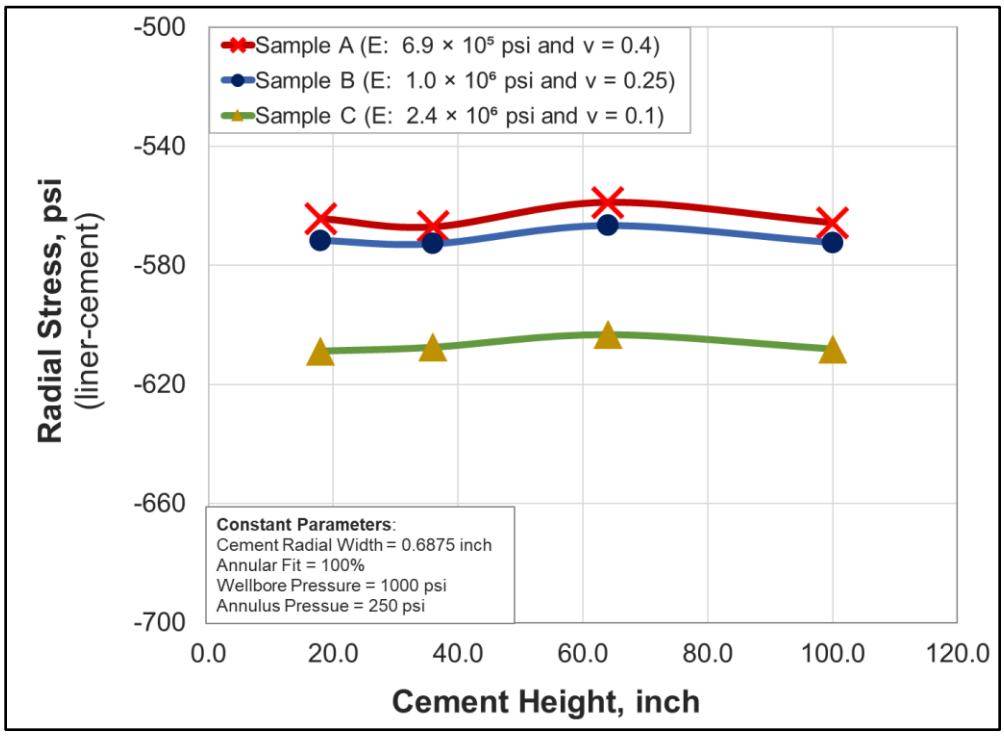

Figure 4.31: Effect of cement sheath height on radial stress in cement at liner-cement interface

THIS REPORT WAS INADVERTENTLY DISSEMINATED IN THE PUBLIC DOMAIN/ONLINE SINCE 12/2018 WITHOUT A DISCLAIMER. DISCLAIMER HAS BEEN ADDED – "THIS INFORMATION IS DISTRIBUTED SOLELY FOR THE PURPOSE OF PEER REVIEW UNDER APPLICABLE INFORMATION QUALITY GUIDELINES. IT HAS NOT BEEN FORMALLY DISSEMINATED BY BSEE. IT DOES NOT REPRESENT AND SHOULD NOT BE CONSTRUED TO REPRESENT ANY AGENCY DETERMINATION OR POLICY."

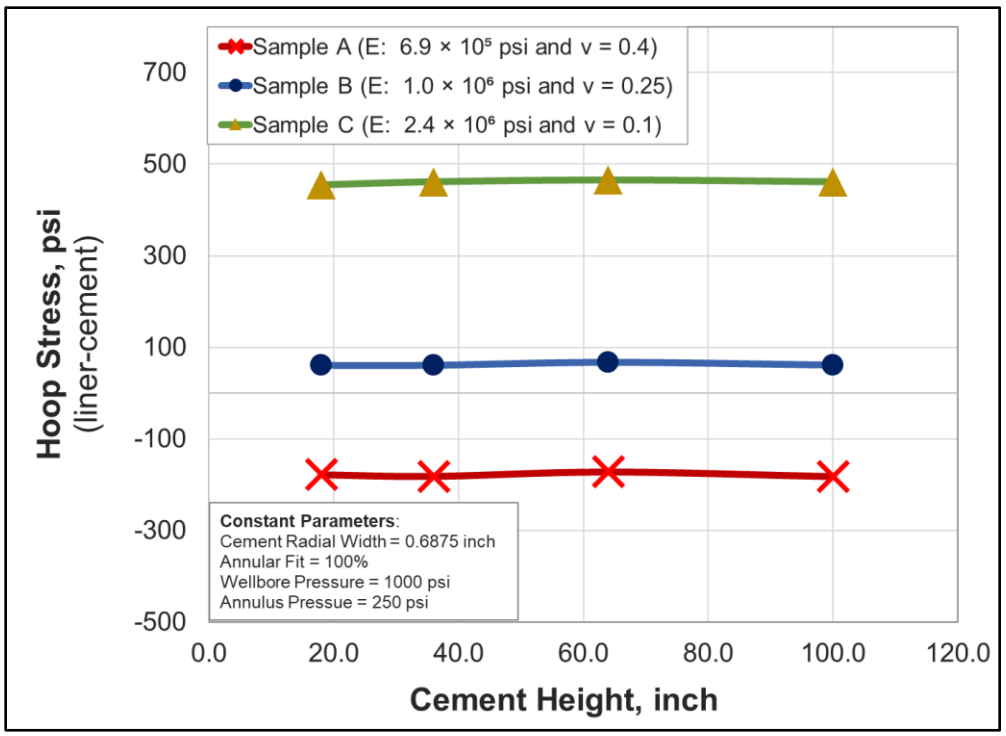

Figure 4.32: Effect of cement sheath height on hoop stress in cement at liner-cement interface

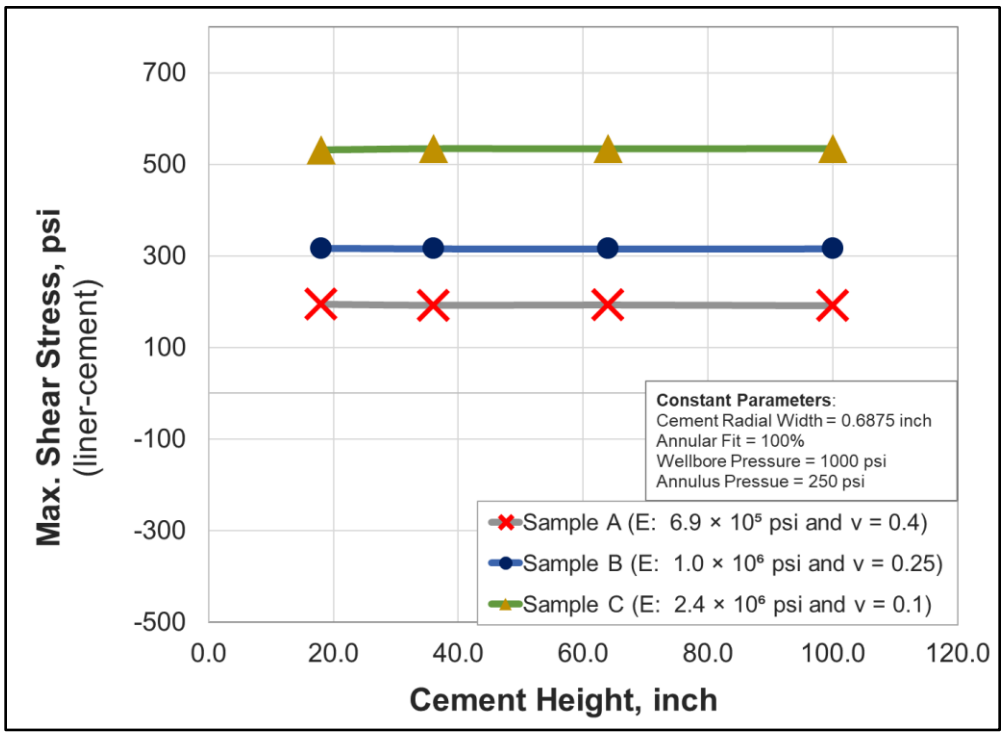

Figure 4.33: Effect of cement sheath height on maximum shear stress in cement at liner-cement interface

Similar to annulus pressure, it is clear that there is no apparent effect of changing the cement height on the stresses developed at liner-cement interface. Change in cement height can affect the end

THIS REPORT WAS INADVERTENTLY DISSEMINATED IN THE PUBLIC DOMAIN/ONLINE SINCE 12/2018 WITHOUT A DISCLAIMER. DISCLAIMER HAS BEEN ADDED – "THIS INFORMATION IS DISTRIBUTED SOLELY FOR THE PURPOSE OF PEER REVIEW UNDER APPLICABLE INFORMATION QUALITY GUIDELINES. IT HAS NOT BEEN FORMALLY DISSEMINATED BY BSEE. IT DOES NOT REPRESENT AND SHOULD NOT BE CONSTRUED TO REPRESENT ANY AGENCY DETERMINATION OR POLICY."

stresses near the top and bottom of cement. However, the stresses at the middle of cement should be free of end effects and independent of cement length. An additional explanation for this result is the presence of bonded type contact between the cement and the liner/casing. This type of contact, similar to adhesion, does not permit any displacement. Modelling contact pairs as 'rough' and permitting separation did not change the results.

4.2.4. Cement Radial Width

Cement radial width (i.e. thickness) of the cement sheath was varied to account for various casing programs and investigate its effect on potential failures. The outer radius of cement was kept constant while the inner radius was varied. The thickness of the liner and the casing were kept constant. The effects of changes in the cement width on radial, hoop, and maximum shear stresses for three different types of cement samples is presented in Figure 4.34, Figure 4.35, and Figure 4.36 respectively.

As expected, increases in cement width resulted in a decrease in magnitude of all three stresses. This means that the tensile stress became less tensile and compressive stress became less compressive. However, each consecutive change was approximately less than 5% meaning there is no practical advantage of having a thicker sheath in terms of reducing the likelihood of failure.

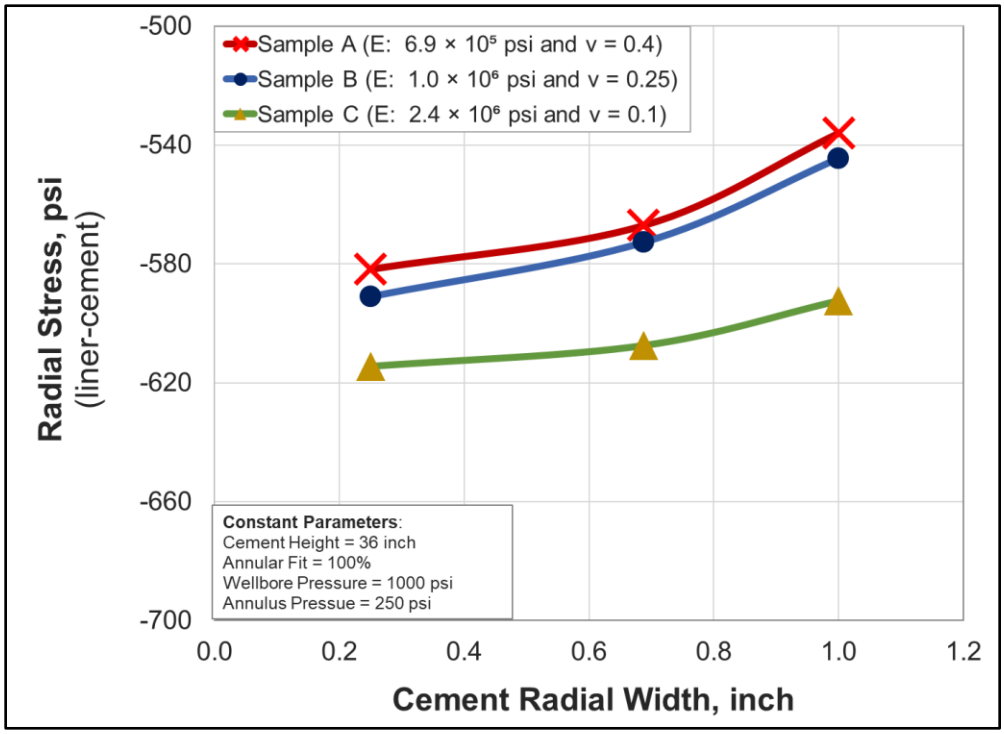

Figure 4.34: Effect of cement radial width on radial stress in cement at liner-cement interface

THIS REPORT WAS INADVERTENTLY DISSEMINATED IN THE PUBLIC DOMAIN/ONLINE SINCE 12/2018 WITHOUT A DISCLAIMER. DISCLAIMER HAS BEEN ADDED – "THIS INFORMATION IS DISTRIBUTED SOLELY FOR THE PURPOSE OF PEER REVIEW UNDER APPLICABLE INFORMATION QUALITY GUIDELINES. IT HAS NOT BEEN FORMALLY DISSEMINATED BY BSEE. IT DOES NOT REPRESENT AND SHOULD NOT BE CONSTRUED TO REPRESENT ANY AGENCY DETERMINATION OR POLICY."

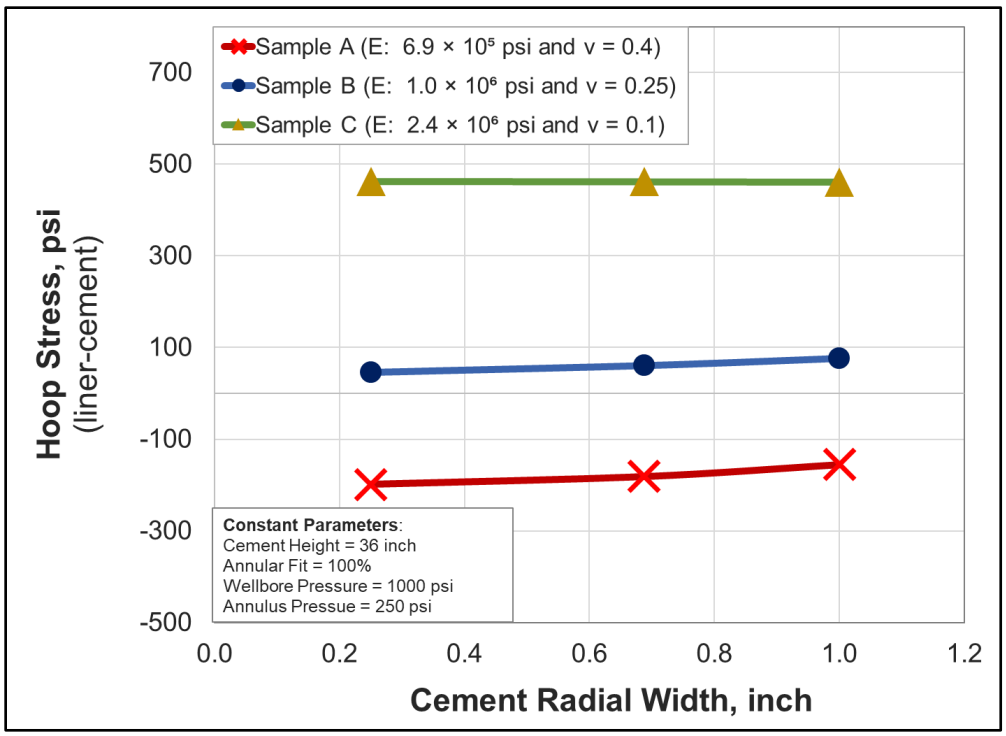

Figure 4.35: Effect of cement radial width on hoop stress in cement at liner-cement interface

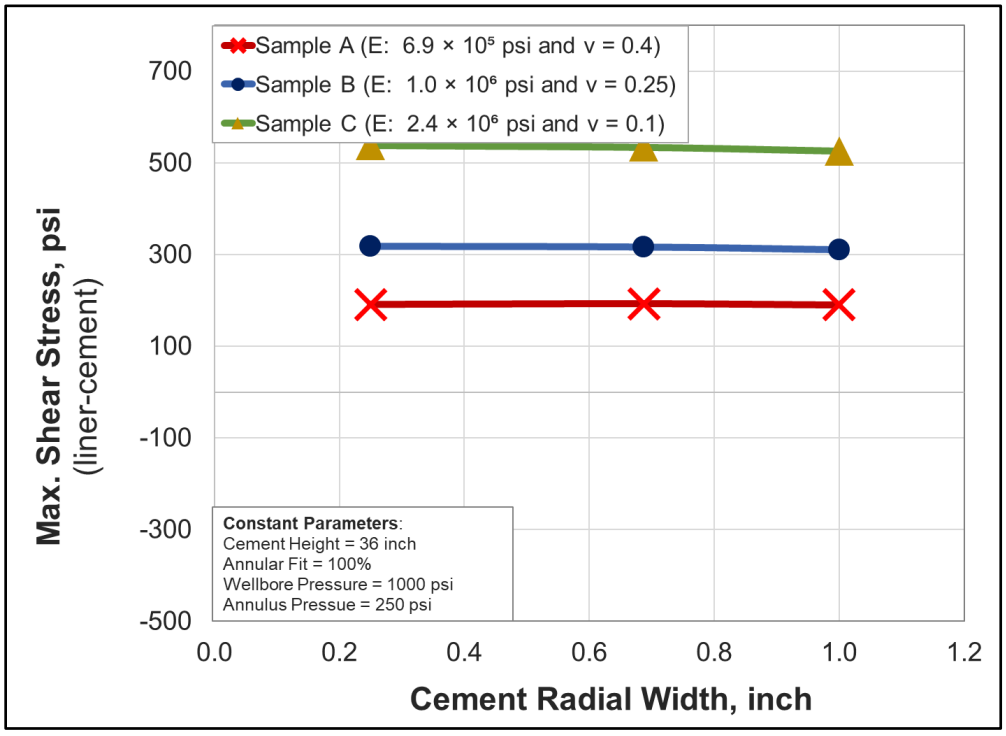

Figure 4.36: Effect of cement radial width on maximum shear stress in cement at liner-cement interface

THIS REPORT WAS INADVERTENTLY DISSEMINATED IN THE PUBLIC DOMAIN/ONLINE SINCE 12/2018 WITHOUT A DISCLAIMER. DISCLAIMER HAS BEEN ADDED – "THIS INFORMATION IS DISTRIBUTED SOLELY FOR THE PURPOSE OF PEER REVIEW UNDER APPLICABLE INFORMATION QUALITY GUIDELINES. IT HAS NOT BEEN FORMALLY DISSEMINATED BY BSEE. IT DOES NOT REPRESENT AND SHOULD NOT BE CONSTRUED TO REPRESENT ANY AGENCY DETERMINATION OR POLICY."

4.2.5. Cement Annular Fit

Cement annular fit is defined as its radial width relative to the annular gap between the liner and the cement. As shown in Figure 4.37, annular fit less than 1 (or 100%) means that the cement sheath is thinner than the annular gap between the pipes. Annular fit more than 1 (or 100%) corresponds to a pre-stress condition within the cement. This parameter will help analyze two distinct conditions: (i) presence of uniform micro-annulus along the liner due to volume shrinkage in set cement, insufficient mud removal, or trapped fluid pressure during setting process and (ii) expansive cement (or pre-stressed cement) versus conventional cement.

In all simulations, wellbore and annulus pressure of 1000 psi and 250 psi were applied after setting of the cement. The annular fit was varied from 99% to 101%. The width of gap or channel along the liner corresponding to 99% and 99.5% annular fit is 175 μm and 87 μm respectively. The annular fit of 100.5% and 101% corresponds to contact stress of approximately 350 psi and 700 psi respectively at the liner-cement interface. For these four different annular fit cases, simulated radial, hoop, and maximum shear stresses are graphically presented in Figure 4.38, Figure 4.39, and Figure 4.40 respectively.

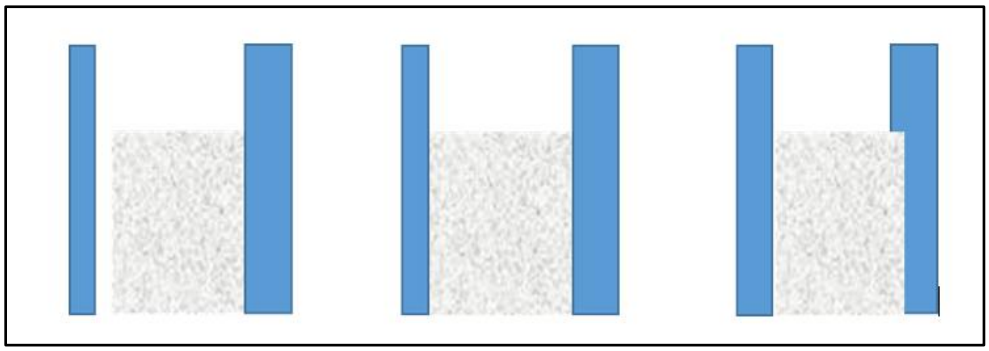

Figure 4.37: Graphical representation of models with different annular fit of cement

THIS REPORT WAS INADVERTENTLY DISSEMINATED IN THE PUBLIC DOMAIN/ONLINE SINCE 12/2018 WITHOUT A DISCLAIMER. DISCLAIMER HAS BEEN ADDED – "THIS INFORMATION IS DISTRIBUTED SOLELY FOR THE PURPOSE OF PEER REVIEW UNDER APPLICABLE INFORMATION QUALITY GUIDELINES. IT HAS NOT BEEN FORMALLY DISSEMINATED BY BSEE. IT DOES NOT REPRESENT AND SHOULD NOT BE CONSTRUED TO REPRESENT ANY AGENCY DETERMINATION OR POLICY."

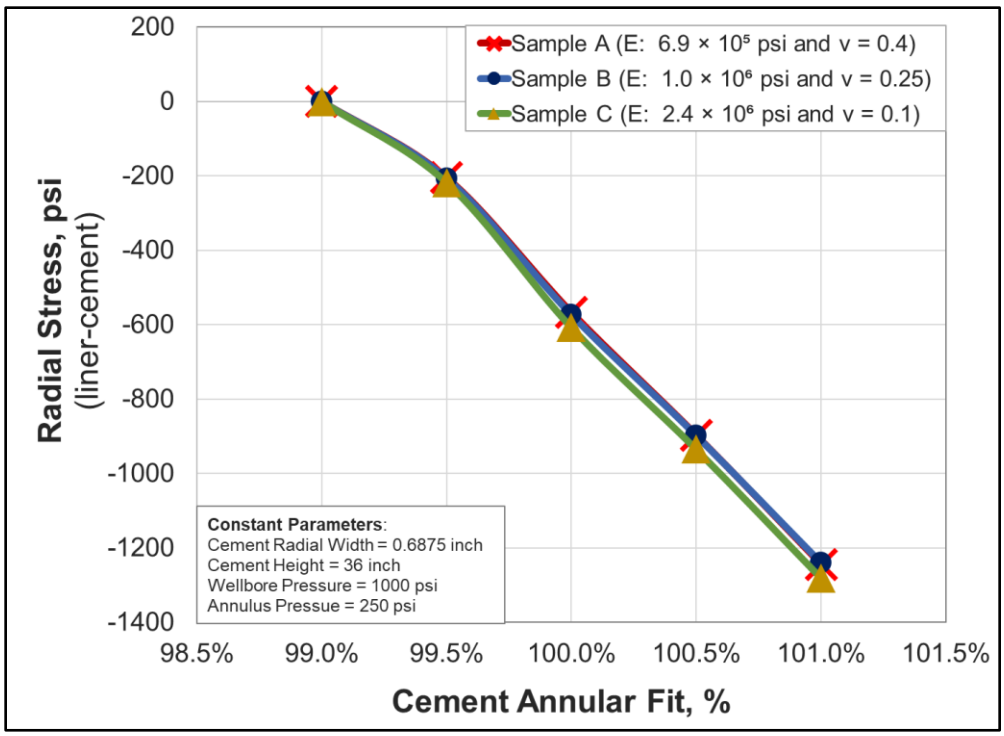

Figure 4.38: Effect of cement annular fit on radial stress in cement at liner-cement interface

As shown in Figure 4.38, all three stresses are zero at annular fit of 99%; indicating that there is no contact established between the liner and the cement. This means that the application of 1000 psi wellbore pressure does not cause sufficient ballooning of the liner to close the gap of 175 μm. Interestingly, in the case of 99.5% annular fit, the 1000 psi wellbore pressure was able to cause sufficient ballooning of the liner to close the gap of 87 μm and achieve contact. Once contact is established, the values of stresses are in accordance with the results obtained in section **4.2.1.** An interesting outcome from this simulation was the observation that theoretically, it is not impossible to have small micro-annuli in set cement masked during a 30-minute pressure test.

THIS REPORT WAS INADVERTENTLY DISSEMINATED IN THE PUBLIC DOMAIN/ONLINE SINCE 12/2018 WITHOUT A DISCLAIMER. DISCLAIMER HAS BEEN ADDED – "THIS INFORMATION IS DISTRIBUTED SOLELY FOR THE PURPOSE OF PEER REVIEW UNDER APPLICABLE INFORMATION QUALITY GUIDELINES. IT HAS NOT BEEN FORMALLY DISSEMINATED BY BSEE. IT DOES NOT REPRESENT AND SHOULD NOT BE CONSTRUED TO REPRESENT ANY AGENCY DETERMINATION OR POLICY."

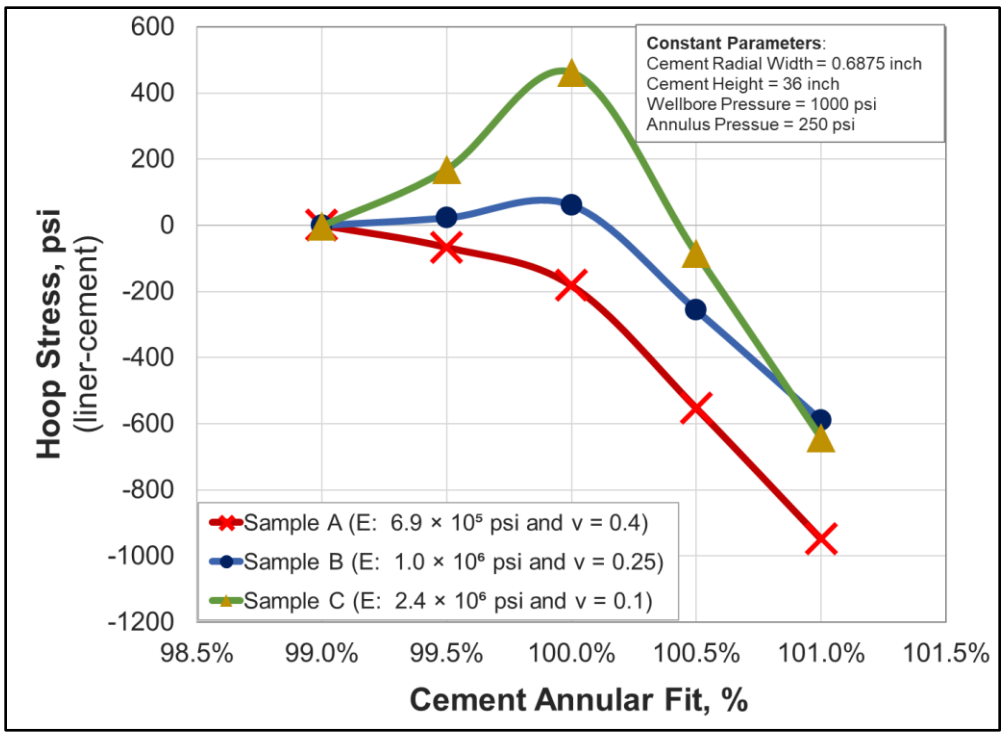

Figure 4.39: Effect of cement annular fit on hoop stress in cement at liner-cement interface

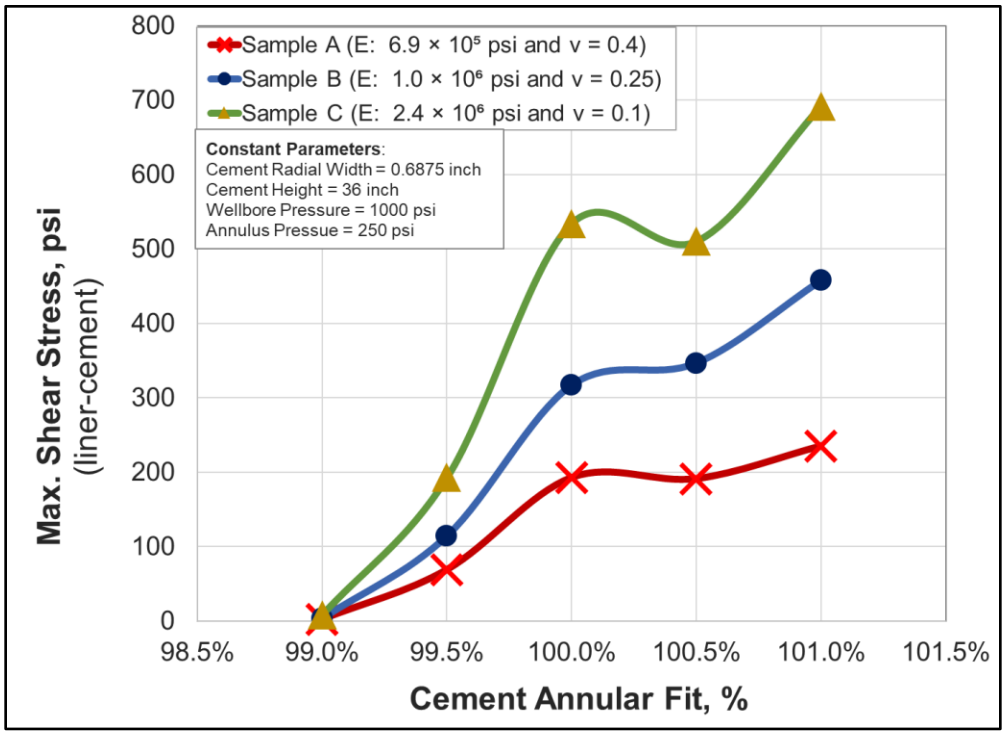

Figure 4.40: Effect of cement annular fit on maximum shear stress in cement at liner-cement interface

THIS REPORT WAS INADVERTENTLY DISSEMINATED IN THE PUBLIC DOMAIN/ONLINE SINCE 12/2018 WITHOUT A DISCLAIMER. DISCLAIMER HAS BEEN ADDED – "THIS INFORMATION IS DISTRIBUTED SOLELY FOR THE PURPOSE OF PEER REVIEW UNDER APPLICABLE INFORMATION QUALITY GUIDELINES. IT HAS NOT BEEN FORMALLY DISSEMINATED BY BSEE. IT DOES NOT REPRESENT AND SHOULD NOT BE CONSTRUED TO REPRESENT ANY AGENCY DETERMINATION OR POLICY."

Annular fit of 100.5% and 101% mimic pre-stress conditions found in special type of cements known as expansive cement (Teodoriu et al. 2008). As shown in Figure 4.41, this type of cement develops internal compressive stresses when set. When a wellbore pressure is applied, the tensile hoop stress generated by the pressure first needs to compensate for the compressive pre-load before a net tensile stress is generated. This leads to reduction in effective magnitude of stresses generated by external loads, provides more margin of safety from failure and minimizes tensile or compressive strength requirement.

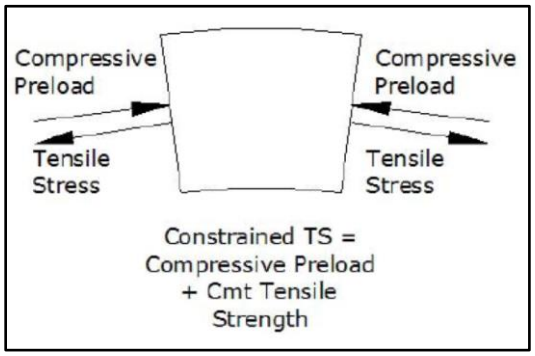

Figure 4.41: Pre-stressed expansive cement system

This effect can be visualized in the simulation results. For the same constant wellbore pressure of 1000 psi, the hoop stress decreases as pre-load (or annular fit) increases. This can significantly minimize the risk of radial crack failure. On the contrary, the maximum shear stress increases because of pre-load. This can make things worse by reducing the safety margin on shear failure. Thus, the selection of expansive cement should be made after carefully weighing potential benefits against the risks.

4.2.6. Young's Modulus

Young's modulus is a critical material property that defines the stiffness of cement. As discussed in section **4.2.1**, a cement sheath with lower Young's modulus and higher tensile strength would have lesser possibility of failure. Neat cement is a brittle material but researchers and manufacturers have tried various recipes to improve flexibility such as adding elastomeric material or creating a foam. The objective of this simulation task was to isolate and observe the effect of Young's modulus on various stresses in cement. For this purpose, the modulus was varied from 6.9×10^5 psi to 2.4×10^6 psi at a constant Poisson's ratio of 0.1, 0.25, and 0.4. The wellbore and annulus pressure were kept constant at 1000 psi and 250 psi respectively. The effect of Young's modulus on radial, hoop, and maximum shear stresses developed in the cement at the liner-cement interface is presented in Figure 4.42, Figure 4.44, and Figure 4.44.

THIS REPORT WAS INADVERTENTLY DISSEMINATED IN THE PUBLIC DOMAIN/ONLINE SINCE 12/2018 WITHOUT A DISCLAIMER. DISCLAIMER HAS BEEN ADDED – "THIS INFORMATION IS DISTRIBUTED SOLELY FOR THE PURPOSE OF PEER REVIEW UNDER APPLICABLE INFORMATION QUALITY GUIDELINES. IT HAS NOT BEEN FORMALLY DISSEMINATED BY BSEE. IT DOES NOT REPRESENT AND SHOULD NOT BE CONSTRUED TO REPRESENT ANY AGENCY DETERMINATION OR POLICY."

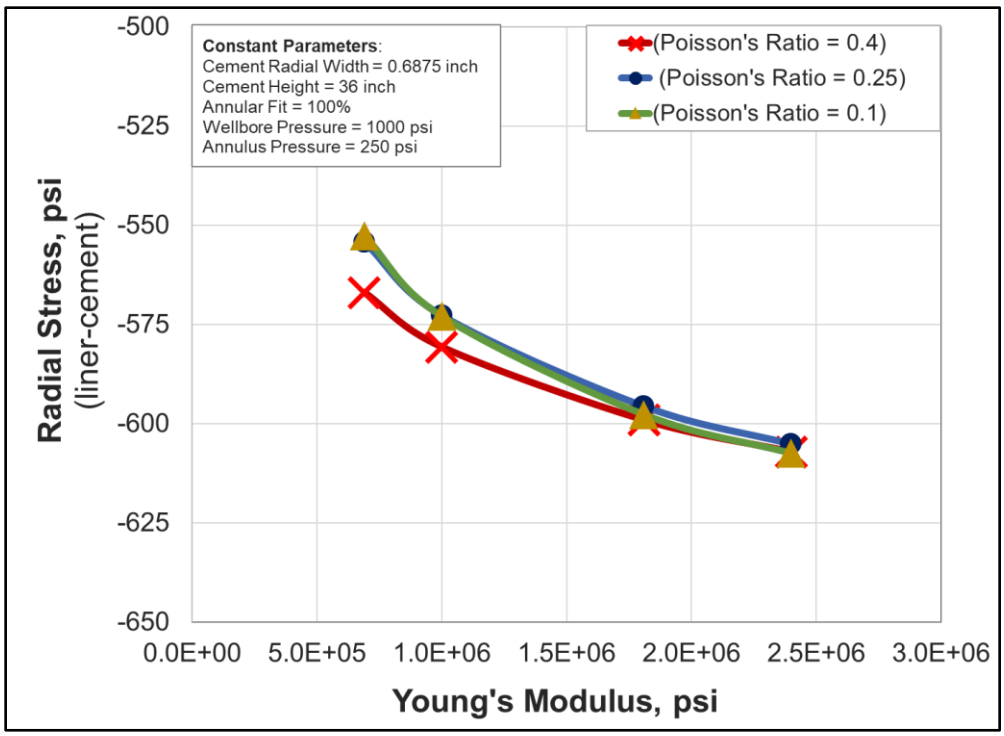

Figure 4.42: Effect of Young's modulus on radial stress in cement at liner-cement interface

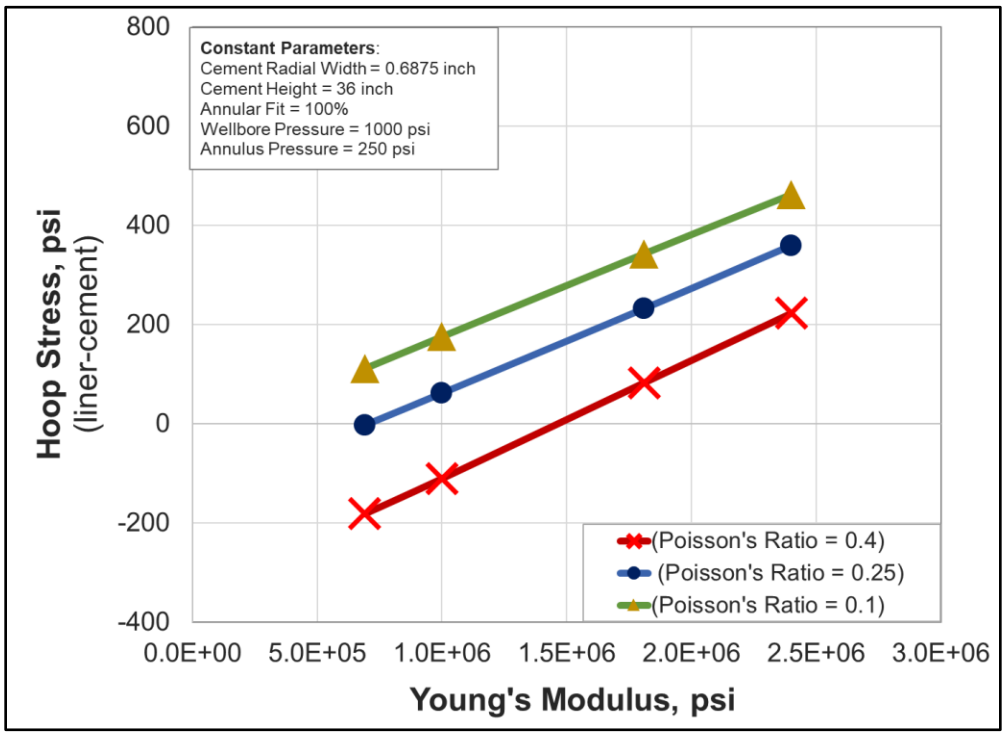

Figure 4.43: Effect of Young's modulus on hoop stress in cement at liner-cement interface

THIS REPORT WAS INADVERTENTLY DISSEMINATED IN THE PUBLIC DOMAIN/ONLINE SINCE 12/2018 WITHOUT A DISCLAIMER. DISCLAIMER HAS BEEN ADDED – "THIS INFORMATION IS DISTRIBUTED SOLELY FOR THE PURPOSE OF PEER REVIEW UNDER APPLICABLE INFORMATION QUALITY GUIDELINES. IT HAS NOT BEEN FORMALLY DISSEMINATED BY BSEE. IT DOES NOT REPRESENT AND SHOULD NOT BE CONSTRUED TO REPRESENT ANY AGENCY DETERMINATION OR POLICY."

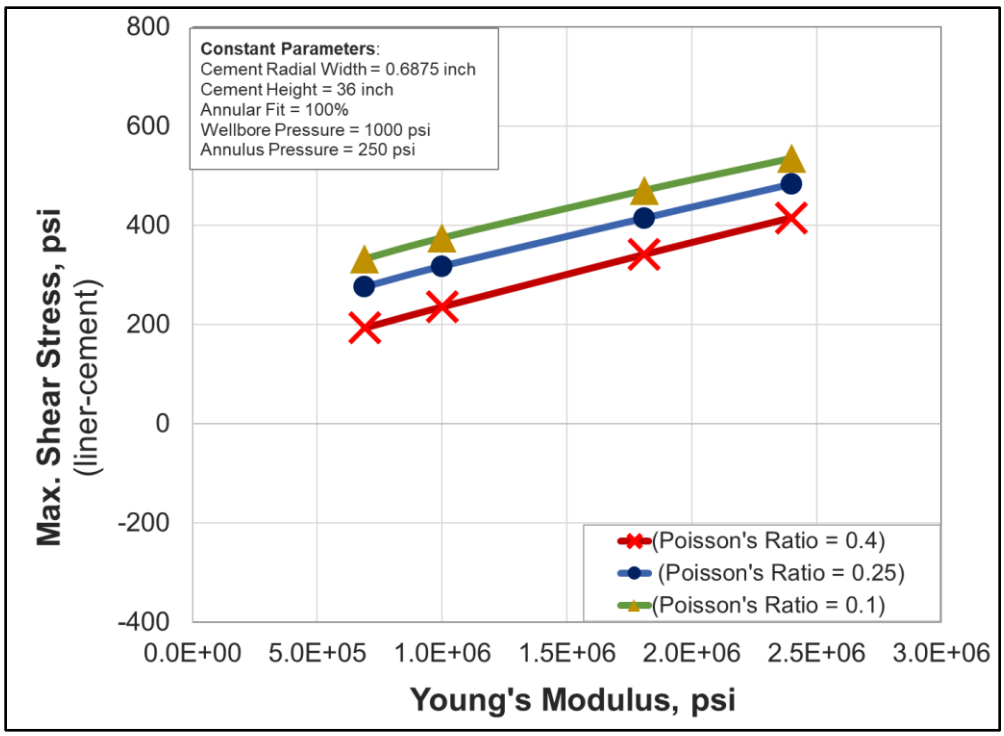

Figure 4.44: Effect of Young's modulus on maximum shear stress in cement at liner-cement interface

As shown in Figure 4.42, radial stress increases in magnitude (i.e. becomes more compressive as Young's modulus increases). This is an expected trend and was also observed in section **4.2.1.** The relationship is quadratic and practically independent of Poisson's ratio. The reduction in magnitude of radial stress is only about 7% after increasing the Young's modulus approximately 43 times. Therefore, the overall effect on radial stress is practically not important.

Unlike radial stress, the hoop and maximum shear stresses exhibit linear correlation with Young's modulus. Increase in Young's modulus resulted in both stresses increasing. The increase is independent of Poisson's ratio. If each of the curve in Figure 4.43 and Figure 4.44 is shifted to coincide, then it can be calculated that each 100,000 psi increase in Young's modulus results in 20 psi to 24 psi and 11 psi to 14 psi increase in hoop and maximum shear stress respectively. The amount may seem low, but it is relatively important when compared with typical tensile strengths of cement such as a neat class H that has the tensile strength of about 400 psi (Iverson et al. 2008). Another important effect can be seen in the case of hoop stress in cement with high Poisson's ratio of 0.4 (Figure 4.43). Any further increase in Young's modulus beyond 1.5×10^6 psi changes hoop stress from compressive to tensile, making tensile strength as the limiting strength and significantly reducing the safety factor.

Overall, all other factors being equal, as cement becomes more brittle (i.e. Young's modulus increases), the likelihood of radial cracking and shear failure increases. Radial bonding on the other hand, has no important dependency to the flexibility of cement.

THIS REPORT WAS INADVERTENTLY DISSEMINATED IN THE PUBLIC DOMAIN/ONLINE SINCE 12/2018 WITHOUT A DISCLAIMER. DISCLAIMER HAS BEEN ADDED – "THIS INFORMATION IS DISTRIBUTED SOLELY FOR THE PURPOSE OF PEER REVIEW UNDER APPLICABLE INFORMATION QUALITY GUIDELINES. IT HAS NOT BEEN FORMALLY DISSEMINATED BY BSEE. IT DOES NOT REPRESENT AND SHOULD NOT BE CONSTRUED TO REPRESENT ANY AGENCY DETERMINATION OR POLICY."

4.2.7. Poisson's Ratio

Similar to Young's modulus, Poisson's ratio is a critical material property that governs material behavior (deformations/stresses) in directions perpendicular to the applied load. It is difficult to control or design Poisson's ratio independent of Young's modulus. Nevertheless, it is important to isolate and understand its effect on the risk of cement failure. In this simulation task, Poisson's ratio was varied from 0.1 to 0.45 at three different Young's moduli (6.9×10^5 psi, 1.0×10^6 psi and 2.4×10^6 psi). The wellbore and annulus pressure were kept constant at 1000 and 250 psi respectively. Simulated radial, hoop, and maximum shear stresses are shown in Figure 4.45, Figure 4.46, and Figure 4.47 respectively.

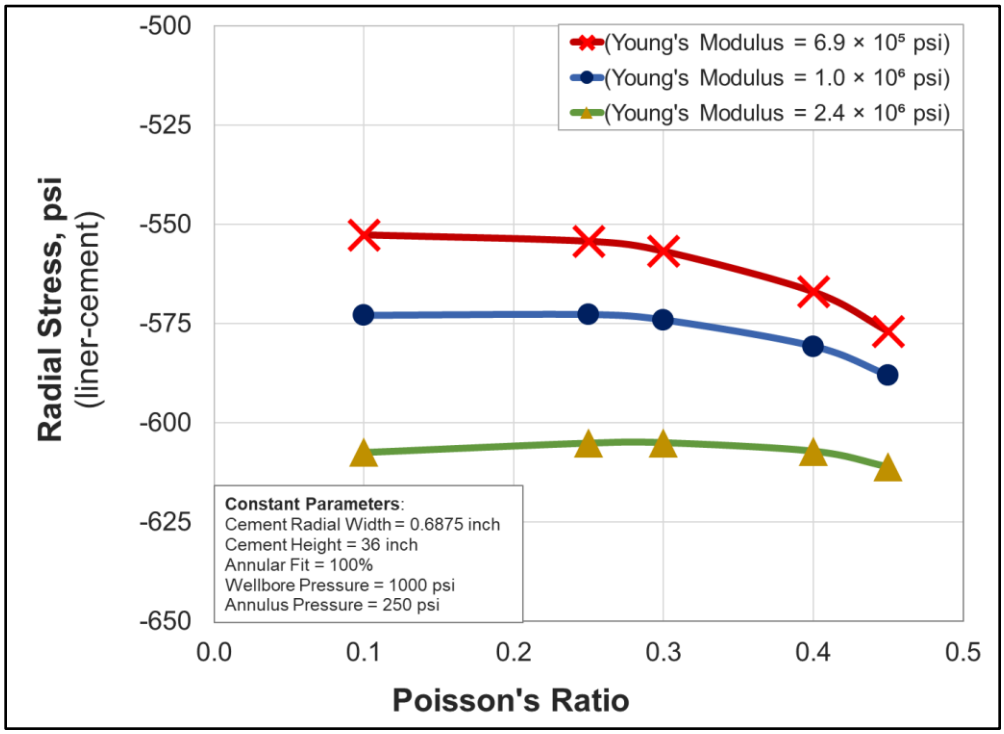

Figure 4.45: Effect of Poisson's ratio on radial stress in cement at liner-cement interface

As shown in Figure 4.45, Poisson's ratio has no effect on radial stress up to 0.3. Further increases resulted in an increased magnitude of radial stress. The trend is similar for all the three cases of Young's modulus. The increment however, is not significant and can be ignored for practical purposes.

It is clear from Figure 4.46 and Figure 4.47 that, unlike radial stress, Poisson's ratio has clear and well defined correlation with both hoop and shear stresses. Increase in Poisson's ratio reduces the stresses (i.e. tensile stresses become less tensile and compressive stress become more compressive). The change is notable and the difference in hoop stress between Poisson's ratio of 0.1 and 0.4 is more than 300 psi. In the case of maximum shear stress, the difference is more than 150 psi. Thus, for wellbore pressure increment of 1000 psi, a higher Poisson's ratio is preferable

THIS REPORT WAS INADVERTENTLY DISSEMINATED IN THE PUBLIC DOMAIN/ONLINE SINCE 12/2018 WITHOUT A DISCLAIMER. DISCLAIMER HAS BEEN ADDED – "THIS INFORMATION IS DISTRIBUTED SOLELY FOR THE PURPOSE OF PEER REVIEW UNDER APPLICABLE INFORMATION QUALITY GUIDELINES. IT HAS NOT BEEN FORMALLY DISSEMINATED BY BSEE. IT DOES NOT REPRESENT AND SHOULD NOT BE CONSTRUED TO REPRESENT ANY AGENCY DETERMINATION OR POLICY."

and has a lower likelihood of failure. It should be noted that the change in wellbore pressure may affect the trend. This is discussed in the next section.

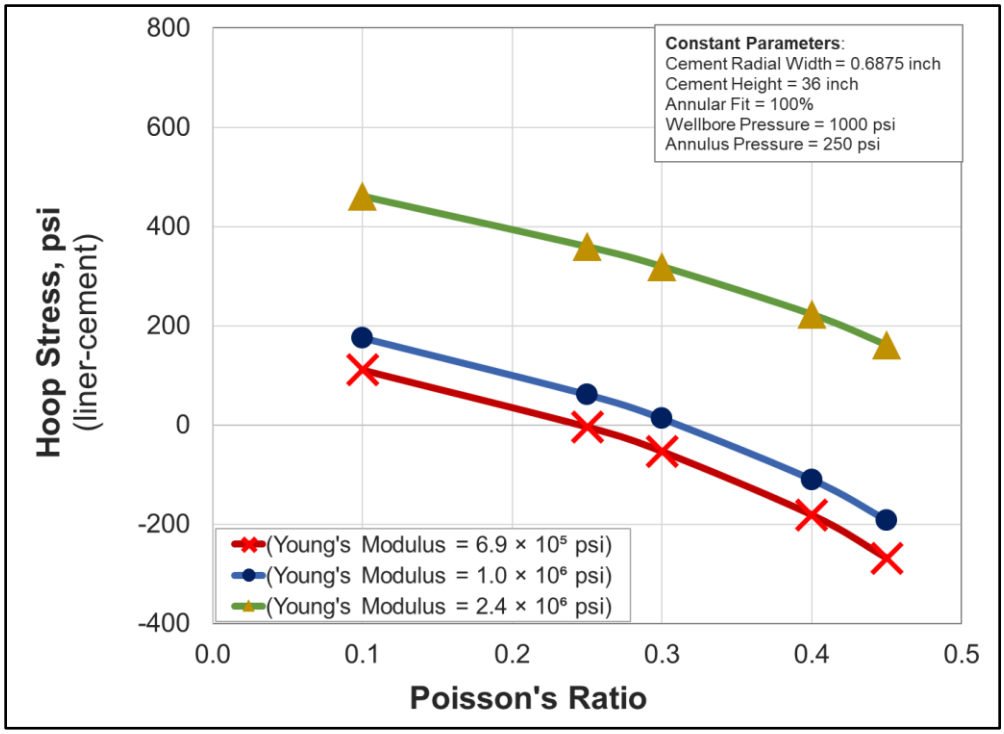

Figure 4.46: Effect of Poisson's ratio on hoop stress in cement at liner-cement interface

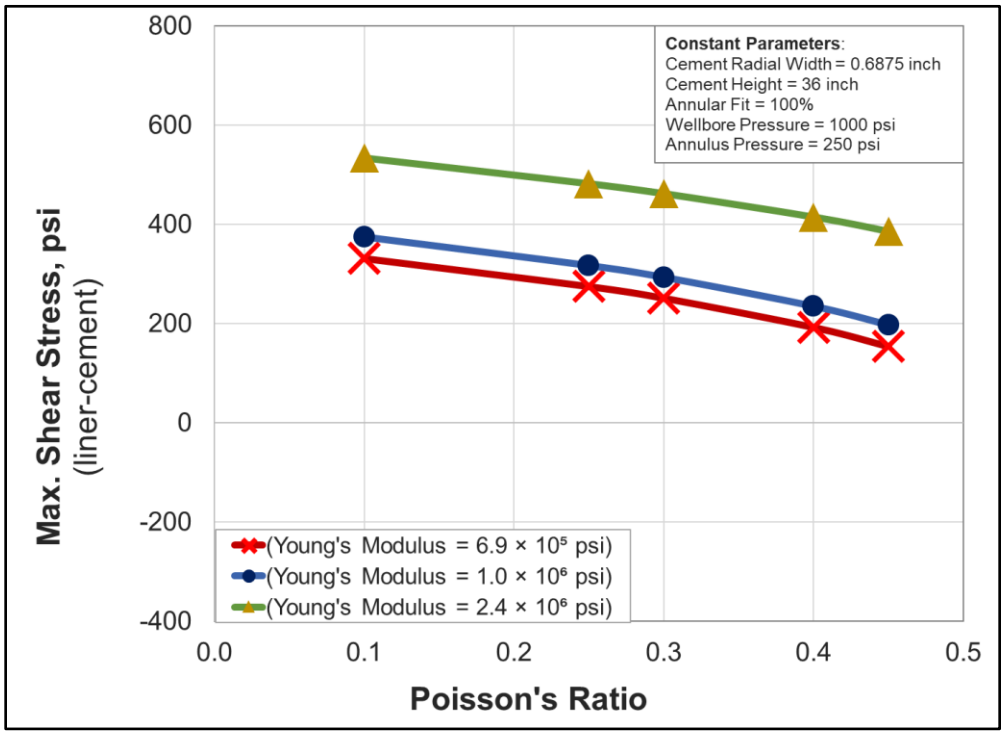

Figure 4.47: Effect of Poisson's ratio on maximum shear stress in cement at liner-cement interface

THIS REPORT WAS INADVERTENTLY DISSEMINATED IN THE PUBLIC DOMAIN/ONLINE SINCE 12/2018 WITHOUT A DISCLAIMER. DISCLAIMER HAS BEEN ADDED – "THIS INFORMATION IS DISTRIBUTED SOLELY FOR THE PURPOSE OF PEER REVIEW UNDER APPLICABLE INFORMATION QUALITY GUIDELINES. IT HAS NOT BEEN FORMALLY DISSEMINATED BY BSEE. IT DOES NOT REPRESENT AND SHOULD NOT BE CONSTRUED TO REPRESENT ANY AGENCY DETERMINATION OR POLICY."

4.2.8. Interdependency of Wellbore Pressure and Material Properties

It was observed that wellbore pressure and material properties are inter-dependent. Hence, for the sake of easier comparison and understanding, the results are discussed based on the type of cement system –

- LYLP: Low Young's modulus & low Poisson's ratio (6.9×10^5 psi and 0.1)
- LYHP: Ductile cement i.e. low Young's modulus & high Poisson's ratio (6.9×10^5 psi and 0.4)
- HYLP: Brittle cement i.e. high Young's modulus & low Poisson's ratio (2.4×10^6 psi and 0.1)
- HYHP: High Young's modulus & high Poisson's ratio (2.4×10^6 psi and 0.4)

The fourth type of cement system is highly unlikely to exist, but it has been included as a theoretical comparison.

Radial Stress

The effect of Young's modulus, Poisson's ratio, and wellbore pressure on radial stress is graphically summarized in Figure 4.48. Important observations are as follows:

- Increases in wellbore pressure leads to a slight increase in magnitude of radial stress. The effect is slightly more pronounced in the case of high Young's modulus cement systems.
- The nature of radial stress is compressive for decreasing wellbore pressure and tensile for increasing. Hence, for the same amount of pressure change, decreasing wellbore pressure is more detrimental than increasing pressure as the cement systems typically have higher compressive strength than tensile strength.
- In terms of magnitude of radial stress, there is no significant difference among the four types of cement systems and there is no conclusive evidence to indicate if one system is more robust to debonding or stress crushing type of failure than the other.

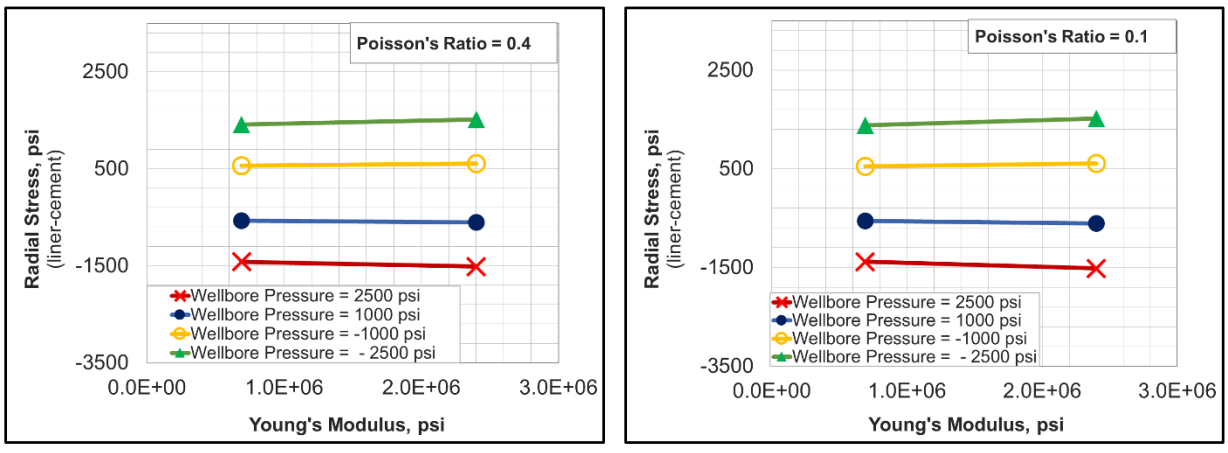

(a) **(b)**

Figure 4.48: Effect of Young's modulus and wellbore pressure on radial stress in cement at liner-cement interface – comparison between Poisson's ratio of 0.4 (a) and 0.1 (b)

THIS REPORT WAS INADVERTENTLY DISSEMINATED IN THE PUBLIC DOMAIN/ONLINE SINCE 12/2018 WITHOUT A DISCLAIMER. DISCLAIMER HAS BEEN ADDED – "THIS INFORMATION IS DISTRIBUTED SOLELY FOR THE PURPOSE OF PEER REVIEW UNDER APPLICABLE INFORMATION QUALITY GUIDELINES. IT HAS NOT BEEN FORMALLY DISSEMINATED BY BSEE. IT DOES NOT REPRESENT AND SHOULD NOT BE CONSTRUED TO REPRESENT ANY AGENCY DETERMINATION OR POLICY."

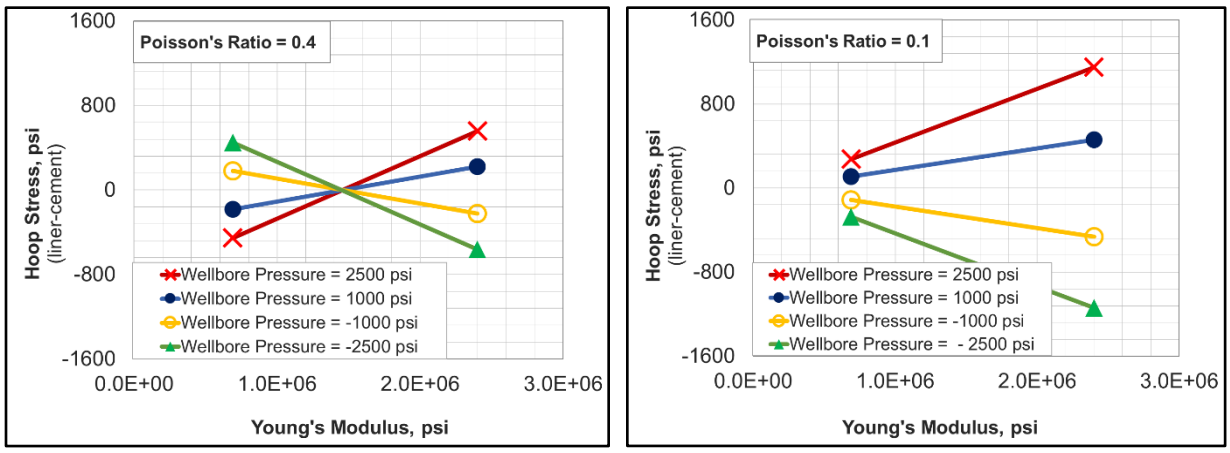

Figure 4.49: Effect of Young's modulus and wellbore pressure on hoop stress in cement at liner-cement interface – comparison between Poisson's ratio of 0.4 (a) and 0.1 (b)

Hoop Stress

The effect of Young's modulus, Poisson's ratio, and wellbore pressure on hoop stress is graphically summarized in Figure 4.49. The following are useful observations:

- Increase in wellbore pressure increases the magnitude of hoop stress in all cement systems. In terms of (i) magnitude of hoop stress at a constant wellbore pressure and (ii) sensitivity to change in wellbore pressure, the decreasing order of cement system is HYLP > HYHP > LYHP > LYLP. That is to say, LYLP system has the least sensitivity to wellbore pressure and also develops the smallest hoop stress in terms of magnitude than any other system at a constant wellbore pressure. Thus, LYLP followed by LYHP should be the preferred cement system to minimize risk of radial cracks.
- Unlike LYHP, all other cement systems developed a tensile hoop stress under increasing wellbore pressure load and developed a compressive hoop stress under decreasing pressure load. This trend is reversed for LYHP cement.
- For each Poisson's ratio, there is a critical Young's modulus at which the hoop stress becomes zero and changes direction. This optimum point does not appear to be changing significantly with change in pressure loads. This point moves towards higher Young's modulus as Poisson's ratio increases.
- Hoop stress and Young's modulus are linearly correlated. The magnitude of the slope (i.e. sensitivity of hoop stress to change in modulus) increases with increasing magnitudes of wellbore pressure. The sensitivity does not depend greatly on Poisson's ratio. At wellbore pressures of 1000 psi and 2500 psi, hoop stress changes by approximately 20 psi and 60 psi respectively per 100,000 psi change in Young's modulus.
- The sensitivity of hoop stress to change in Poisson's ratio depends on Young's modulus as well as wellbore pressure. At wellbore pressures of 1000 psi and 2500 psi and a Young's

THIS REPORT WAS INADVERTENTLY DISSEMINATED IN THE PUBLIC DOMAIN/ONLINE SINCE 12/2018 WITHOUT A DISCLAIMER. DISCLAIMER HAS BEEN ADDED – "THIS INFORMATION IS DISTRIBUTED SOLELY FOR THE PURPOSE OF PEER REVIEW UNDER APPLICABLE INFORMATION QUALITY GUIDELINES. IT HAS NOT BEEN FORMALLY DISSEMINATED BY BSEE. IT DOES NOT REPRESENT AND SHOULD NOT BE CONSTRUED TO REPRESENT ANY AGENCY DETERMINATION OR POLICY."

modulus of 2.4×10^6 psi, hoop stress changes by approximately 80 psi and 200 psi respectively per 0.1 change in Poisson's ratio.

Maximum Shear Stress

The effect of Young's modulus, Poisson's ratio, and wellbore pressure on hoop stress is graphically summarized in Figure 4.50. Unlike hoop stress, the trends are straight forward.

- Increase in magnitude of wellbore pressure load linearly increases the maximum shear stress. At a given pressure load, in terms of magnitude of maximum shear stress, the decreasing order of cement systems is – HYLP > HYHP > LYLP > LYHP. This indicates that the cement system LYHP has the lowest risk of shear failure followed by LYLP. Overall, low Young's modulus cement systems are more robust to shear failures.
- Maximum shear stress is linearly correlated to Young's modulus. The sensitivity of stress magnitude to change in the modulus (i.e. the slope of line) increases with increase in wellbore pressure. The sensitivity does not change with Poisson's ratio. At wellbore pressures of 1000 and 2500 psi, maximum shear stress changes by approximately 10 psi and 30 psi respectively per 100,000 psi change in Young's modulus.

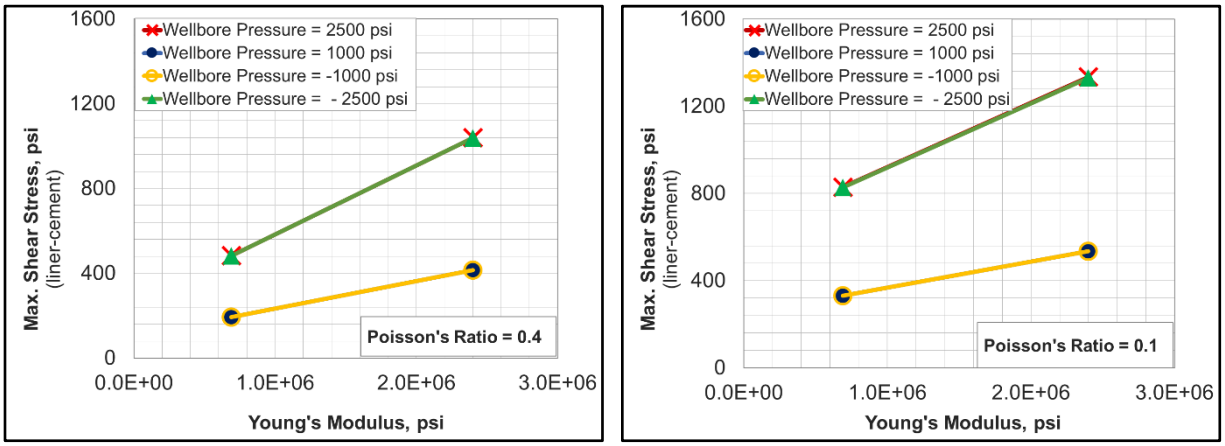

Figure 4.50: Effect of Young's modulus and wellbore pressure on maximum shear stress in cement at liner-cement interface – comparison between Poisson's ratio of 0.4 (a) and 0.1 (b)

4.2.9. Analytical Validation

The FEA model of cement was validated by comparing the analytically derived radial and hoop stresses at the liner-cement interface with the ones predicted by the FEA model. As discussed in section **2.2.1**, the analytical model is based on plane strain equations for composite thick cylinders. The derivation of contact stress at liner-cement and cement-casing interface is provided in Appendix **A**.

THIS REPORT WAS INADVERTENTLY DISSEMINATED IN THE PUBLIC DOMAIN/ONLINE SINCE 12/2018 WITHOUT A DISCLAIMER. DISCLAIMER HAS BEEN ADDED – "THIS INFORMATION IS DISTRIBUTED SOLELY FOR THE PURPOSE OF PEER REVIEW UNDER APPLICABLE INFORMATION QUALITY GUIDELINES. IT HAS NOT BEEN FORMALLY DISSEMINATED BY BSEE. IT DOES NOT REPRESENT AND SHOULD NOT BE CONSTRUED TO REPRESENT ANY AGENCY DETERMINATION OR POLICY."

As shown in Figure 4.51 and Figure 4.52**,** the accuracy of the FEA model is good. The error in radial stress prediction was between 0 to 0.4% while in case of hoop stress, it ranged from 0 to about 4.4%.

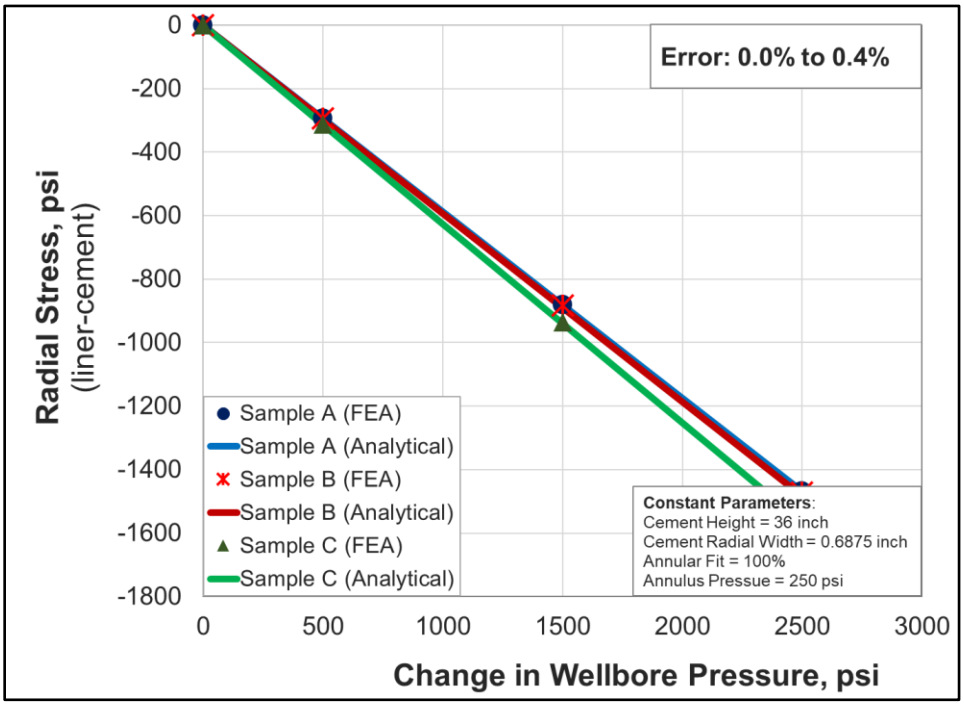

Figure 4.51: Comparison between FEA simulated and analytically calculated radial stress

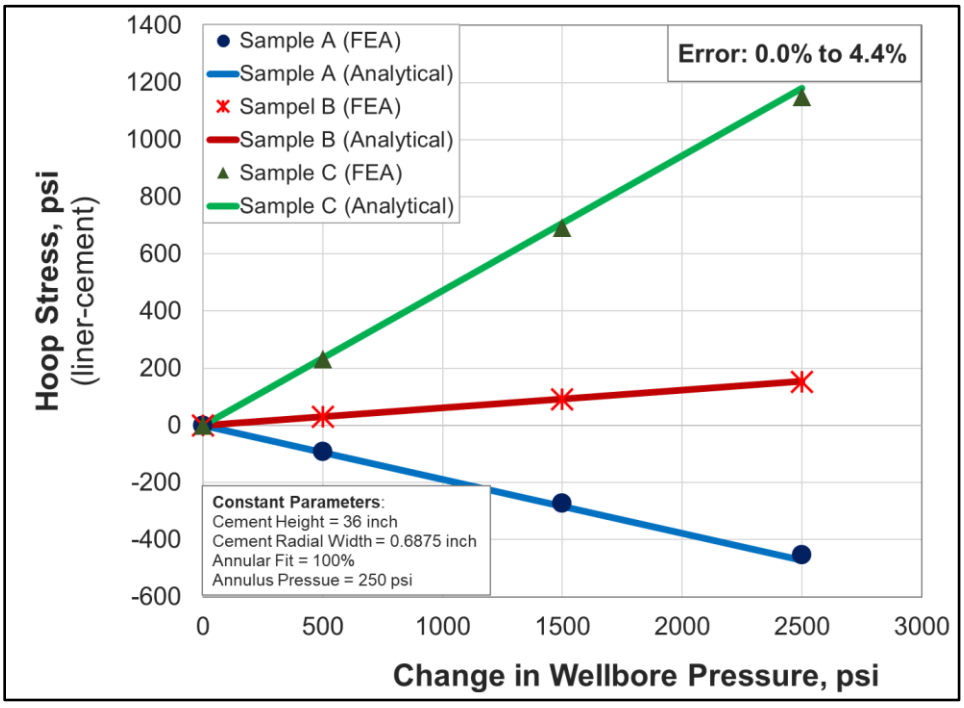

Figure 4.52: Comparison between FEA simulated and analytically calculated hoop stress

THIS REPORT WAS INADVERTENTLY DISSEMINATED IN THE PUBLIC DOMAIN/ONLINE SINCE 12/2018 WITHOUT A DISCLAIMER. DISCLAIMER HAS BEEN ADDED – "THIS INFORMATION IS DISTRIBUTED SOLELY FOR THE PURPOSE OF PEER REVIEW UNDER APPLICABLE INFORMATION QUALITY GUIDELINES. IT HAS NOT BEEN FORMALLY DISSEMINATED BY BSEE. IT DOES NOT REPRESENT AND SHOULD NOT BE CONSTRUED TO REPRESENT ANY AGENCY DETERMINATION OR POLICY."

5. CONCLUSIONS

Three-dimensional FEA models were used to evaluate "fitness-for-service" of wellbore barrier components. Parametric analysis was performed to examine the effect of various operational, design, and failure parameters on barrier performance. The FEA generated results were matched with analytical calculations with reasonable accuracy. The following conclusion are drawn from the simulation results:

5.1. Seal Assembly Model

- Annular fit (i.e. radial width of seal relative to annular space) is the most critical parameter affecting sealability. If the radial gap between seal and casing is x% higher than anticipated, then it can effectively reduce compression by x% and vice versa. A radial gap of 1% higher than the designed value can reduce the effective contact pressure by an amount approximately equal to 16 times the elastic modulus of the seal.
- Contact pressure increases gradually with increase in Poisson's ratio up to 0.425 beyond which it increases exponentially and even faster. Elastic modulus on the other hand is directly proportional to contact pressure.
- Compression ratio (% change in axial seal length) is an important operational parameter affecting sealability. Contact pressure exhibits a positive liner correlation with the compression ratio. The force required to achieve certain compression ratios depends on the elastic modulus and seal axial length.
- Axial seal length and radial thickness (for 100% annular fit) has practically no significant effect on sealability. Contact pressure shows an insignificant reduction (up to 2-3%) with approximately 5 times increase in seal length. Significant changes (±40%) in seal thickness results in a minor change (< 2%) in contact pressure.
- Material failure can have significant impact on sealability. The average % reduction in contact pressures due to gas exposure was found to be equal to the % reduction in elastic modulus of the material. The worst case in aging tests was observed to be 7 days exposure to pure CO_2 at 180°F. It resulted in a sealability reduction of NBR (40%), EPDM (29%), VITON (9%), and PTFE elastomer (2%).
- Operational failure such as non-uniform seal energization or faulty support while energizing can result in 13% to 95% less contact pressure than the designed value, depending on the severity. Overall, the loss is more pronounced and detrimental in the case of an axially shorter seal.
- All the major predictors namely elastic modulus, Poisson's ratio, compression ratio, and annular fit were incorporated into an empirical correlation that can be used to estimate contact pressure with ±2% error.

THIS REPORT WAS INADVERTENTLY DISSEMINATED IN THE PUBLIC DOMAIN/ONLINE SINCE 12/2018 WITHOUT A DISCLAIMER. DISCLAIMER HAS BEEN ADDED – "THIS INFORMATION IS DISTRIBUTED SOLELY FOR THE PURPOSE OF PEER REVIEW UNDER APPLICABLE INFORMATION QUALITY GUIDELINES. IT HAS NOT BEEN FORMALLY DISSEMINATED BY BSEE. IT DOES NOT REPRESENT AND SHOULD NOT BE CONSTRUED TO REPRESENT ANY AGENCY DETERMINATION OR POLICY."

5.2. Cement Model

- Annular fit has significant impact on radial, hoop, and maximum shear stresses at the liner-cement interface. Smaller than 100% annular fit (e.g. presence of micro-annuli or lack of bonding between cement and pipe is the most likely first mode of sealability failure for cement. This could be caused by volume shrinkage, improper centralization, shallow gas channeling, etc.
- Radial mode of failure (debonding and stress crushing) is highly unlikely for shallow wells. Radial debonding can only occur in the event of decreasing wellbore pressure when radial stresses become tensile. Stress crushing is highly unlikely because the cement would fail by radial cracking when the hoop stress exceeds tensile strength, before it fails by compressive radial stress exceeding compressive strength.
- Radial cracking and shear failure are the most likely modes of failures for set cement with 100% annular fit. The likelihood and order of these failure modes depends on the cement's Young's modulus, Poisson's ratio, and limiting strength.
- Cement with low Young's modulus and low Poisson's ratio (LYLP) develops smaller hoop stress in terms of magnitude and exhibits more robustness to change in wellbore pressure than any other cement system. Thus, LYLP followed by LYHP should be the preferred cement systems to minimize the risk of failure by radial cracks.
- Cement systems with low Young's modulus are overall more robust to shear failures. LYHP cement system has the lowest risk of shear failure followed by LYLP cement system.
- Variations in material properties can have notable impact on the designed values of hoop and maximum shear stresses. For example, at wellbore pressures of 2500 psi, hoop stress changes by approximately 60 psi respectively per 100,000 psi change in Young's modulus and by approximately 200 psi respectively per 0.1 change in Poisson's ratio.
- Pre-stressed cement system can significantly minimize the risk of radial crack failure by providing compensatory compressive stress. However, this pre-stressed system is more likely to fail by shear because the pre-load condition led to higher values of maximum shear stress than a conventional cement system.
- For all three cement samples, a wellbore pressure increase of 1000 psi was able to close 87 μm wide channel (99.5% annular fit). This indicates that if pressure increase is sufficiently high to balloon the liner, then it may mask the presence of a small micro-annuli in set cement.
- For shallow depth wells, height of cement column and annular pressure are not important factors contributing to the structural failure of cement.

Overall, this study provided useful information on seal assembly and cement sheath as barriers. This work filled-in some of the existing knowledge gaps and help regulators and operators alike in improving design, selection, and qualification of these barrier elements.

THIS REPORT WAS INADVERTENTLY DISSEMINATED IN THE PUBLIC DOMAIN/ONLINE SINCE 12/2018 WITHOUT A DISCLAIMER. DISCLAIMER HAS BEEN ADDED – "THIS INFORMATION IS DISTRIBUTED SOLELY FOR THE PURPOSE OF PEER REVIEW UNDER APPLICABLE INFORMATION QUALITY GUIDELINES. IT HAS NOT BEEN FORMALLY DISSEMINATED BY BSEE. IT DOES NOT REPRESENT AND SHOULD NOT BE CONSTRUED TO REPRESENT ANY AGENCY DETERMINATION OR POLICY."

ACKNOWLEDGEMENT

We extend our sincere gratitude to BSEE for funding this project and providing the research team with valuable feedback.

NOMENCLATURE

Acronyms

EPDM	:	Ethylene Propylene Diene Monomer
HYLP	:	High Young's Modulus Low Poisson's Ratio
HYHP	:	High Young's Modulus High Poisson's Ratio
LYLP	:	Low Young's Modulus Low Poisson's Ratio
LYHP	:	Low Young's Modulus High Poisson's Ratio
NBR	:	Nitrile Butadiene Rubber
PTFE	:	Polytetrafluoroethylene
SF	:	Safety Factor
VITON	:	A brand of synthetic Flouropolymer elastomer

Symbols

a	:	Inner radius of liner
b	:	Outer radius of liner / inner radius of cement
c	:	Outer radius of cement / inner radius of casing
d	:	Outer radius of casing
r	:	Radius of cylidner
r_1	:	Outer radius of liner
t	:	Radial width of seal / cement
w	:	Width/thickness of cylinder
A	:	Integration constant in Lame's Equation
B	:	Integration constant in Lame's Equation
C_0	:	Uni-axial Compressive strength of material
E	:	Elastic modulus
K	:	Bulk modulus
V	:	Volume of seal
P_c	:	Contact pressure
P_{c1}	:	Contact Stress at liner-cement interface
P_{c2}	:	Contact Stress at cement-casing interface
P_i	:	Pressure acting internally on liner
P_{max}	:	Maximum contact pressure
P_o	:	Pressure acting externally on casing
T_0	:	Uni-axial Tensile strength of material

THIS REPORT WAS INADVERTENTLY DISSEMINATED IN THE PUBLIC DOMAIN/ONLINE SINCE 12/2018 WITHOUT A DISCLAIMER. DISCLAIMER HAS BEEN ADDED – "THIS INFORMATION IS DISTRIBUTED SOLELY FOR THE PURPOSE OF PEER REVIEW UNDER APPLICABLE INFORMATION QUALITY GUIDELINES. IT HAS NOT BEEN FORMALLY DISSEMINATED BY BSEE. IT DOES NOT REPRESENT AND SHOULD NOT BE CONSTRUED TO REPRESENT ANY AGENCY DETERMINATION OR POLICY."

GREEK SYMBOLS

δ	:	Seal Compression ratio
δ_r	:	Radial compression/expansion
λ	:	Annular gap between seal and pipe
ν	:	Poisson's ratio, dimensionless
σ_1	:	Maximum principle stress
σ_3	:	Minimum principle stress
σ_r	:	Radial stress
σ_θ	:	Hoop stress
σ_z	:	Axial stress
ς	:	Cohesion or intrinsic shear strength of cement
τ_{max}	:	Maximum shear stress

REFERENCES

Al-Hiddabi, S. A., Pervez, T., Qamar, S. Z. et al. 2015. Analytical model of elastomer seal performance in oil wells. *Applied Mathematical Modelling*: **39**(10-11), 2836–2848. http://dx.doi.org/10.1016/j.apm.2014.10.028

Al-Kharusi, M. S. M., Qamar, S. Z., Pervez, T. et al. 2011. Non-Linear Model for Evaluation of Elastomer Seals Subjected to Differential Pressure. Presented at SPE/DGS Saudi Arabia Section Technical Symposium and Exhibition, 15-18 May, Al-Khobar, Saudi Arabia. SPE-149032-MS. https://doi.org/10.2118/149032-MS

Alzebdeh, K., Pervez, T., and Qamar, S.Z. 2010. Finite Element Simulation of Compression of Elastomeric Seals in Open Hole Liners. *Journal of Energy Resources Technology:* **132**(3). 031002. http://dx.doi.org/10.1115/1.4002244

Ansys®, 2017. Workbench 17.2 User Manual

API 11D1, Packers and Bridge Plugs, Third Edition. 2015. Washington, DC: API

API Spec 17D, Specification for Design and Operation of Subsea Production Systems—Subsea Wellhead and Tree Equipment, Second Edition. 2011. Washington, DC: API

API Standard 65-2, Isolating Potential Flow Zones During Well Construction, Second Edition. 2010. Washington, DC: API

API RP 10B-2, Recommended Practice for Testing Well Cements, Second Edition. 2013. Washington, DC: API

THIS REPORT WAS INADVERTENTLY DISSEMINATED IN THE PUBLIC DOMAIN/ONLINE SINCE 12/2018 WITHOUT A DISCLAIMER. DISCLAIMER HAS BEEN ADDED – "THIS INFORMATION IS DISTRIBUTED SOLELY FOR THE PURPOSE OF PEER REVIEW UNDER APPLICABLE INFORMATION QUALITY GUIDELINES. IT HAS NOT BEEN FORMALLY DISSEMINATED BY BSEE. IT DOES NOT REPRESENT AND SHOULD NOT BE CONSTRUED TO REPRESENT ANY AGENCY DETERMINATION OR POLICY."

API RP 10B-4, Preparation and Testing of Foamed Cement Formulations at Atmospheric Pressure, Second Edition. 2015. Washington, DC: API

API RP 10B-5, Recommended Practice on Determination of Shrinkage and Expansion of Well Cement Formulations at Atmospheric Pressure, First Edition. 2005. Washington, DC: API

API RP 10B-6, Recommended Practice on Determining the Static Gel Strength of Cement Formulations, First Edition. 2010. Washington, DC: API

API SPEC 10A, Specification for Cements and Materials for Well Cementing, Twenty Fourth Edition. 2010. Washington, DC: API

API TR 10TR1, Cement Sheath Evaluation, Second Edition. 2008. Washington, DC: API

Arias, H. 2013. Use of Finite-Element Analysis to Improve Well Cementing in HTHP Conditions. PhD Dissertation, Texas A&M University, College Station, Texas (August 2013).

Bellarby, J. 2009. *Well Completion Design*, volume 56, first edition. Amsterdam, Amsterdam : Elsevier Science.

Berger, S. 2004. Experimental and Finite Element Analysis of High Pressure Packer Elements. MS Thesis, Massachusetts Institute of Technology, Cambridge, Massachusetts (September 2004)

Bois, A.P., Garnier, A., Rodot, F. et al. 2011. How To Prevent Loss of Zonal Isolation Through a Comprehensive Analysis of Microannulus Formation. *SPE Drilling & Completion*: **26**(01), 13–31. SPE-124719-PA. http://dx.doi.org/10.2118/124719-pa

Bosma, M., Ravi, K., van Driel, W. et al. 1999. Design Approach to Sealant Selection for the Life of the Well. Presented at SPE Annual Technical Conference and Exhibition, 3-6 October, Houston, Texas, USA. SPE-56536-MS. https://doi.org/10.2118/56536-MS

Bosma, M. G. R., Cornelissen, E. K., and Schwing, A., 2000. Improved Experimental Characterisation of Cement/Rubber Zonal Isolation Materials. Presented at SPE Asia Pacific Oil and Gas Conference and Exhibition, 16-18 October, Brisbane, Australia. SPE-64395-MS. http://dx.doi.org/10.2118/64395-ms

BSEE. 2014. QC-FIT Evaluation of Seal Assembly & Cement Failures Interim Summary of Findings. Internal QC-FIT Report #2014-02, Bureau of Safety and Environmental Enforcement, Washington, DC.

Bustgaard, M., and Nesheim, M. H. 2016. Model for Prediction of Cement Sheath Failure. MS Thesis, Norwegian University of Science and Technology, Trondheim, Norway (June 2016).

THIS REPORT WAS INADVERTENTLY DISSEMINATED IN THE PUBLIC DOMAIN/ONLINE SINCE 12/2018 WITHOUT A DISCLAIMER. DISCLAIMER HAS BEEN ADDED – "THIS INFORMATION IS DISTRIBUTED SOLELY FOR THE PURPOSE OF PEER REVIEW UNDER APPLICABLE INFORMATION QUALITY GUIDELINES. IT HAS NOT BEEN FORMALLY DISSEMINATED BY BSEE. IT DOES NOT REPRESENT AND SHOULD NOT BE CONSTRUED TO REPRESENT ANY AGENCY DETERMINATION OR POLICY."

Cantu, J., Smith, P., and Nida, R. 2004. Expandable Liner Hanger Application in Arduous Well Conditions Proves Reliability: A Case History. Presented at SPE Asia Pacific Oil and Gas Conference and Exhibition, 18-20 October, Perth, Australia. SPE-88510-MS. https://doi.org/10.2118/88510-MS

Chu, W., Shen, J., Yang, Y. et al. 2015. Calculation of micro-annulus size in casing-cement sheath-formation system under continuous internal casing pressure change. Petroleum Exploration and Development: 42(3), 414–421. https://doi.org/10.1016/S1876-3804(15)30033-1

Dagle, O., Johnson, J., and Moeller, D. 2016. Metal-to-Metal Sealing and Anchoring Expandable Hanger in Gulf of Mexico: Development, Collaboration, and Execution. Presented at SPE Deepwater Drilling and Completions Conference, 14-15 September, Galveston, Texas, USA. SPE-180304-MS. https://doi.org/10.2118/180304-MS

De Andrade, J. 2015. Cement Sheat Integrity During Thermal Cycling. PhD Dissertation, Norwegian University of Science and Technology, Trondheim, Norway.

De Andrade, J., and Sangesland, S. 2016. Cement Sheath Failure Mechanisms: Numerical Estimates to Design for Long-Term Well Integrity. *Journal of Petroleum Science and Engineering*: **147**, 682–698. https://doi.org/10.1016/j.petrol.2016.08.032

Edgley, K., D., Sabins, F., L. and Watters, L., T. 2005. Supercement for Annular Seal and Long-Term Integrity in Deep, Hot Wells "Deep Trek." Final Report, Contract No. DE-FC26-06NT41836, US DOE, Washington, DC (August 2005). http://dx.doi.org/10.2172/908315

Feng, Y., Podnos, E., and Gray, K. 2016. Well Integrity Analysis: 3D Numerical Modeling of Cement Interface Debonding. Presented at 50th U.S. Rock Mechanics/Geomechanics Symposium, 26-29 June, Houston, Texas, USA. ARMA-2016-246.

Feng, D., Yuan, Y., Tan, B. et al. 2010. Finite Element Analysis of The Packer Rubbers on Sealing Process. 2010 International Conference on Mechanic Automation and Control Engineering, 26-28 June, Wuhan, China. 11461585. http://dx.doi.org/10.1109/mace.2010.5535502

Guo, Z., Li, Q., Wang, Y. et al. 2011. Analysis and structural improvement of the rubber part in packer in a way of non-linearity finite element. 2011 Second International Conference on Mechanic Automation and Control Engineering, 15-17 July, Hohhot, China. 12242645. https://dx.doi.org/10.1109/mace.2011.5986860

Hearn, E. J. 1997. *Mechanics of Materials I: An Introduction to the Mechanics of Elastic and Plastic Deformation of Solids and Structural Materials*, Third Edition. Jordan Hill, Oxford: Butterworth-Heinemann.

THIS REPORT WAS INADVERTENTLY DISSEMINATED IN THE PUBLIC DOMAIN/ONLINE SINCE 12/2018 WITHOUT A DISCLAIMER. DISCLAIMER HAS BEEN ADDED – "THIS INFORMATION IS DISTRIBUTED SOLELY FOR THE PURPOSE OF PEER REVIEW UNDER APPLICABLE INFORMATION QUALITY GUIDELINES. IT HAS NOT BEEN FORMALLY DISSEMINATED BY BSEE. IT DOES NOT REPRESENT AND SHOULD NOT BE CONSTRUED TO REPRESENT ANY AGENCY DETERMINATION OR POLICY."

Hu, G., Zhang, P., Wang, G. et al. 2017. The influence of rubber material on sealing performance of packing element in compression packer. *Journal of Natural Gas Science and Engineering*: **38**(Feb 2017), 120–138. https://doi.org/10.1016/j.jngse.2016.12.027

Iverson, B., Darbe, R., and McMechan, D. 2008. Evaluation of Mechanical Properties of Cements. Presented at the 42nd U.S. Rock Mechanics Symposium (USRMS), 29 June-2 July, San Francisco, California. ARMA-08-293.

Izon, D., Danenberger, E. P., and Melinda, M. 2007. Absence of fatalities in blowouts encouraging in MMS study of OCS incidents 1992-2006. *Drilling Contractor*: July/August 2017, 84-90. http://drillingcontractor.org/dcpi/dc-julyaug07/DC_July07_MMSBlowouts.pdf

Jimenez, C., Soto, S., Leon, A. et al. 2009. New Liner-Hanger Technology Improves Safety and Reduces Non-Productive Time in Deviated High-Temperature Wells in South Central Venezuela. SPE Annual Technical Conference and Exhibition, 4-7 October, New Orleans, Louisiana. SPE-124396-MS. https://doi.org/10.2118/124396-MS

Khandka, R. K. 2007. Leakage Behind Casing. MS Thesis, Norwegian University of Science and Technology, Trondheim, Norway (June 2007).

Lavrov, A. and Torsæter, M. 2016. *Physics and Mechanics of Primary Well Cementing*, First Edition. Springer. http://dx.doi.org/10.1007/978-3-319-43165-9.

Li, W., Wang, Y., and Miao, D. 2015. Finite Element Analysis on Rubber Sealing Ring of the Rotary Liner Hanger Bearing. Proc. of the 2015 International Conference on Modeling, Simulation and Applied Mathematics, 23-24 August 2015, Phuket, Thailand. http://dx.doi.org/10.2991/msam-15.2015.52

Lin, Z. C. 2013. The Strength Analysis and Structure Optimization of Packer Slip Based on ANSYS. *Applied Mechanics and Materials*: **423-426**, 1967–1971. https://doi.org/10.4028/www.scientific.net/AMM.423-426.1967

Liu, Q., Wang, Z., Lou, Y., and Suo, Z. 2014. Elastic leak of a seal. *Extreme Mechanics Letters*: **1**, 54–61. http://dx.doi.org/10.1016/j.eml.2014.10.001

Lohoefer, C. L., Mathis, B., Brisco, D. et al. 2000. Expandable Liner Hanger Provides Cost-Effective Alternative Solution. Presented at IADC/SPE Drilling Conference, 23-25 February, New Orleans, Louisiana. SPE-59151-MS. https://doi.org/10.2118/59151-MS

Ma, M., Jia, W., Bu, Y. et al. 2014. Study on Rubber Seal Design of a Swellpacker in Oil Well Cementing. *Open Access Library Journal*: **01**(09), 1–8. http://dx.doi.org/10.4236/oalib.1101082

THIS REPORT WAS INADVERTENTLY DISSEMINATED IN THE PUBLIC DOMAIN/ONLINE SINCE 12/2018 WITHOUT A DISCLAIMER. DISCLAIMER HAS BEEN ADDED – "THIS INFORMATION IS DISTRIBUTED SOLELY FOR THE PURPOSE OF PEER REVIEW UNDER APPLICABLE INFORMATION QUALITY GUIDELINES. IT HAS NOT BEEN FORMALLY DISSEMINATED BY BSEE. IT DOES NOT REPRESENT AND SHOULD NOT BE CONSTRUED TO REPRESENT ANY AGENCY DETERMINATION OR POLICY."

Ma, W., Qu, B., and Guan, F. 2014. Effect of the friction coefficient for contact pressure of packer rubber. *Proc. of the Institution of Mechanical Engineers, Part C: Journal of Mechanical Engineering Science*: **228**(16), 2881–2887. http://dx.doi.org/10.1177/0954406214525596

Mccormick, J., Matice, M., and Cramp, S. 2012. Big Bore Expandable Liner Hangers for Offshore and Deepwater Applications Reduces Cost and Increases Reliability : Global Case History. Presented at SPETT 2012 Energy Conference and Exhibition, 11-13 June, Port-of-Spain, Trinidad. SPE-158856-MS. https://doi.org/10.2118/158856-MS

Mohamed, A. O., and Al-Zuraigi, A. 2013. Liner Hangers Technology Advancement and Challenges. Presented at SPE Middle East Oil and Gas Show and Conference, 10-13 March, Manama, Bahrain. SPE-164367-MS. https://doi.org/10.2118/164367-MS

Moore, M.J., Campo, D.B., Hockaday, J. et al. 2002. Expandable Liner Hangers: Case Histories. Presented at Offshore Technology Conference, 6-9 May, Houston, Texas. OTC-14313-MS. https://doi.org/10.4043/14313-MS.

Mullins, F., 2016. Metal-Formed Liner Hanger Avoids High-Setting-Pressure Requirements. *Journal of Petroleum Technology*: 68(01), 4-8. https://doi.org/10.2118/0116-0022-JPT

Nelson, E. B. and Guillot, D. 2006. *Well cementing*, First Edition, Amsterdam: Elsevier.

NORSOK D-010, Well integrity in drilling and well operations, Revision 4, 2013. Lysaker, Norway: Standards Norway

Nygaard, R., Salehi, S., Weideman, B. et al. 2014. Effect of Dynamic Loading on Wellbore Leakage for the Wabamun Area CO2-Sequestration Project. *Journal of Canadian Petroleum Technology*: **53**(01), 69-82. http://dx.doi.org/10.2118/146640-pa

Rahimi, R. 2014. The effect of using different rock failure criteria in wellbore stability analysis. MS Thesis, Missouri University of Science and Technology, Rolla, Missouri, USA (May 2014).

Ravi, K., Bosma, M., and Gastebled, O. 2002. Safe and Economic Gas Wells through Cement Design for Life of the Well. Presented at SPE Gas Technology Symposium, 30 April-2 May, Calgary, Alberta, Canada. SPE-75700-MS. https://doi.org/10.2118/75700-MS

Smith, P., and Williford, J. 2006. Case Histories : Liner-Completion Difficulties Resolved With Expandable Liner-Top Technology. Presented at Canadian International Petroleum Conference, 13-15 June, Calgary, Alberta. PETSOC-2006-103. https://doi.org/10.2118/2006-103

Speer, M. 2006. Introduction to Wellhead Systems. In: *Petroleum Engineering Handbook*, Vol. 2, ed. Lake, L.W. Chap. 8, 344-369. Richardson, Texas: Society of Petroleum Engineers.

THIS REPORT WAS INADVERTENTLY DISSEMINATED IN THE PUBLIC DOMAIN/ONLINE SINCE 12/2018 WITHOUT A DISCLAIMER. DISCLAIMER HAS BEEN ADDED – "THIS INFORMATION IS DISTRIBUTED SOLELY FOR THE PURPOSE OF PEER REVIEW UNDER APPLICABLE INFORMATION QUALITY GUIDELINES. IT HAS NOT BEEN FORMALLY DISSEMINATED BY BSEE. IT DOES NOT REPRESENT AND SHOULD NOT BE CONSTRUED TO REPRESENT ANY AGENCY DETERMINATION OR POLICY."

Stautzenberger, A., Baird, S., and Lundgård, G.. 2016. Expandable Liner Hanger Technology Provides Metal-to-Metal Sealing and Improved Anchoring Solution for ERD Wells : Case History in North Sea. Presented at SPE Bergen One Day Seminar, 20 April, Grieghallen, Bergen, Norway. SPE-180012-MS. https://doi.org/10.2118/180012-MS

Teodoriu, C., Yi, M. C., Ichim, A. et al. 2018. A Novel View of Cement Failure with Application to Geothermal Well Construction. Presented at 43rd Workshop on Geothermal Reservoir Engineering, February 12-14, Stanford University, Stanford, California, USA.

Teodoriu, C., Schubert, J., and Ugwu, I. 2008. Cement Fatigue and HPHT Well Integrity with Application to Life of Well Prediction. Final Report, Contract No. MMS/OTRC CRA 1435-01-04-CA-35515. Minerals Management Service, Herndon, VA. (December 2008).

Van Dort, R. 2009. Metal-to-Metal Seals Meet Downhole Hazard Demands. *Journal of Petroleum Technology*. **61**(01), 24–26. SPE-0109-0024-JPT. https://doi.org/10.2118/0109-0024-JPT

Walvekar, S., and Jackson, T. 2007. Development of an Expandable Liner-Hanger System To Improve Reliability of Liner Installations. Presented at Offshore Technology Conference, 30 April-3 May, Houston, Texas, USA. OTC-18730-MS. https://doi.org/10.4043/18730-MS

Wang, J., Han, X., Wang, J. et al. 2015. Research on Packer Material Stress Analysis. Proc. of the 2015 Asia-Pacific Energy Equipment Engineering Research Conference, 13-14 June, Zhuhai, China. https://doi.org/10.2991/ap3er-15.2015.47

Wang, Z., Chen, C., Liu, Q. et al. 2017. Extrusion, slide, and rupture of an elastomeric seal. *Journal of the Mechanics and Physics of Solids:* **99**, 289–303. https://doi.org/10.1016/j.jmps.2016.12.007

Williford, J. W., and Smith, P. E. 2007. Expandable Liner Hanger Resolves Sealing Problems and Improves Integrity in Liner Completion Scenarios. Presented at Production and Operations Symposium, 31 March-3 April, Oklahoma City, Oklahoma, USA. SPE-106757-MS. https://doi.org/10.2118/106757-MS

Zhang, H., Shen, R., Yuan, G.et al. 2017. Cement sheath integrity analysis of underground gas storage well based on elastoplastic theory. *Journal of Petroleum Science and Engineering*: **159**, 818–829. http://dx.doi.org/10.1016/j.petrol.2017.10.012

Zhong, A., Johnson, M., Kohn, G. et al. 2015. Performance Evaluation of a Large Bore Expandable Liner Hanger for Field Operations in the Gulf of Mexico. Presented at Offshore Technology Conference, 04-07 May, Houston, Texas, USA. https://doi.org/10.4043/25995-MS

THIS REPORT WAS INADVERTENTLY DISSEMINATED IN THE PUBLIC DOMAIN/ONLINE SINCE 12/2018 WITHOUT A DISCLAIMER. DISCLAIMER HAS BEEN ADDED – "THIS INFORMATION IS DISTRIBUTED SOLELY FOR THE PURPOSE OF PEER REVIEW UNDER APPLICABLE INFORMATION QUALITY GUIDELINES. IT HAS NOT BEEN FORMALLY DISSEMINATED BY BSEE. IT DOES NOT REPRESENT AND SHOULD NOT BE CONSTRUED TO REPRESENT ANY AGENCY DETERMINATION OR POLICY."

APPENDIX A: ANALYTICAL CALCULATION OF CONTACT STRESS IN CEMENT

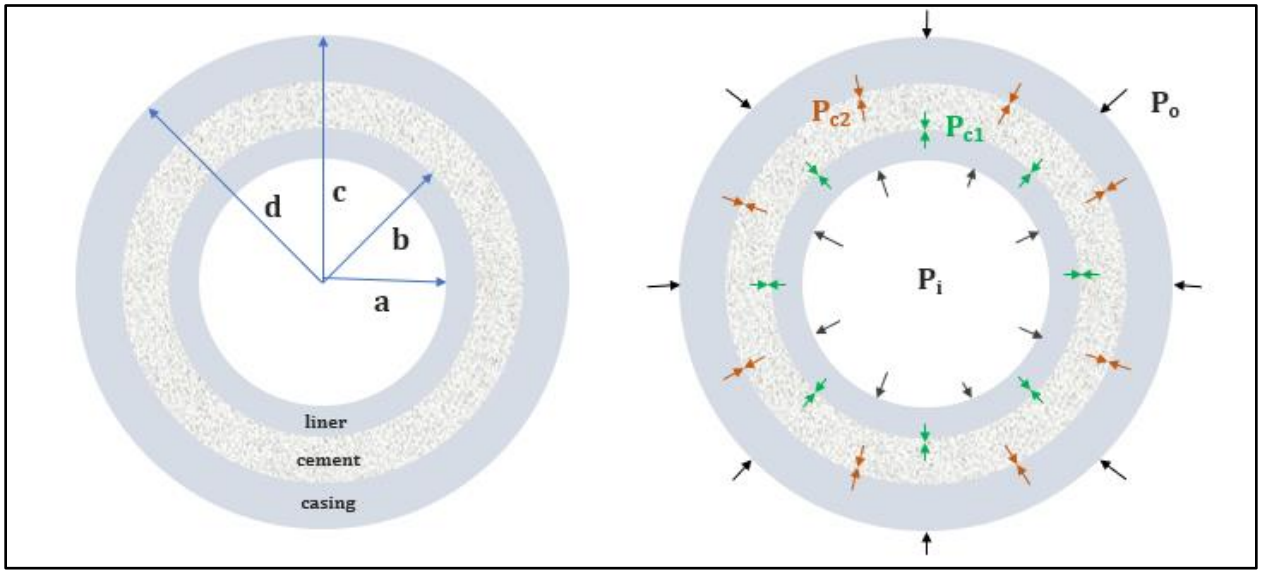

Figure A-1: Schematic of liner-cement-casing system for derivation of analytical equations

As discussed in section **2.2.1,** the liner-cement-casing system can be considered as composite thick cylinder system. Since the liner and casing are restrained in the z direction, the model can be considered as a plane strain axisymmetric problem. According to Lamé's theory (Hearn 1997), the axial strain can be calculated as following,

$$\varepsilon_z = \frac{1}{E}[\sigma_z - \upsilon(\sigma_\theta + \sigma_r)] \quad \text{(A.1)}$$

Where σ_z, σ_θ, and σ_r are axial, hoop, and radial stresses respectively. E and ν are Young's modulus and Poisson's ratio respectively.

Because of the plane strain assumption that $\varepsilon_z = 0$, the above equation can be rearranged as,

$$\sigma_z = \upsilon\,[\sigma_\theta + \sigma_r] \quad \text{(A.2)}$$

The radial expansion can be calculated as,

$$\delta_r = r \times \left[\frac{1}{E}\{\sigma_\theta(1-\upsilon^2) - (\upsilon+\upsilon^2)\sigma_r\}\right] \quad \text{(A.3)}$$

Considering, the liner as thin walled cylinder, radial and hoop stresses at liner-cement interface can be written as

$$\sigma_r = -(P_i - P_{c1}) \quad and \quad \sigma_\theta = \frac{-(P_i - P_{c1})\, r_{ml}}{t_l} \quad \text{(A.4)}$$

THIS REPORT WAS INADVERTENTLY DISSEMINATED IN THE PUBLIC DOMAIN/ONLINE SINCE 12/2018 WITHOUT A DISCLAIMER. DISCLAIMER HAS BEEN ADDED – "THIS INFORMATION IS DISTRIBUTED SOLELY FOR THE PURPOSE OF PEER REVIEW UNDER APPLICABLE INFORMATION QUALITY GUIDELINES. IT HAS NOT BEEN FORMALLY DISSEMINATED BY BSEE. IT DOES NOT REPRESENT AND SHOULD NOT BE CONSTRUED TO REPRESENT ANY AGENCY DETERMINATION OR POLICY."

Where r_{ml} and t_l are mean radius and thickness of liner respectively. P_i and P_{c1} are liner internal pressure and contact stress at liner-cement interface as shown in the Figure A-1.

Substituting equation A.4 in A.3, and putting r = a, the radial expansion at liner-cement interface can be calculated

$$\delta_{r-liner} = \left[\frac{a(P_i - P_{c1})}{E_l}\left\{\frac{r_{ml}(1-\nu_l^2)}{t_l} + (\upsilon_l + \nu_l^2)\right\}\right] \quad \text{(A.5)}$$

Now, let's calculate radial expansion at the liner-cement interface. Based on Lamé's theory of thick cylinder, radial and hoop stresses at the liner-cement interface are,

$$\sigma_{r-liner-cement} = -P_{c1} \quad \text{(A.6)}$$

$$\sigma_{\theta-liner-cement} = P_{c1}\left(\frac{c^2+b^2}{c^2-b^2}\right) - P_{c2}\left(\frac{2c^2}{c^2-b^2}\right) \quad \text{(A.7)}$$

Substituting above two equations in equation A.3, radial expansion at liner-cement interface can be calculated as,

$$\delta_{r-liner-cement} = \frac{b}{E_c}\left\{(1-\nu_{cs}^2)\left\{P_{c1}\left(\frac{c^2+b^2}{c^2-b^2}\right) - P_{c2}\left(\frac{2c^2}{c^2-b^2}\right)\right\} + P_{c1}(\upsilon_{cs} + \nu_{cs}^2)\right\} \quad \text{(A.8)}$$

Where subscript cs represents cement sheath properties

Both the radial expansions in equations A.5 and A.8 should approximately be the same and hence, equating those two equations and rearranging them leads to,

$$AP_{c1} + BP_{c2} = C \quad \text{(A.9)}$$

Where,

$$A = \frac{b}{E_c}\left[(1-\nu_{cs}^2)\left(\frac{c^2+b^2}{c^2-b^2}\right) + (\upsilon_{cs} + \nu_{cs}^2)\right] + \frac{a}{E_l}\left[\frac{r_{ml}(1-\nu_l^2)}{t_l} + (\upsilon_l + \nu_l^2)\right] \quad \text{(A.10)}$$

$$B = -\frac{b}{E_c}\left[(1-\nu_{cs}^2)\left(\frac{2c^2}{c^2-b^2}\right)\right] \quad \text{(A.11)}$$

$$C = \frac{aP_i}{E_l}\left[\frac{r_{ml}(1-\nu_l^2)}{t_l} + (\upsilon_l + \nu_l^2)\right] \quad \text{(A.12)}$$

Now, similar calculation will be performed at the cement-casing interface

Hoop and radial stresses at cement-casing interface using contact stress at cement-liner interface can be calculated as,

THIS REPORT WAS INADVERTENTLY DISSEMINATED IN THE PUBLIC DOMAIN/ONLINE SINCE 12/2018 WITHOUT A DISCLAIMER. DISCLAIMER HAS BEEN ADDED – "THIS INFORMATION IS DISTRIBUTED SOLELY FOR THE PURPOSE OF PEER REVIEW UNDER APPLICABLE INFORMATION QUALITY GUIDELINES. IT HAS NOT BEEN FORMALLY DISSEMINATED BY BSEE. IT DOES NOT REPRESENT AND SHOULD NOT BE CONSTRUED TO REPRESENT ANY AGENCY DETERMINATION OR POLICY."

$$\sigma_{r-liner-cement} = -P_{c2} \quad \text{(A.13)}$$

$$\sigma_{\theta-liner-cement} = P_{c1}\left(\frac{2b^2}{c^2-b^2}\right) - P_{c2}\left(\frac{c^2+b^2}{c^2-b^2}\right) \quad \text{(A.14)}$$

Putting these values in equation A.3 and calculating radial expansion at r = c,

$$\delta_{r-cement-casing} = \frac{c}{E_{cs}}\left\{(1-\nu_{cs}^2)\left\{P_{c1}\left(\frac{2b^2}{c^2-b^2}\right) - P_{c2}\left(\frac{c^2+b^2}{c^2-b^2}\right)\right\} + P_{c2}(\upsilon_{cs}+\nu_{cs}^2)\right\}. \quad \text{(A.15)}$$

Now, calculating the radial expansion at the same interface but using cement-casing properties, by calculating radial and hoop stress and using them in equation A.3.

$$\sigma_{r-liner-cement} = -P_{c2} \quad \text{(A.16)}$$

$$\sigma_{\theta-liner-cement} = P_{c2}\left(\frac{d^2+c^2}{d^2-c^2}\right) - P_o\left(\frac{2d^2}{d^2-c^2}\right) \quad \text{(A.17)}$$

The radial expansion at cement-casing interface,

$$\delta_{r-cement-casing} = \frac{c}{E_c}\left\{(1-\nu_c^2)\left\{P_{c2}\left(\frac{d^2+c^2}{d^2-c^2}\right) - P_o\left(\frac{2d^2}{d^2-c^2}\right)\right\} + P_{c2}(\upsilon_c+\nu_c^2)\right\} \quad \text{(A.18)}$$

Equating equations A.15 and A.18 and rearranging them provides,

$$DP_{c1} + KP_{c2} = F \quad \text{(A.19)}$$

Where,

$$D = -\frac{c}{E_{cs}}\left[(1-\nu_{cs}^2)\left(\frac{2b^2}{c^2-b^2}\right)\right] \quad \text{(A.20)}$$

$$K = \frac{c}{E_c}\left[(1-\nu_c^2)\left(\frac{d^2+c^2}{d^2-c^2}\right) + (\upsilon_c+\nu_c^2)\right] + \frac{c}{E_{cs}}\left[(1-\nu_{cs}^2)\left(\frac{c^2+b^2}{c^2-b^2}\right) - (\upsilon_{cs}+\nu_{cs}^2)\right] \quad \text{(A.21)}$$

$$F = \frac{cP_o}{E_c}\left[(1-\nu_f^2)\left(\frac{2d^2}{d^2-c^2}\right)\right] \quad \text{(A.22)}$$

Simultaneously solving equation A.9 and A.19,

$$P_{c1} = \frac{FB-KC}{DB-AK} \quad \text{(A.23)}$$

$$P_{c2} = \frac{C}{B} - \frac{A}{B}\left(\frac{FB-KC}{DB-AK}\right) \quad \text{(A.24)}$$

THIS REPORT WAS INADVERTENTLY DISSEMINATED IN THE PUBLIC DOMAIN/ONLINE SINCE 12/2018 WITHOUT A DISCLAIMER. DISCLAIMER HAS BEEN ADDED – "THIS INFORMATION IS DISTRIBUTED SOLELY FOR THE PURPOSE OF PEER REVIEW UNDER APPLICABLE INFORMATION QUALITY GUIDELINES. IT HAS NOT BEEN FORMALLY DISSEMINATED BY BSEE. IT DOES NOT REPRESENT AND SHOULD NOT BE CONSTRUED TO REPRESENT ANY AGENCY DETERMINATION OR POLICY."

The above contact pressure can then be used to calculate radial and hoop stress within cement using following equation,

$$\sigma_{r-cement} = \frac{P_{c1}b^2}{c^2-b^2}\left(1-\frac{c^2}{r^2}\right) - \frac{P_{c2}c^2}{c^2-b^2}\left(1-\frac{b^2}{r^2}\right) \quad \text{(A.25)}$$

$$\sigma_{r-cement} = \frac{P_{c1}b^2}{c^2-b^2}\left(1+\frac{c^2}{r^2}\right) - \frac{P_{c2}c^2}{c^2-b^2}\left(1+\frac{b^2}{r^2}\right) \quad \text{(A.26)}$$

Stresses in liner and cement can be calculated using equations similar to above two by replacing corresponding radii and pressures.